CHARACTERIZATION AND ENHANCEMENT OF IR OPTICAL AND TRIBOLOGICAL PROPERTIES OF DLC FILMS SYNTHESIZED BY RF-PECVD

A THESIS SUBMITTED TO
THE GRADUATE SCHOOL OF NATURAL AND APPLIED SCIENCES
OF
MIDDLE EAST TECHNICAL UNIVERSITY

BY
VAHİT EREN TABUROĞLU

IN PARTIAL FULFILLMENT OF THE REQUIREMENTS
FOR
THE DEGREE OF MASTER OF SCIENCE
IN
MICRO AND NANOTECHNOLOGY

JULY 2017

Approval of the thesis:

CHARACTERIZATION AND ENHANCEMENT OF IR OPTICAL AND TRIBOLOGICAL PROPERTIES OF DLC FILMS SYNTHESIZED BY RF-PECVD

submitted by Vahit Eren Taburoğlu in partial fulfillment of the requirements for the degree of Master of Science in Micro and Nanotechnology Department, Middle East Technical University by,

Prof. Dr. Gülbin Dural Ünver
Dean, Graduate School of Natural and Applied Sciences _____

Assoc. Prof. Dr. Burcu Akata Kurç
Head of Department, Micro and Nanotechnology _____

Prof. Dr. A. Macit Özenbaş
Supervisor, Metallurgical and Materials Engineering Dept., METU _____

Assoc. Prof. Dr. Burcu Akata Kurç
Co-Supervisor, Micro and Nanotechnology, METU _____

Examining Committee Members:

Prof. Dr. M.Vedat Akdeniz
Metallurgical and Materials Engineering Dept., METU _____

Prof. Dr. A. Macit Özenbaş
Metallurgical and Materials Engineering Dept., METU _____

Prof. Dr. Caner Durucan
Metallurgical and Materials Engineering Dept., METU _____

Assoc. Prof. Dr. Burcu Akata Kurç
Micro and Nanotechnology, METU _____

Assist. Prof. Dr. Kazım Tur
Metallurgical and Materials Engineering Dept., Atılım University _____

Date: 12.07.2017

I hereby declare that all information in this document has been obtained and presented in accordance with academic rules and ethical conduct. I also declare that, as required by these rules and conduct, I have fully cited and referenced all material and results that are not original to this work.

Name, Last name: Vahit Eren Taburoğlu

Signature:

ABSTRACT

CHARACTERIZATION AND ENHANCEMENT OF IR OPTICAL AND TRIBOLOGICAL PROPERTIES OF DLC FILMS SYNTHESIZED BY RF-PECVD

Taburoğlu, Vahit Eren

M.Sc., Department of Micro and Nanotechnology

Supervisor : Prof. Dr. A. Macit Özenbaş

Co-Supervisor: Assoc. Prof. Dr. Burcu Akata Kurç

July 2017, 146 pages

This thesis analyzes the hydrogenated amorphous diamond like carbon (a-DLC) films coated on aluminum substrates by the technique of plasma enhanced chemical vapor deposition (PECVD). Effects of film thickness, hydrogen content and RF power on the tribology, optical characteristics and structure are observed and studied in detail. DLC films have compressive intrinsic stresses by default. Surface topography revealed by an interferometer shows that too low/high compressive stress is detrimental to the film. In order to obtain the targeted results in terms of optical reflectivity, hardness, elasticity and durability of the film, one should use a well thought combination of thickness, hydrogen content and RF power in design and production stages. Frictional effects, recovery power (ratio of hardness ([H] to Young's modulus [E]; namely H/E) and restoration power are studied under a continuous predetermined scratching attack to decide on optimum initial coating

conditions. As a promising candidate for superlubricity, DLC films have exceptional hardness and friction coefficient which are core parameters to work on. Film robustness and durability under harsh environmental conditions are other pillars of the study. Furthermore by using X-ray photoemission spectrometer (XPS), it is proved that sp^3/sp^2 distribution is not uniform throughout the films, but sp^3/sp^2 ratio can be increased via some methods like increasing in hydrogen content. Hence this thesis aims to achieve optimum DLC film properties in terms of optical, tribological and/or mechanical aspects on the polished and highly reflective aluminum substrates.

Keywords: Quarter Wave Optical Thickness (QWOT), Optical Power, Friction, Hardness, Superlubricity, Recovery Power (H/E), Restoration Power.

ÖZ

RF-PECVD YÖNTEMİ İLE BÜYÜTÜLEN DLC FİLMLERİN IR OPTİK VE TRİBOLOJİK ÖZELLİKLERİ BAKIMINDAN KARAKTERİZASYONU VE GELİŞTİRİLMESİ

Taburoğlu, Vahit Eren

Yüksek Lisans, Mikro ve Nanoteknoloji Bölümü

Tez Yöneticisi: Prof. Dr. A. Macit Özenbaş

Ortak Tez Yöneticisi: Doç. Dr. Burcu Akata Kurç

Temmuz 2017, 146 sayfa

Bu tez çalışmasında plazma destekli kimyasal buharlaştırma yöntemi (PECVD) ile alüminyum altlık üzerine kaplaması yapılan, hidrojence zenginleştirilmiş amorf elmas benzeri karbon (DLC) ince filmler analiz ve karakterize edilmiştir. Film kalınlığı, film içerisindeki hidrojen yoğunluğu ve kaplama işlemi esnasındaki RF (radyo frekansı) gücü değişimlerinin filmin tribolojik, optik ve yapısal özelliklerine etkileri gözlemlenmiş ve bu parametreler üzerinde, optimum sonuçları elde etmek için çalışmalar yapılmıştır. DLC filmler doğaları gereği içsel basma gerilimlerine sahiptir. İnterferometri ölçümleri göstermiştir ki çok yüksek ve çok düşük içsel basma gerilimleri filmin bütünlüğünü korumasında zorluklar yaratmaktadır. Optik yansıtma, sertlik, elastisite ve dayanıklılık açılarından hedeflenen sonuçları elde etmek için film kalınlığı, hidrojen içeriği ve RF gücü, tasarım ve üretim aşamalarında çok iyi hesaplanmalı ve kontrol edilmelidir. Sürtünmeye ilişkin sonuçlar, kurtarma gücü (sertlik/elastisite modülü [H/E]) ve geri-gelme gücü yapılan sürtünme testleri ile incelenerek en uygun kaplama başlangıç değişkenleri belirlenmeye çalışılmıştır. Bir "süper kaygan" adayı olarak DLC filmler üzerinde çalışılmaya değer sıra dışı sertlik

ve sürtünme katsayılarına sahiptir. Çetin çevre koşullarında filmlerin sağlamlığının ve dayanıklılığının karakterize edilmesi, çalışmanın dayandığı ana ayaklardan birisidir. DLC filmlerin sp^3 ve sp^2 dağılım oranlarının filmin her noktasında tekdüze olmadığı X-ışını foto-emisyon spektrometre (XPS) cihazı yardımıyla anlaşılmıştır. Bununla birlikte sp^3/sp^2 oranının, hidrojen içeriğinin artırılması gibi çeşitli yöntemlerle başarılması mümkün görünmektedir. Sonuç olarak bu tez çalışmasıyla DLC filmler için optik ve tribolojik ve/veya mekanik açılardan optimum sonuçları, parlatılmış ve yüksek yansıma değerlerine sahip alüminyum altlıklar üzerinde elde etmek amaçlanmıştır.

Anahtar Kelimeler: Çeyrek Dalga Optik Kalınlık (ÇDOK), Optik Güç, Sürtünme, Sertlik, Süperkayganlık, Kurtarma Gücü (H/E), Geri-gelme Gücü.

To My Family and my Dearie Daughter Zeynep Helin

ACKNOWLEDGEMENTS

The author wishes to express his deepest gratitude to his supervisor Prof. Dr. A. Macit Özenbaş for his patience, guidance, advice, criticism, encouragements and insight throughout the research.

I would like to thank Assoc. Prof.Dr. Burcu Akata Kurç for being co-supervisor of my thesis work.

I would like to thank to all specialists of XPS and Nanomechanical Testing Laboratories in METU Central Laboratory for their great technical support and assistances.

TABLE OF CONTENTS

LIST OF TABLES

TABLES

LIST OF FIGURES

FIGURES

CHAPTER 1

INTRODUCTION

Carbon has been the core element in the life on world from the very early beginnings. Actually we are all living species in a carbon world. Furthermore, we are not only composed of mainly carbon and its compounds but also carbon as a material has shaped the world history irreversibly. It is accepted that modern age starts with 1st Industrial revolution, this was also known as the first carbon era. Although this age is mostly related with energy, it is for sure that as a neighbor of silicon and aluminum carbon does not leave us to the very end in space.

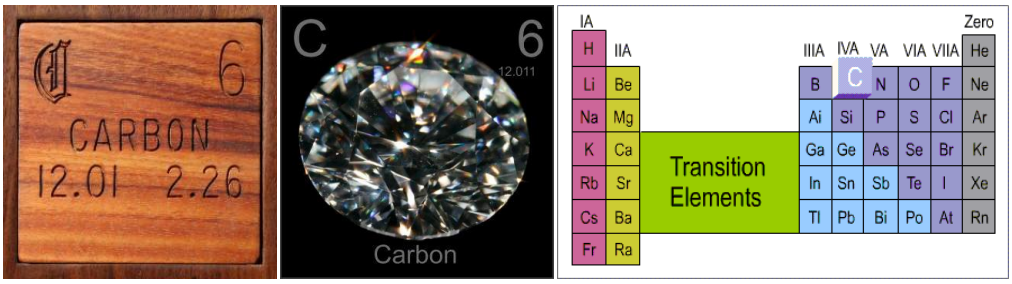

Figure 1.1 Carbon is an element in IVA in periodic table

For about 30 years carbon has also been the key element in the synthesis of thin film coatings like diamond, diamond-like carbon (DLC), carbon nitride, boron carbide, titanium carbide coatings. Exceptional mechanical and tribological properties make these coatings very popular in many engineering applications especially when friction

and wear are taken into consideration. Furthermore it is well known that diamond is one of the most technologically and scientifically valuable crystalline solids found in nature, as it has a combination of properties unrivaled by any other known material. The word diamond is derived from the Greek “adamas”, meaning "unconquerable, invincible". As a solid film diamond-like carbon, as the name suggests, inherits its basic chemical and physical properties from diamond. For example, diamond has the highest atom number density of any solid material ($1.76x10^{23}$ cm^3) at normal atmospheric pressures. As a result of its high atom number density and the strong covalent bonding, diamond has the highest hardness of any material and is the least compressible substance known. At 300 K diamond has the highest thermal conductivity and the smallest thermal expansion coefficient among all materials. Diamond is also a very wide band gap semiconductor (Eg=5.5 eV), has a high breakdown voltage (107 V/cm), and it is transparent almost in the whole spectral region. Although the DLC coatings are studied largely nowadays, DLC as a coating was discovered in early 1950s by Schmellenmeier. However it had to wait for 1970s and 1980s to reborn, then it took scientific attraction thanks to the studies done by Eisenberg and Chabot [1].

Amorphous diamond-like carbon (DLC) coatings are, similarly, known for their outstanding properties such as low friction coefficients, high hardness and wear resistance, chemical inertness, optical transparency in the IR spectral range and low electrical conductivities etc. These properties and their combinations are very promising for a variety of technical applications. Properties of the film depend mostly on bonding type and hydrogen content. Hence characteristics can be engineered by changing these inputs.

Today DLC films are used worldwide on a large industrial scale to improve the performance of tools and of components, thanks to its uncanny resistance to abrasion, salts, acids, alkalis, and oil. For automotive applications with more than 100 million parts are coated with DLC per year and a market volume of several €100 million [2]. Another application with large market shares is protective DLC films (a few nm thick) for high storage density hard disks and recording heads as well as razor blades where thin DLC films improve the performance of sharp cutting edges.

A single layer of hard carbon, deposited using highly specialized coating methods, offers an attractive combination of highly protective properties coupled with good anti-reflective performance. It was discovered that DLC adheres extremely well to Germanium and Silicon.

Optical parts deployed on military vehicles and outdoor thermal cameras can be coated with DLC, it protects the outer optical surfaces from high velocity airborne particles, seawater, engine fuel and oils, high humidity, improper handling, etc.

Throughout the infrared wavelength region in which it is employed, DLC exhibits moderate absorption and scattering. With a refractive index of approximately 2.0, DLC delivers good Broadband Anti-reflective (BBAR) performance on some semiconductor elements. DLC, because it consists of a single layer, is optimized for a specific wavelength region (most commonly 3-5 μm and 8-14 μm bands) by adjusting the layer thickness during the coating process. Although DLC is used in antireflective coating applications it is possible to use it in reflective side. In other words there is a promising possibility to use it on mirrors or mirror like tools.

In addition to its outstanding tribological properties, DLC is tolerated well by the body. Due to this advantageous combination of properties, research and development efforts have been made toward the use of DLC coatings in biomedical applications. Together with its blood biocompatibility, DLC surfaces also have an excellent haemocompatibility and DLC coated cardiovascular implants such as artificial heart valves, bloods pumps, and stents are already commercially available. Furthermore coatings for tissue culture flasks, microcarriers, cell culture containers are also in the application fields for DLC [3].

The major drawback of today's DLC coatings is having lack of high temperature resistance, which may preclude them from many cutting and grinding tool applications together with the limitations in thickness to a few microns due to intrinsic stresses. On the other hand, in moulding applications, for examples ejectors, moulds, they are effectively used to reduce wear and friction. Another application area of DLC is textile industry. Especially textile needles in textile machines are coated with DLC thanks to its high wear resistance.

Besides, high temperature together with oxygen especially atomic oxygen with energy (plasma) is the well-known enemy of DLC. Although in earth atmosphere it is a serious drawback, there seems to be a high potential to use DLC technologies on low weight metals or materials like aluminum in space applications.

The substrates used in this study are one side polished (to optical grade) pure aluminum and DLC film is to be deposited on these surfaces. Aluminum is selected because it has one of the highest optical reflectivity for the broad range of spectrum. The main concern and aim in this thesis is to create robust and durable DLC thin films on aluminum substrates with maximum optical reflectivity. Of course it is almost impossible to go beyond reflection values of optically polished bare aluminum surface, but the aim is rather keeping it as high as possible with enhanced tribological features. Hence durability and maximum hardness are other concerns. In other words the optimum film properties are going to be searched during this study.

The writer would feel successful if this thesis can add a drop of knowledge and scientific courage for further technological researches into the ocean of DLC in the universe of micro and nano technology.

Film thickness is the one of the parameters that is to be tailored. Furthermore, hydrogen content is also going to be changed and effects are monitored.

Compressive stress is frequently added up in the DLC films. Actually all DLC films tend to develop intrinsic compressive stresses in their body. Both film thickness and amount of hydrogen in the film affect the stresses developed in the film and consequently durability and lifetime is deadly fated by them.

This thesis consists of five chapters. First chapter is separated for literature survey. Secondly film structure and composition are explained. Optical, mechanical and tribological properties of DLC films are investigated in literature. The third chapter gives the details of experimental procedure. In chapter four, each experiment with their inputs and initial conditions are briefly introduced, results of the experiments were also given and discussed in detail. The discussions are also based on theoretical

approaches and analyses. Lastly in chapter five, the outcome of the study was defined and further suggestions were proposed.

CHAPTER 2

LITERATURE SURVEY

2.1 Bonding Structure in Diamond-Like Character

Diamond is accepted as carbon allotrope, in other words it is a formation of carbon atoms bonded in certain order with covalent bonds. Carbon is a unique and versatile element because of the short, medium and long range configurations it forms with itself and with other elements. A neutral single carbon atom has six electrons surrounding the nucleus. The arrangement of the electron orbitals in the ground state of C-atom is noted as the $1s^2 2s^2 2p^2$ configuration [4]. In order to form compounds during the bonding process with other atoms, the four $2s^2$ and $2p^2$ electrons are transformed into one out of three basic hybridization configurations, sp^1, sp^2 and sp^3 (Figure 2.2). In sp^1 configuration, two of the four valence electrons enter σ orbitals, each forming σ bond directed along the ± x-axis and two other valence electrons forms weaker π bonds (form polymers). In sp^2 configuration carbon forms graphite, the stable carbon allotrope with sp^2 trigonal bonding (3 σ bonds with 120 degrees separation, 1 π bond perpendicular to the plane) and in sp^3 configuration (diamond) an allotrope with sp^3 tetragonal bonding (4 σ bonds with 109.5 degree angles). The extreme physical properties of diamond are derived from its strong, directional σ bonds [5].

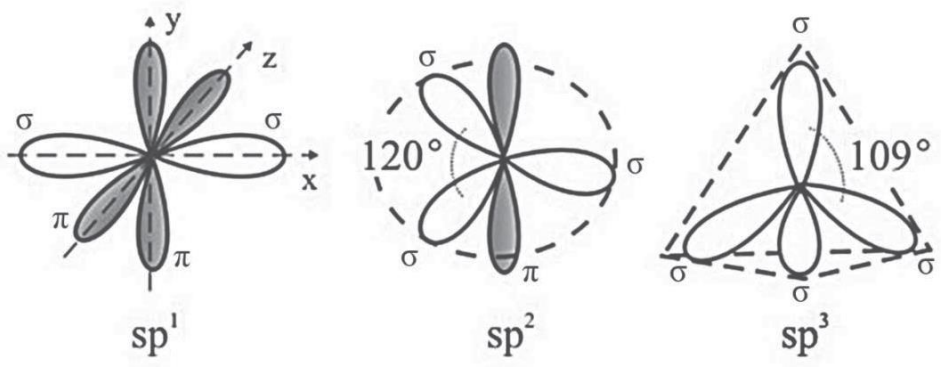

Figure 2.1 Three hybridization configurations of carbon atom with possible σ and π bond structures [5]

Although DLC owes its "diamond-like character" to C-C sp^3 bonds in the film, in order to call a film as DLC it should contain other type of bonds and atoms in it, otherwise it will be called as diamond because only diamond is composed almost full of C-C sp^3 type bonds. In fact literature says if a film has less than 70% sp^3 fraction it may then be accepted as amorphous DLC [5].

DLC films have meta-stable mixed phase which can be composed of different type of bonds: C-C sp^3, C-C sp^2, C-H. General characters of Young's modulus and hardness are dominated by C-C sp^3. C-C sp^2 bonds do not contribute much. Furthermore C-H bonds do not link up the network, this does not always create a handicapped situation, and on the contrary it can help to overwhelm the inelasticity character of pure diamond by causing relaxation throughout the film, hence it adds some elasticity to the film. Moreover, thanks to C-H bonds it is easier to make conformal DLC coatings to sophisticated geometries [6].

Hydrogen atoms usually participate to film by covalent bonds with carbon (C-H). These bonds are extremely strong (even stronger than C-C bonds) and it is difficult to remove it from carbon surface. Especially on the surface these bonds give the inertness character concerning many chemicals (including acids and bases) and make the film robust. However some hydrogen can be immersed freely into the film and these may be lost upon heating. Moreover these free hydrogen atoms can serve as reservoir and

can replace or replenish those hydrogen atoms that may be lost or removed especially from the surface mechanically [7].

Ion energies play an important role in the formation of bonds. For both hydrogen free and hydrogenated DLC films, the optimum ion energy is about 100 eV (Figure 2.2). For hydrogenated DLC's above this point, sp^2 fraction increases and the film gets more graphitic. On the other hand, in hydrogen free DLCs as the energy drops under 100 eV the film gets also more graphitic with increasing sp^2 fraction. However in hydrogenated DLC films, as the ion energy drops below 100 eV C(sp^3)-H bond fraction increases and the film gets more polymeric [6].

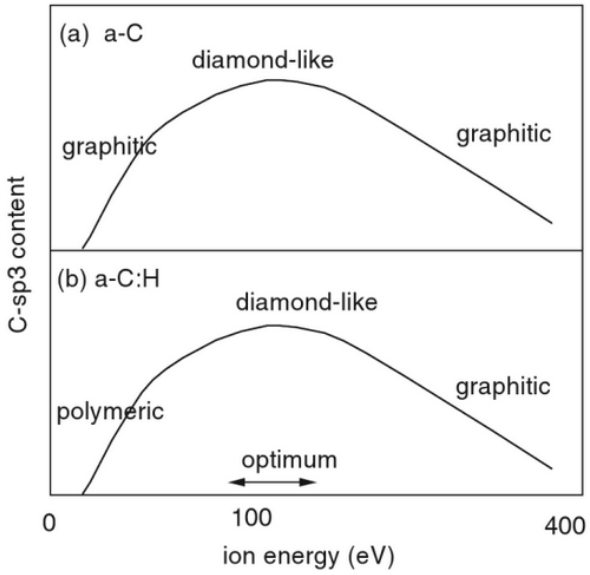

Figure 2.2 Schematic variation of fractional diamond-like character of (a) a-C and (b) a-C:H with deposition ion energy [6]

Binding energies of sp^2, sp^3 and other type of bonds can be differentiated by techniques like XPS (Figure 2.3). The characteristic carbon C peak 1s exits in the range of 283 eV to 290 eV, and it can be decomposed into several components basically on the structure of carbon and other possible elements. Fitted peaks within the C 1s can possibly relate to C-C bonds. C-C bonds are detected by three peaks; a

peak from sp^2 hybridized atoms appearing at 284.25 ± 0.30 eV known as C 1s-2 and another representing the sp^3 hybridized atoms appears at 285.33 ± 0.38 eV known as C 1s-3, lastly a sp^1 peak that appears at 283 eV. Carbon oxygen bonding peaks can appear at higher binding energies than the C-C peaks, each referring to a different state of bonding. In identified peaks, C 1s-4 for (C-O) appears around 285.5 eV, C 1s-5 for (C=O) is appearing around 287.7 eV and C 1s-6 for carboxylic (O=C-O) group is appearing around 290 eV, respectively. For DLC, these peaks are referred to as satellite peaks as they aren't used in analyzing the samples [8]. The C 1s-3 peak can also refer to C-H bonding; which was reported to appear at the same position as sp^3 connected carbon atoms (C-C) and by using only XPS it is hard to differentiate if it is C-C or C-H [9].

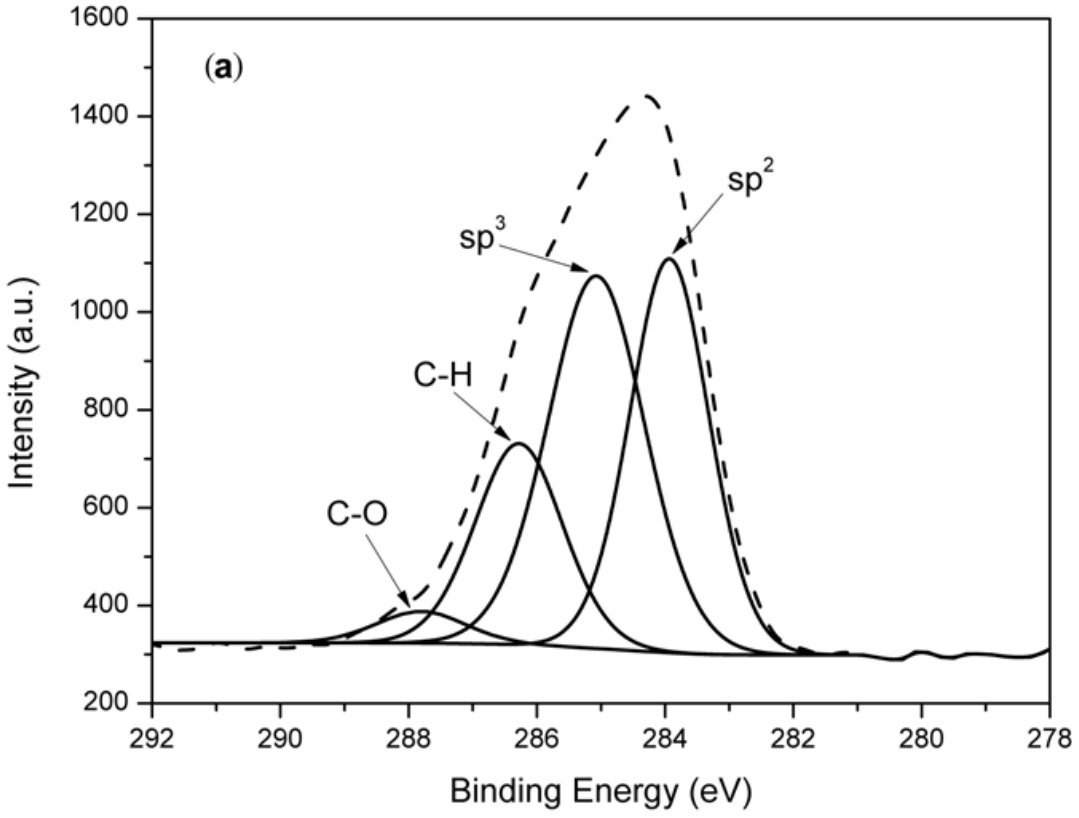

Figure 2.3 A sample XPS monitoring DLC on Si substrate [10]

2.2 A General View on Properties of Diamond-like Carbon Film

Typically, DLC thin films composed of sp^3, sp^2 bonds. The third defining factor is hydrogen content. In Figure 2.4 the ternary diagram shows the composition depended film structure. Hence as the sp^3 concentration increases the film characteristics gains more diamond –like properties, that is tetrahedral amorphous (ta) carbon. On the other hand sp^2 is graphitic and mechanically soft.

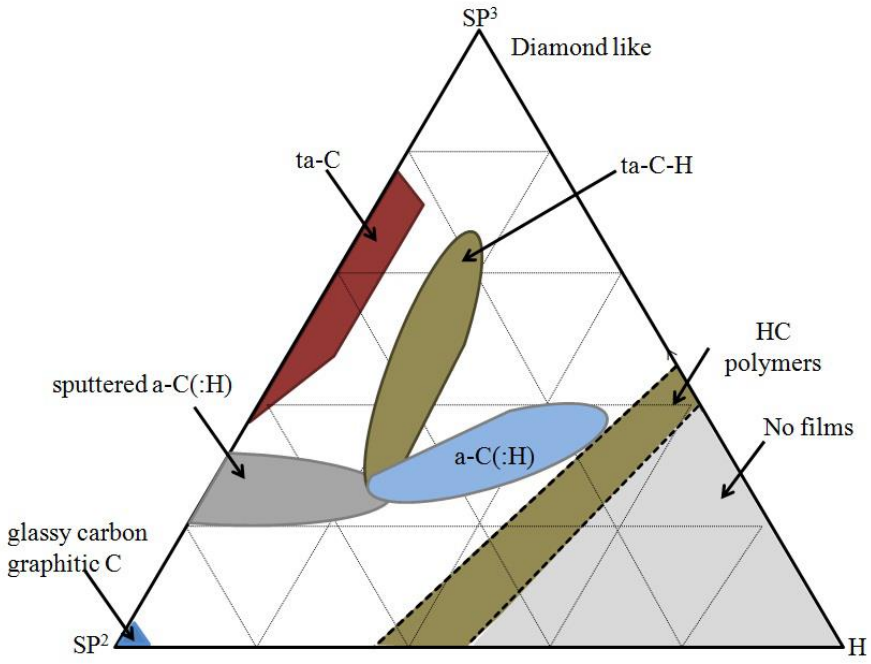

Figure 2.4 Ternary phase diagram for various DLC films with respect to their sp^2, sp^3 and hydrogen contents [11].

Diamond is the hardest material ever known in the nature. DLC film as the name suggests has similar characteristics with diamond. It has superior hardness values and coefficient of friction is very low hence its wear resistance is comparatively better than other known hard thin films. In able 2.1 some properties of diamond, ta-C (tetrahedral amorphous carbon) DLC, a-C:H (hydrogenated amorphous carbon) DLC and graphite are comparatively tabulated.

High sp^3 to sp^2 ratio increases not only hardness, but also optical refractive index and intrinsic stress. Mean optical refractive index is about 2.0.

Hydrogen percentage is less than 1% for a-C (amorphous carbon) films, if hydrogen concentration exceeds 1%, the film is then called as a-C:H (hydrogenated amorphous carbon). The presence of H is essential for optical transparency. Furthermore, hydrogen (H) in plasma etches sp^2 bonds, hence it favors formation of sp^3. It was shown that as DC bias voltage increases, H-to-C ratio increases with increasing sp^3 to sp^2 ratio [12]. Generally speaking in hydrogenated DLC (α-C:H) films H content is more than 30%, and commercially available DLC films consist predominantly of sp^3 vs sp^2 bonds.

Table 2.1 Comparison of properties of diamond, ta-C, a-C:H and graphite [11]

	Diamond	DLC(ta-C)	DLC(a-C:H)	Graphite
Crystal system	Diamond cubic	Amorphous	Amorphous	Hexagonal
Mass density (g/cm^3)	3.51	2.5-3.3	1.5-2.4	2.26
sp^3 Content (%)	100	50-90	20-60	0
Hydrogen content (%)	0	-1	10-50	0
Hardness (GPa)	100	50-80	10-45	<5
Friction coefficients in humid air	0.1	0.05-0.25	0.02-0.3	0.1-0.2
Friction coefficients in dry air	0.1	0.6	0.02-0.2	>0.6
Band gap (eV)	5.5	1-2.5	1-4	-0.04
Electrical resistivity (Ω cm)	10^{18}	10^6-10^{10}	10^4-10^{12}	10^{-6}-10^{-2}
Thermal stability in air (°C)	800	400-600	300-350	>500

The precursor gases can be among some well-known hydrocarbons; namely, CH_4 (methane), C_2H_2 (acetylene), C_2H_6 (ethane), C_2H_4 (ethylene), C_6H_{12} (cyclohexane).

Table 2.2 Characteristics of DLC coatings and aluminum [13], [4], [14], [15]

Chemical properties	DLC	Aluminum
Composition	Carbon, hydrogen	Aluminum
Structure	Mixture of sp^3 (tetrahedral diamond type) and sp^2 (trigonal graphitic) and amorphous	Metallic
Reactivity	Generally inert to acids, alkalis, solvents, salts, water, and other reagents at ambient temperature	Not inert to acids, alkalis, solvents, salts, water, and other reagents at ambient temperature
Physical properties		
Density	1.8-2.1 g/cm^3	2,7 g/cm^3
Thermal conductivity	10 W/cm x K	2,35 W/cm x K
Coefficient of expansion	9 x 10^{-6}/C	23 x 10^{-6}/C
Electrical resistance	Several MΩ x cm	2.6×10^{-8} m Ω
Dielectric constant	varies between 4 and 11	
Adhesion	34.473 MPa std. pull strength	
Permeability	Barrier to hydrogen and other gases	

Table 2.2 (cont'd) Characteristics of DLC coatings and aluminum [13], [4], [14],[15]

Optical properties	DLC	Aluminum
Optical transparency	From NIR to FIR	Highly reflective IR bands
Refractive index	1.85 - 2.0	N/A
Thickness	Depends but generally max:3μm	
Surface roughness	Depends on selected substrate	
Stresses	Not measurable	
Other properties	DLC	
Deposition temperature	10 °C approximately	
Operational temperatures	-60 °C to +400 °C	
Biocompatibility	Maintains cell integrity, no inflammatory response	
Durability performance	Adhesions, severe abrasion and mechanical strikes, high humidity, high and low temperature influence, thermal shock, salt spray fog, salt solubility, water solubility and resistance to atmospheric precipitation, dust and sand impact, resistance to some acids, resistance to oil and diesel fuel as per the following standards (where applicable): MIL-C-675C, MIL-STD-810	

In addition to hydrocarbon precursor gas it is not rare to use molecular hydrogen (H_2) in literature.

The DLC films can be deposited by a variety of methods, including filtered cathodic vacuum arc (FCVA), ion beam assisted deposition, DC- and RF-plasma-assisted chemical vapor deposition and sputtering. Among them plasma enhanced (RF assisted [13,56mHz]) vapor deposition (PECVD) is very reliable and repeatable process. Although most of the CVD techniques suffer high temperatures, DLC can be deposited by PECVD at comparatively low temperature like 100-150°C. Besides creating plasma from which film is constructed, RF source used in this technique also

create activated species in the plasma: ions, excited species, electrons. These make the process more energetic.

It is also possible to make the film more durable by using argon as a plasma etching agent. Ar+ preferential etching of weaker bonds reduces sp^2 bond concentration, increases stable sp^3 and "diamond-like" properties.

For a film to have good adhesion and long term durability, it is important having similar surface and physical properties with the substrate. Hence choosing right substrate for the film is important, and vice versa. Aluminum as a substrate may not be the best choice but certainly it does not reject DLC; actually with DLC it can tolerate many practical harsh conditions and creates some sort of synergy. Furthermore since metal aluminum is very light and comparatively cheap, it can be found abundantly in the market. Table 2.2 gives respective basic properties of DLC films and aluminum.

2.3 Growth Mechanisms and Structural Observations on Hydrogenated Amorphous Diamond-Like Carbon Films

Because of the amorphous structure of hydrogenated diamond-like films there is a structural diversity and growth mechanism causing this diversity is essentially affected by energies of incoming ions or molecules, abundancy of precursor gases and so on. That is to say there is no unique growth mechanisms and structural model.

In literature one can find out that there have been studies those are using molecular dynamic (MD) simulations on microstructure and growth mechanism of hydrogenated amorphous carbon films. One of a study is released on 8 May 2014 [16]. The substrate is diamond and the precursor gas is C_2H_2 as selected in this study.

One of its insertions is that at low energies, molecular adsorption dominates the process of the film growth, so the incident molecules tend to preserve their original molecular structures [17]. In case of an increase in incident energy, the film density

first increases and then gets stabilized, at the mean time hydrogen content decreases because of molecular fragmentation [18].

Furthermore, hydrogen atoms play an important role in the growth of hydrogenated amorphous carbon films. There was approximately a linear correlation between the H flux and H incorporation in the film. In addition to that, hydrogen adsorption, the formation of C–H bonds and the formation of sp^3 structure is favored by low energies. On the other hand, at high energies the sub-plantation of carbon atoms and formation of C–C bonds are most responsible to the formation of sp^3 structures.

Besides, increase of hydrogen content or increase in flow rate in source gas decreases film density and increases sp^3 fraction.

In the MD study, the effect of incident energy of deposited agents is also investigated. Behaviors of C_2H_2 molecules under the incident energy ranging from 5 to 150 eV per carbon atom are observed. The substrate is again diamond. Below 20 eV dense, thick and homogeneous films could not be obtained due to high hydrogen content as simulated in Figure 2.5. The reason is below 20 eV the hydrogen content is very high on the surface that results in a high rebound ratio and low deposition yield. Furthermore results show also that at low energy levels intermixing with the film due to the soft landing of the incident atoms is not observed at all. Moreover at higher energies as 80 eV and above, long monoatomic carbon chains and rings comprised of sp1-C atoms appear on the surface with very few hydrogen atoms. This films with sp^1-C atoms and low hydrogen content are very unstable and can easily be etched by oxygen in the air. On the other hand with increasing energy, film-substrate intermixing is more obvious (Figure 2.5).

This study shows specially the atomic structures and depth profiles obtained at 30 eV C_2H_2 incidence. Relative densities, sp^3 fractions and hydrogen contents are calculated starting from substrate surface to very top surface of the film. The sp^3 fraction is the number of sp^3 bonded carbon atoms to total number of carbon atoms. Hydrogen content is referred to as the ratio of the number of hydrogen atoms to the total number

of atoms. Consequently there can be observed three distinct regions in the Figure 2.6. These are namely; transition region, intrinsic region, and surface region.

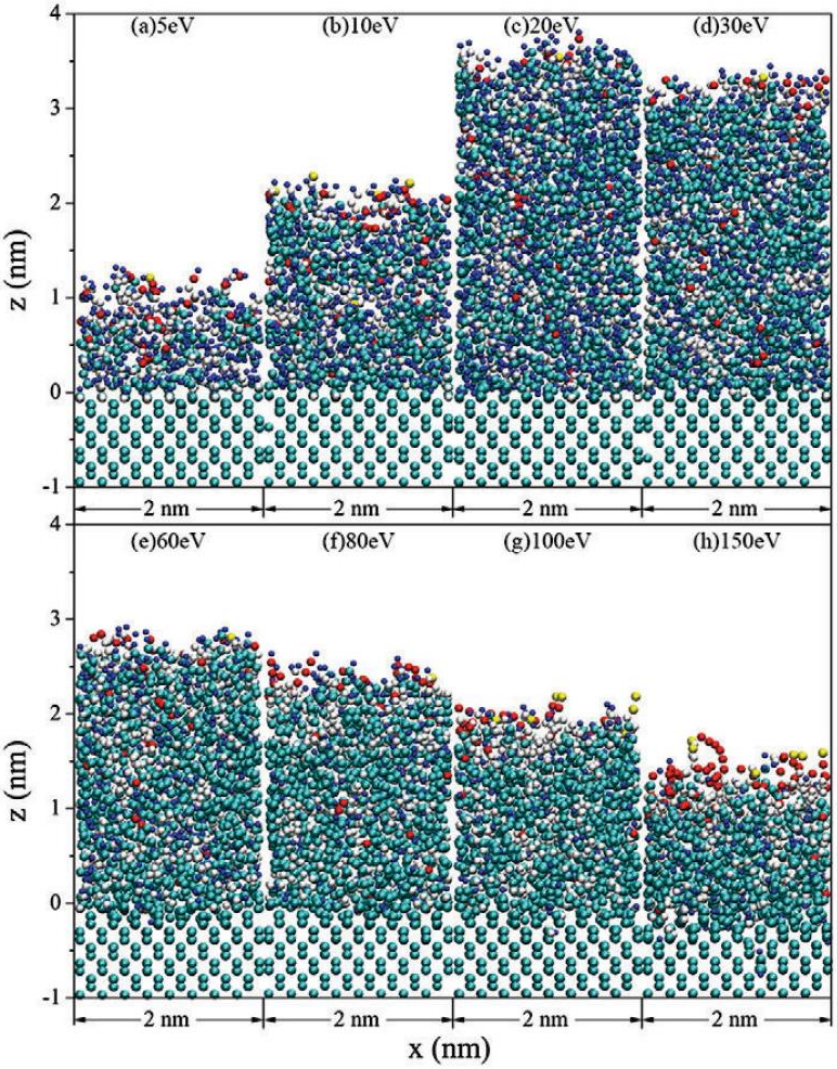

Figure 2.5 Molecular Dynamic (MD) Simulation model: Final configurations of deposited films derived from 1000 incident C_2H_2 molecules at different incident energies. Yellow balls represent one-fold carbon atoms, red balls are two-fold (sp^1) atoms, white balls are three-fold (sp^2) atoms, cyan ones are four-fold (sp^3) atoms, and blue ones are hydrogen atoms. [16]

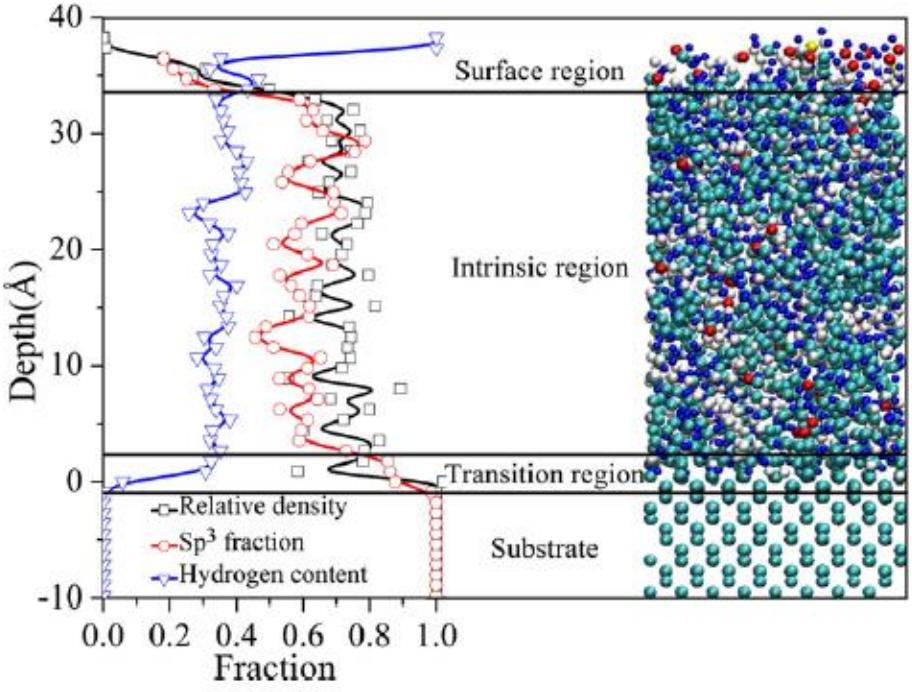

Figure 2.6 Atomic structures and depth profiles obtained at 30 eV C_2H_2 incidence. [16]

Generally film properties in intrinsic region represent the properties of the entire film. In spite of small fluctuations structural parameters keep basically invariable. In other words sp^3 fraction is approximately 60% and hydrogen content is about 35%. The hydrogen content in the surface region shows a rapid increase, which means hydrogen atoms tend to cluster in surface region [16]. High hydrogen content near or on the surface resulting in the super-low friction properties of a-C:H films by surface passivation.

Further change upon incident energy is also studied and results plotted on the graph (Figure 2.7).

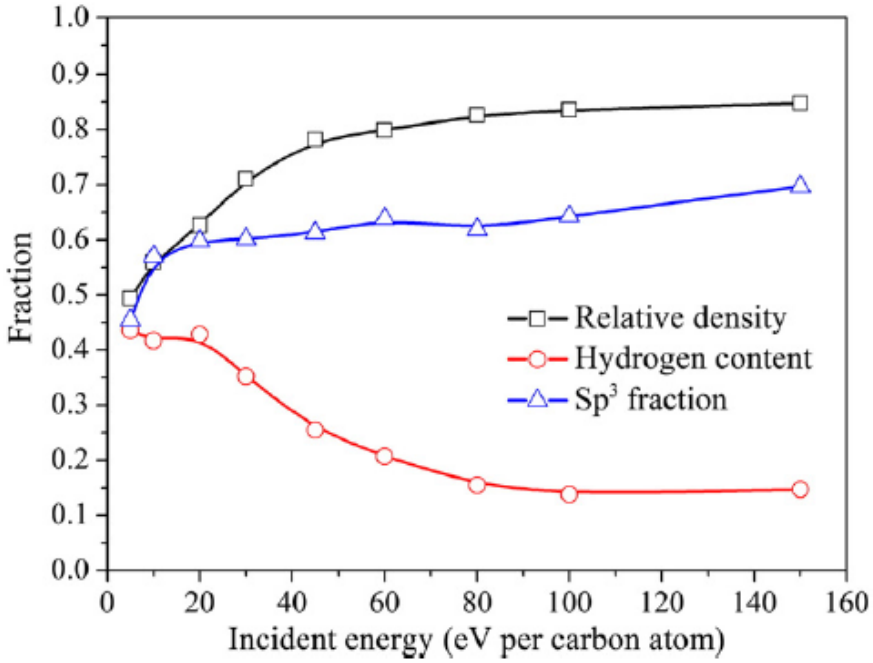

Figure 2.7 Incident energy vs relative density, hydrogen content, sp^3 fraction [16]

As for sp^3 fraction, a gradual rise is observed, from 45% at 5 eV to 70% at 150 eV, showing more diamond-like character and better mechanical properties. Moreover hydrogen content keeps decreasing with increasing energy as mentioned before and it is called as the dehydrogenation [16].

2.4 Residual Stress in DLC

For a good adhesion to substrate surface, stress developed in the film is a fundamental factor. In film technology stresses can be classified as two: intrinsic and extrinsic [19].

Thanks to the nature of CVD, films deposited on the surface quite slow and conformal, hence there is not enough temperature difference to create residual thermal stress during the deposition. However if there exist a thermal expansion coefficient difference between film and the substrate, in case of change in temperature, stress can develop in the film.

As an extrinsic type, stress due to thermal expansion can be formulated as:

$$S_{TCE} = Y_f (\alpha_f - \alpha_s) (T_d - T_m) \qquad \text{(Equation 2.1)}$$

where "f" is film, "s" is substrate, Y_f is film's yield strength, α_f and α_s are thermal expansion coefficients of film and substrate respectively, "T_d" means temperature during deposition, "T_m" means temperature after the run and during measurement [12].

On the other hand, intrinsic stresses result from compressive or tensile forces built into the film layer. Origins of intrinsic stress can be complicated and can be due to:

- Material properties
- Deposition process
- Growth method of nano-structure
- Defects and contamination.

Generally speaking, compressive intrinsic stress develops in thin films with particles having high energies or in other words due to energetic deposition processes. According to Y.Pauleau these energetic particles can be atoms, molecules, ions and radicals either condensed on the film surface and incorporated in the film, or simply reflected at the film surface and backscattered to the gas phase. Energetic particles have average energy above 0.5 eV and particles below this value can be accepted as non-energetic [20]. Furthermore carbon species having high kinetic energies (2.5 to 25 eV) are prone to create sp^3 configurations which are mainly responsible diamond-like properties. Hence there should be a tradeoff between high sp^3 content and compressive stress in the film.

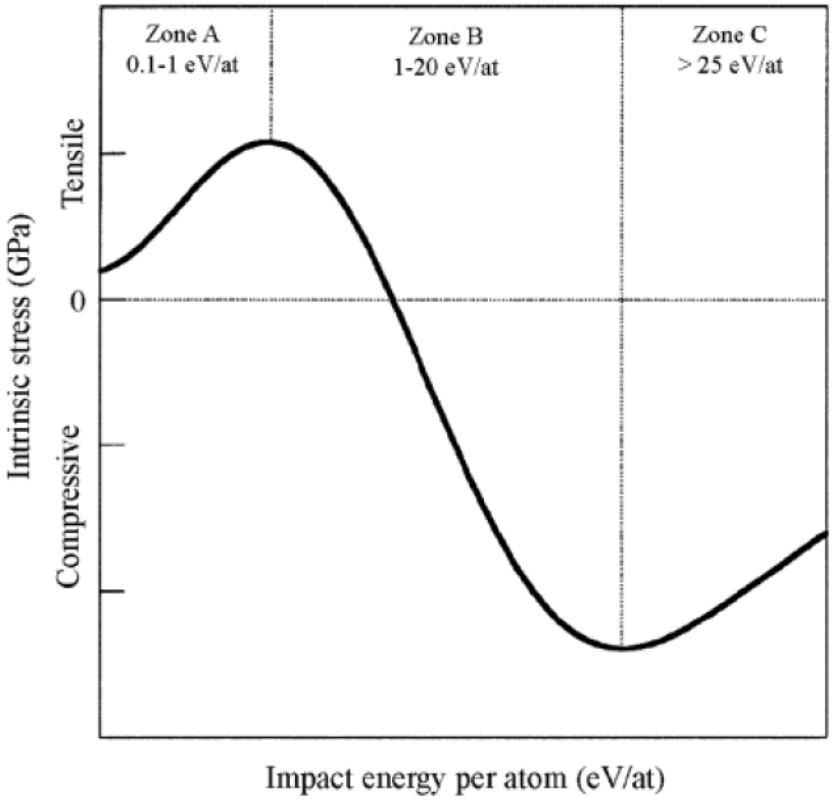

Figure 2.8 Idealized intrinsic stress versus impact energy per atom [20]

On the other hand tensile stresses develop and increase in films because of non-energetic particles and micro voids which are generated in the film due to these non-energetic particles. Figure 2.8 shows the relation between impact energy and intrinsic stress.

The stress is compressive when film on the surface is convex and tensile when film contracts parallel to surface, then the film is concave (Figure 2.9).

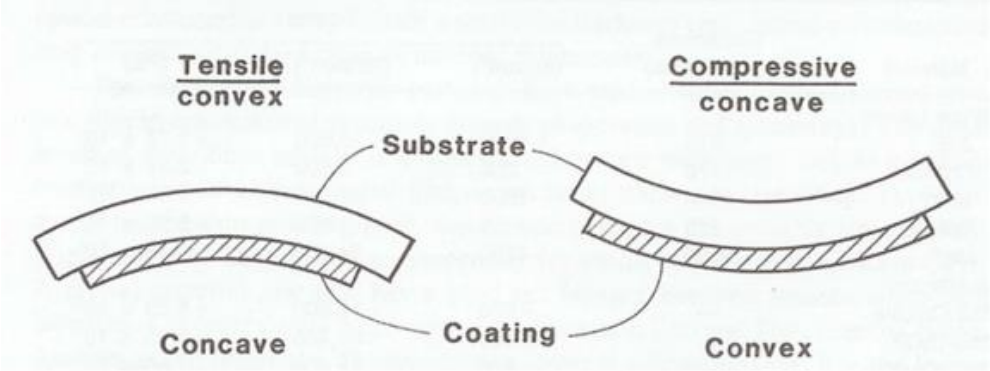

Figure 2.9 Relationship between stress and change of surface geometry [12]

Moreover tension T (not stress) increases with increasing thickness: T = S x t, (where "S" is stress and "t" is the thickness) consequently shear stress is developed between coating and substrate. DLC thin films generally tend to have intrinsic compressive stress. When this stress exceeds the adhesive force then the film fails [12].

2.5 A Review for Optical Reflectance

Light is a progressive electromagnetic disturbance traveling in space or in material. It is composed of two fields, namely electrical field wave, and magnetic field wave. These two waves progress in space always perpendicular into each other. In other words, the electric field [E], the magnetic field [H] and the direction of propagation of the wave can be shown to be mutually perpendicular and to form a right-handed set. Figure 2.10 shows a schematic review of a mechanical wave and a light wave.

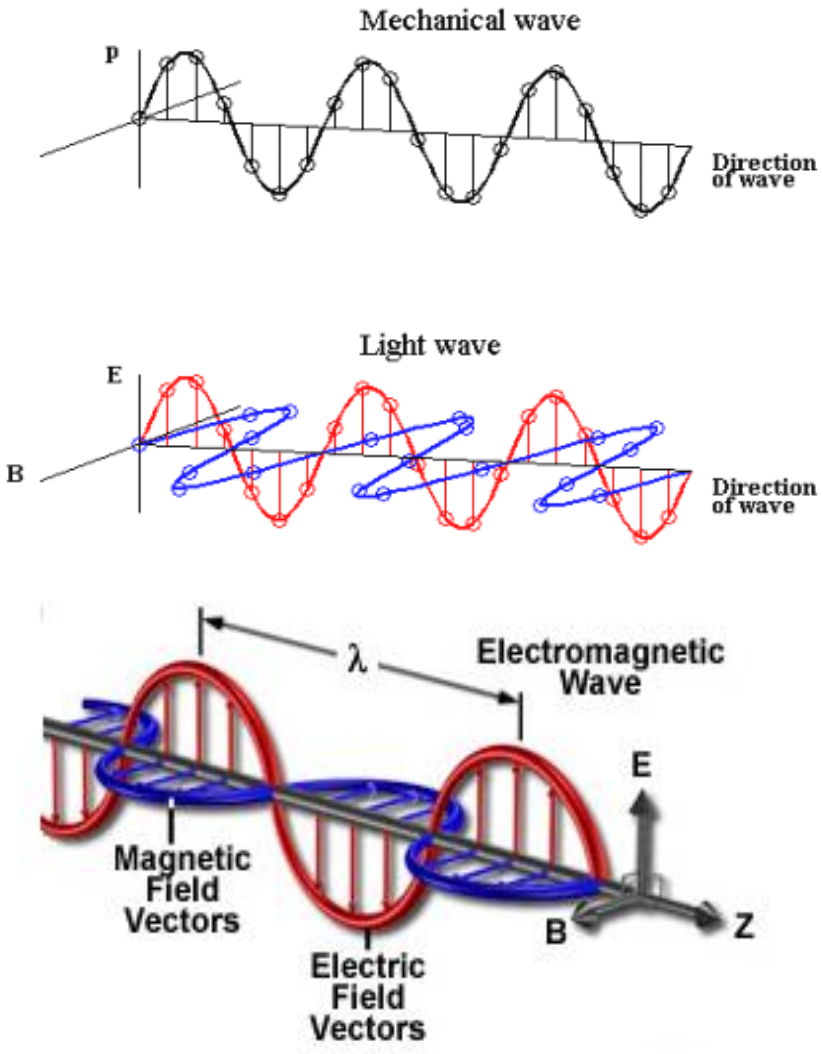

Figure 2.10 Light propagates with its mutually perpendicular components [13]

The material properties are dependent on the action of the fields of the electromagnetic wave with the charged particles, in particular the valence and/or free electrons, in the material through which it propagates. An electric field can exert a force on a stationary charged particle but a magnetic field can interact only with a moving charged particle, and the interaction is negligible unless the speed is very high. Optical frequencies are so high, and the fields of normal optical waves sufficiently low, that the velocity of this vibrational motion never reaches a value where the magnetic action can become

significant. Hence in calculations, it can readily be supposed that the electric field is the only one to care about [13].

For a linearly polarized plane harmonic wave, electric field equation can be written in complex form:

$$E = \varepsilon \exp(i\phi)\exp[i\omega(t-z/v)] \qquad \text{(Equation 2.2)}$$

where E, because of the linear polarization, will be confined to a fixed direction. ε is the electric field amplitude, ϕ is relative phase, ω the angular frequency, t is time, z is distance and v the velocity of this wave. A relative phase (ϕ) is included and $\varepsilon \exp(i\phi)$ is usually referred to as the complex amplitude and the second part of the expression as the phase factor.

Furthermore magnetic field (H) and electrical field (E) can be related:

$$H = yE \qquad \text{(Equation 2.3)}$$

where y is the admittance and admittance can be written in complex form of optical refractive index.

$$y = n - ik \qquad \text{(Equation 2.4)}$$

the refractive index (n) is defined as wave velocity in free space / wave velocity in material [15]. Equation 2.4 is a very useful simplification but can lead to the confused idea that somehow refractive index and optical admittance are the same. They are completely different physical quantities and at lower frequencies this assumption no longer applies.

For light the Irradiance, I, mean power per unit area Wm^{-2} can be defined as:

$$I = 1/2Re(EH) \qquad \text{(Equation 2.5)}$$

Where "Re" is to symbolize the real part of (EH). Then after some simplifications Irradiance can be written as:

$$I = \tfrac{1}{2}\,Re(y)\ |\varepsilon|^{2} \exp[-(4\pi kz/\lambda)] \text{ or } I = \tfrac{1}{2}\,n\ |\varepsilon|^{2} \exp[-(4\pi kz/\lambda)] \qquad \text{(Equation 2.6)}$$

Where, λ is the wavelength of the light. Reflectance can be defined as irradiance reflected divided by irradiance incident:

$$R = (I_{ref.} / I_{inc.}) \qquad \text{(Equation 2.7)}$$

As it can be seen in Figure 2.10 light propagates with its mutually perpendicular components where electrical component of light shows a sinusoidal wave character as it travels. If light hits and reflects on a surface of medium and this second medium has higher refractive index than the medium where the light just comes from (first medium), electrical field wave (E) changes its phase as 180° (π).

Rule of energy conservation states that, light is actually certain type of energy and total incident (I) light (or energy) should be equal to the sum of reflected (R) light, transmitted (T) light and absorbed (A) light. This assumption should be kept in mind throughout the thesis.

$$I = T + R + A \qquad \text{(Equation 2.8)}$$

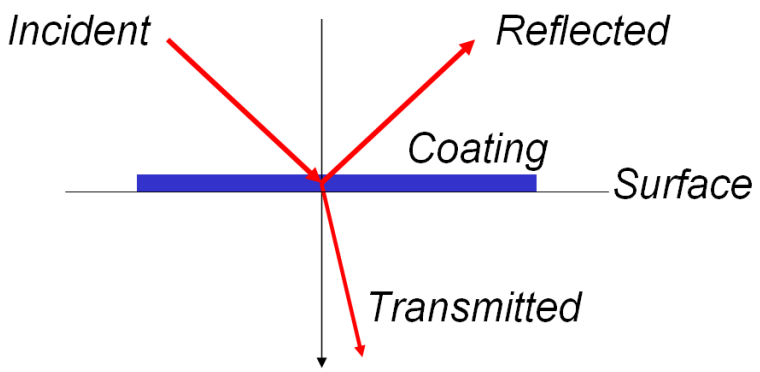

Figure 2.11 Component of light incident on a film [13]

2.5.1 Why Thin Film?

Actually the term thin implies that the film has surfaces that are sufficiently flat and parallel that when illuminated by a plane harmonic wave the infinite number of waves reflected back and forth between the two surfaces have a constant unambiguous phase relationship that does not depend on their lateral position [13].

Thanks to the wave nature of light, interference may the most important and interesting phenomenon in optics. As mentioned above we always take the electrical field part of the light in calculations. Thin films' superiority on thick films or bulk materials relies on this interference effect. In other words thin films use interference properties and that implies creating and changing the shape of interference fringes. Thick materials give fringes that are too closely spaced to be useful. Hence the broad fringes that we require imply thin films.

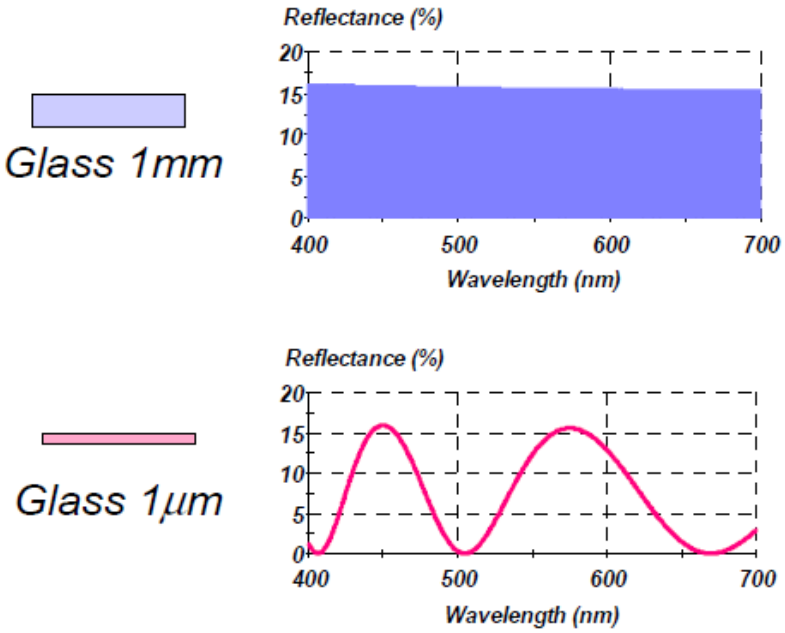

Figure 2.12 Comparison of fringes produced by a 1mm thickness of glass and a 1μm thickness. The thicker glass produces fringes that are essentially unusable [13]

The governing mechanism is based on the created phase difference between reflected light beams. Incident light coming from a medium having a refractive index of n_1 first hits the thin films upper surface which has refractive index of n_2. Some of the light reflected and some is refracted (transtmitted) and goes through from the surface into the substrate. This refracted portion of the light also reflected and refracted on the second interface (thin film-substrate). Hence reflected two rays shown in Figure 2.13 are parallel and there is a phase difference between them. This phase difference (δ) depends on thin films refractive index (n-ik), wavelength (λ) and film thickness (d):

$$\delta = 2 \pi (n\text{-}ik)\, d / \lambda \qquad \text{(Equation 2.9)}$$

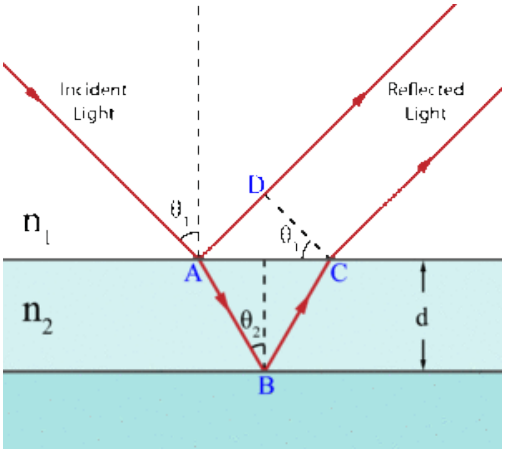

Figure 2.13 Demonstration of the optical path length difference for light reflected from the upper and lower interfaces of a thin film [13].

If the film is dielectric then losses can be neglected in infrared region, then the phase difference equation can be simplified as:

$$\delta = 2 \pi n d / \lambda \qquad \text{(Equation 2.10)}$$

In general, rather than physical thickness (d), optical thickness (nd/ λ_0) is used in thin film literature.

Furthermore, as mentioned before, 180° phase shift also can occur if the light is reflected on surface of a material which has higher refractive index than the medium where the light comes from ($n_1 > n_0$) (Figure 2.14).

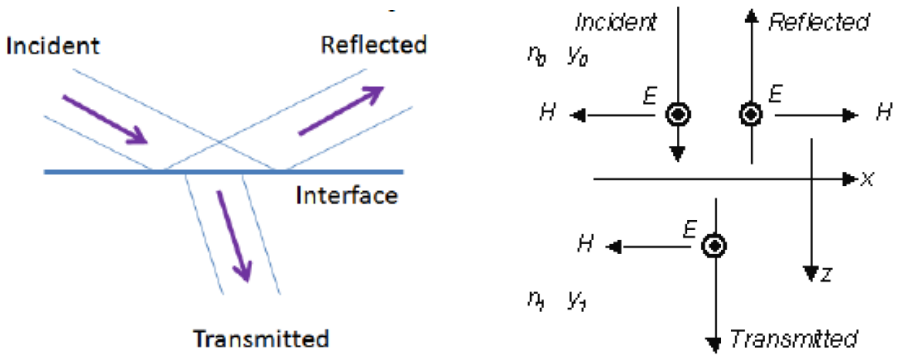

Figure 2.14 Light passing through and reflected on an interface [13]

The phase shift is one of the main principles used in anti-reflective or reflective thin film designs. Actually in an interference phenomenon, two waves add up if there is no phase difference and two waves with the same amplitude and 180° phase shift cancel each other (Figure 2.15). These are the two extreme cases of the rule. Hence according to the conservation rule and if the absorbance can be neglected, in order to strength up reflectance, waves should have minimum phase differences.

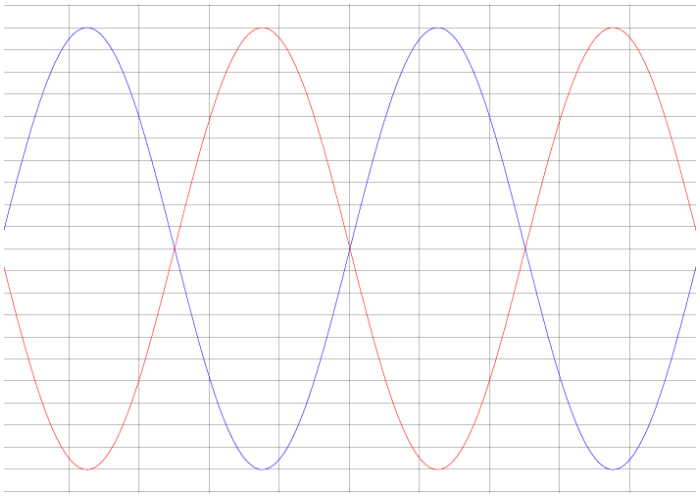

Figure 2.15 Two typical sinusoidal waves having 180° phase shift between each other [13]

2.5.2 Quarter Wave Rule

If optical losses can be neglected it is possible to set up a relationship between film thickness and reflectance / transmittance measurements. Quarter wave rule states that a single layer thin film which has quarter wave optical thickness regarding of the target wavelength, has maximum transmittance and minimum reflectance in a band which centers the target wavelength; this is also valid for odd (1,3,5 etc.) multiples of optical thicknesses of quarter wavelength. On the other hand, if the optical thickness of the film is half of the target wavelength, reflectance will be maximum so transmittance is going to be minimum, again it is valid also if the thickness is multiple of half wavelength (Figure 2.18). These rules can be further extrapolated for all angles by some mathematical and geometrical calculations.

Please note that optical thickness (nd/λ_0) is the crucial parameter rather than physical thickness, where n is the refractive index, d is the physical thickness, λ_0 is the target wavelength. Hence a thin film which is of odd number multiples of quarter wave optical thickness (QWOT), creates 180° phase difference between primary and secondary reflected rays and maximize the interference effect. Hence reflectance will be minimum (if not zero) and according to the conservation rule ($T + R + A = 1$) transmittance will be maximized. On the contrary, in order to maximize reflectance, waves must reinforce each other. In other words there must be no phase difference between reflected rays. This is possible if the thin film has half wave optical thickness. For example in infrared region for target wavelength of 10 000 nm with about 2.0 refractive index a single layer of about 2500 nm physical thickness will maximize the reflectance. Actually half wave optical thick thin films are accepted as “absentee” layers, because they have not any interference effect and almost leave the substrate surface as if it was not coated in terms of optical transmittance/reflectance.

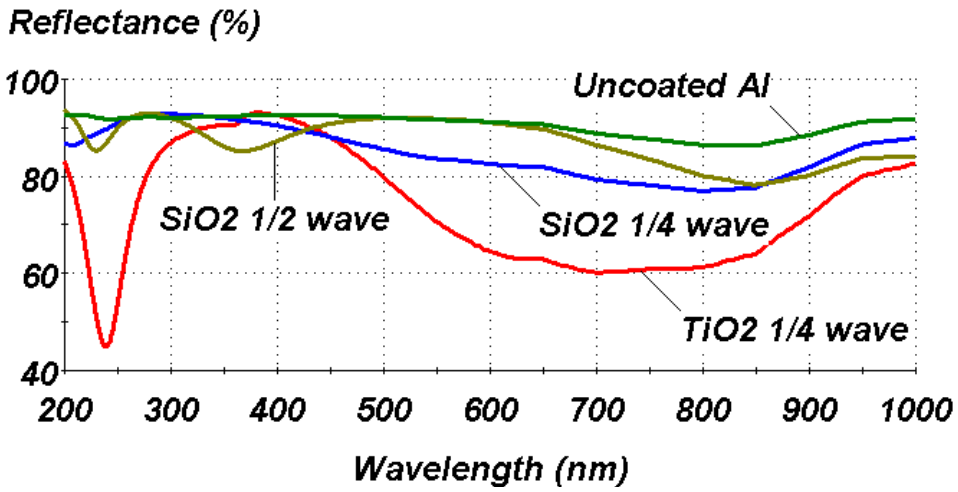

Figure 2.16 Various overcoats for an aluminum front-surface mirror. The halfwave of SiO_2 is the usual one. [13]

Quarterwave layers have maximum interference effect that can be expressed as a transformation of a surface admittance. A quarterwave of characteristic film admittance (y_f) transforms the admittance of a surface (Y) into a new value (y_f^2/Y) (Figure 2.17). This is known as the Quarterwave Rule and is probably the most useful concept in optical coating design [13].

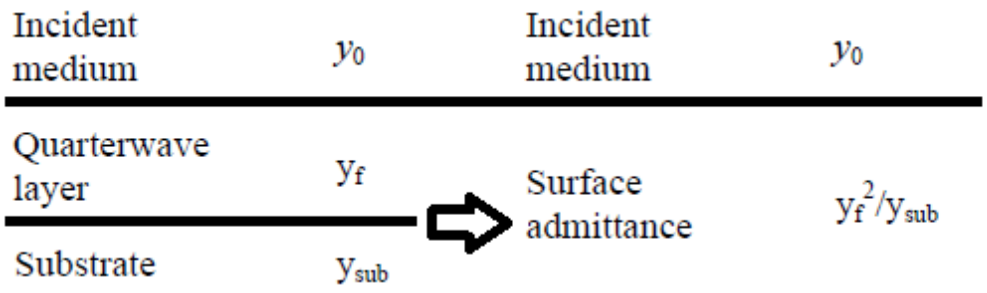

Figure 2.17 Transformation of optical admittance (Y) by thin film (Quarter Wave Optical Thick) on substrate [13]

Where y_{sub} and y_f mean admittances of substrate and film respectively. It is the optical admittance of a surface that tells us how easy or difficult for a light beam to pass through it. If we know the optical admittance we can calculate the reflectance.

$$R = [(y_0 - Y) / (y_0 + Y)]^2 \qquad \text{(Equation 2.11)}$$

where y_0 is the characteristic admittance of the incident medium and Y is the admittance of the surface. At optical frequencies it is possible to make use of a useful simplification. The admittance of free space is constant at 1/377 siemens. If it is possible to express optical admittance in units of the admittance of free space, then the characteristic admittance of a material is numerically equal to its refractive index.

The Quarterwave Rule shows us that reflectance can be reduced to zero if we have a thin film of quarterwave optical thick with characteristic admittance which is the square root of the product of incident admittance and substrate admittance. It is easy to show this by replacing Y with y_f^2/Y in Figure 2.17.

$$y_f = (y_0 * y_{sub})^{1/2} \qquad \text{(Equation 2.12)}$$

as the thickness of the film vary reflectance changes like an extended sinusoidal wave.

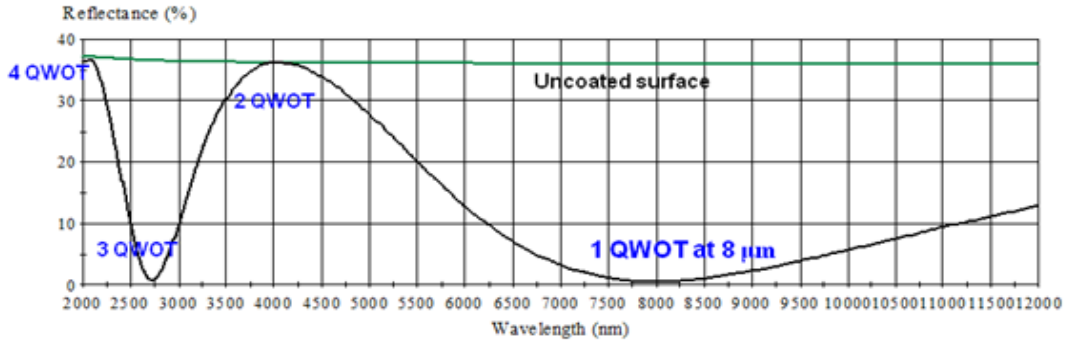

Figure 2.18 Graphical representation of reflectance vs thickness variation of a thin film. Maxima and minima occur at multiples of quarter wave optical thicknesses of the target wavelength [12]

For reflective coatings, metals tend to be used very often as substrates (Figure 2.19). For example chromium and rhodium are used for applications where environmental resistance is important, aluminum for general instrumentation, gold for the infrared region and silver when the ultimate reflectance in the visible and infrared regions is required [13].

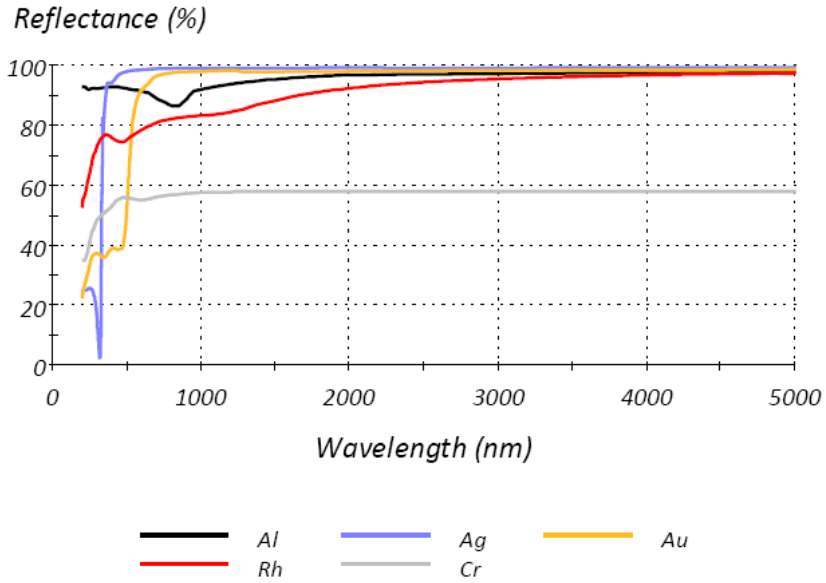

Figure 2.19 Front surface reflectance versus wavelength for a number of commonly used metals [13]

If the substrate is metal and it is not tough enough like rhodium or chromium, front-surface reflectors are generally protected from the environment by a single dielectric overcoating layer. Metals like aluminum are actually quite soft and easily damaged and a dielectric overcoat makes them much more rugged. The coating, as mentioned, has an interference effect on the reflectance of the metal. The dielectric layer, as long as its index is greater than that of the incident medium, always shows falling reflectance. High-index layers give enormous reductions in reflectance at their minima and are unsuitable in most applications. As a handicapped situation little can be done to maximize the reflectance in the near infrared region.

2.6 Tribo-Mechanical View

2.6.1 Wear Mechanisms

Although in most industrial applications, e.g. for plastic injection molding, and for various components like valves and cylinders, the main wear mechanism is related to the fluid-to-body interfaces, the great majority of the wear mechanisms identified is related to contact interfaces between solid bodies [21].

Naturally, the specific wear mechanism depends on the contact mode. Contact modes [22] for various body-to-body interactions can be due to:

- Purely sliding mode
- Purely rolling mode
- Mixed mode; a combination of rolling and sliding
- Purely impact mode
- Mixed impact and sliding mode

The most dominant wear mechanisms occurring in well-designed coating systems are:

- Abrasive wear
- Adhesive wear
- Fatigue wear
- Erosive wear

- Corrosive wear
- Impact wear

For improperly designed coating systems, one of the key wear mechanisms is related to the load carrying capacity. Overloading may result in cohesive failure, and thus delamination in the film, or adhesive failure due to flaking of the film from the substrates or components .

In Table 2.3 various contact modes and wear mechanisms are grouped for 2-body interactions [22].

Table 2.3 Dominant wear mechanisms for various contact modes [22]

	Abrasive wear	Adhesive wear	Fatigue wear
Sliding mode	x	x	
Rolling mode	x		x
Mixed mode	x	x	x
Impact mode			x
Impact + sliding	x		x

For majority of industrial applications, a combination of sliding and impact wear may occur, where the contact loads are as high as possible and very close to the yield point of the base materials. Consequently, the near surface regions of these materials need to be designed and optimized in such a way as to counteract abrasive, impact and fatigue wear by increasing the load-carrying capacity.

Various contact mechanisms are given in Table 2.4 Contact mechanisms for practical applications [22] which consist of contact modes given in Table 2.3

Table 2.4 Contact mechanisms for practical applications [22]

	Sliding	Rolling	Sliding + rolling	Impact	Impact + sliding
Roller bearing		x	x		
Plunger	x			x	
Sliding bearing	x				
Piston pin	x				
Valve				x	x
Tappet	x				x
Gear			x		x
Camshaft	x				x
Ejector pin	x				

2.6.2 Hardness and Friction

Hardness and friction is the core topic for surfaces especially of moving parts and/or surfaces those are subjected to harsh environmental conditions. Hence it is a matter of durability and/or efficiency.

In industry where liquid lubricants are either cannot be used or insufficient to overcome friction, solid lubricant coatings and super hard coatings are becoming prevalent [14]. There are two distinct classes of coatings: “soft coatings” (solid lubricants) which exhibit low friction coefficients and “hard coatings” which are generally good for wear resistance and hence can have long term durability. Generally soft metals, polymers and lamellar solids like graphite are among the soft coatings, on the other hand hard ceramics, nitrides, carbides, borides, oxides are among the hard coatings. In literature the threshold is 10 GPa and if the hardness is above 10 GPa the coating is accepted as hard; elsewhere if it has hardness below 10 GPa the coating is then accepted as soft. Similarly for friction coefficient, 0.3 is the limiting line between solid lubricants and anti-wear coatings [14]. Figure 2.20 is showing this separation clearly.

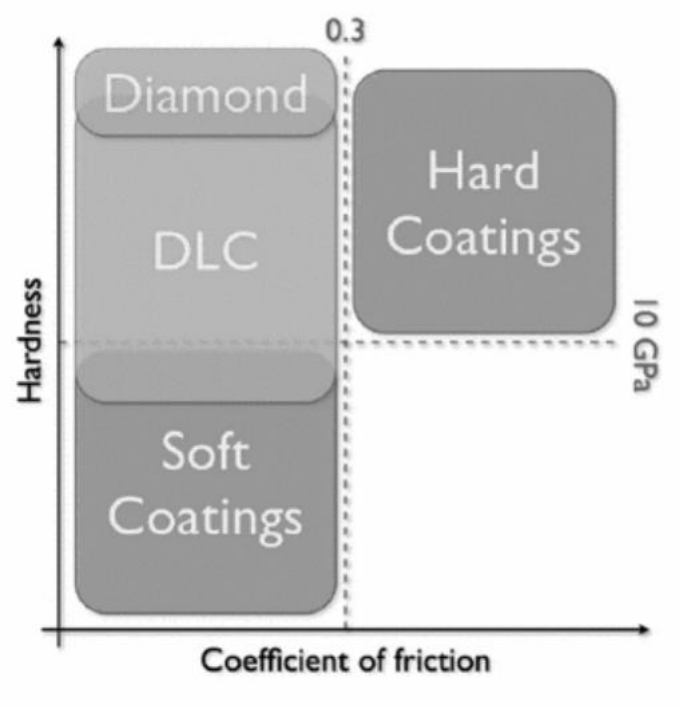

Figure 2.20 Classification of coatings with respect to hardness and coefficient of friction, highlighting the special case of carbon-based coatings [14]

Although it is very difficult to have high wear resistance and low friction values at the same time, there is an extraordinary solution: DLC coating. DLC coatings can afford both low coefficient of friction and low wear rates at the same time. Among other CVD films DLC can have highest hardness values (Table 2.5) and this plays an important role in the wear resistance.

Friction force between solid bodies is the result of three phenomena; namely abrasion, shearing and adhesion forces (Figure 2.21).

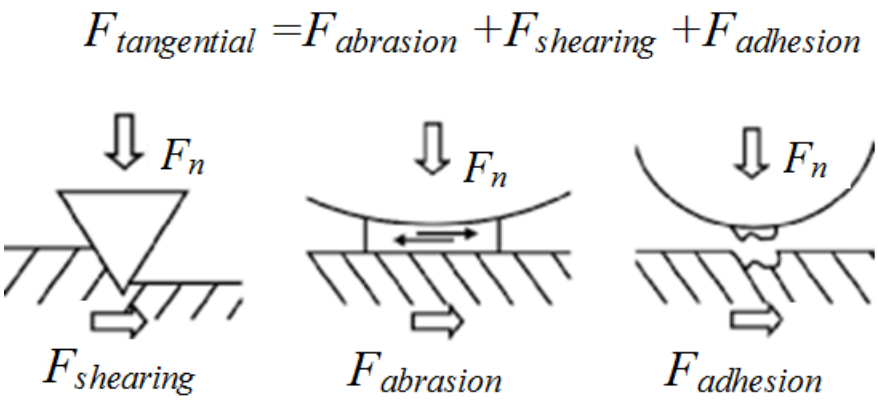

Figure 2.21 Schematic diagram of the three main fundamental contributions to friction (or tangential) force F_t with a normal force F_n [14]

Abrasive force arises from debris or asperities and seen if one body is harder than the other [23]. Shearing force results from plastic or viscous flow. Furthermore adhesive force can be due to electrostatic force, capillary force, polarization forces (van der Waals), and bonding forces (covalent, ionic, metallic, or hydrogen bonding) [14].

For a protective coating which designed to reduce wear, wear-volume (V) can be calculated using F_N (normal force), k (wear coefficient), H (hardness) and L (sliding distance) by Archard's law [14]:

$$V = (k/H)LF_N \qquad \text{(Equation 2.13)}$$

There wear coefficient (k) depends on mainly on the materials and wear regime.

Furthermore hardness (H) and elastic modulus (E) are fundamental parameters on the tribological behavior of the film. For a wear resistant hard coating; plastic work of indentation or in other words the ratio of hardness (H) to Young's modulus (E) namely H/E defines how the film strain tolerant is. High H/E ratios bring also high elastic

recovery rates. For example highest value achievable with heat-treated tool steel is about 0.04, ceramics like Al_2O_3, ZrO_2, Si_3N_4, SiC have values around 0.06, nitride-based coatings (TiN, CrN) have values around 0.08. However DLC films can have values as high as 0.2.

Table 2.5 Hardness (H), Young's modulus (E), and H/E ratio of the different families of DLC films (a = amorphous; ta = tetrahedral amorphous) [14]

	a-C	a-C:H	ta-C	ta-C:H
Hardness (GPa)	12-18	7-30	28-65	28-60
Elastic modulus (GPa)	160-190	60-210	210-650	175-290
H/E ratio	0.08	0.1-0.16	0.1-0.2	0.16-0.21

Moreover increasing hydrogen content has tendency to reduce both the hardness and Young's modulus, and yet also increases sp^3 fraction that improves these mechanical properties (H, E).

Actually a coating needs to be hard to avoid abrasive or adhesive wear, but it also need to be strain tolerant and though to prevent crack propagation and follow substrate deformations, especially when there are large differences in elastic modulus between the coatings and its substrates, this can be very limiting in some cases hence should be considered in designing the coating procedure.

2.6.3 Superlubricity

As a subtopic of tribology, superlubricity defines a sliding regime where there is no friction, even in sliding there is virtually no resistance. In other words there is no contribution to friction especially by adhesion. Friction is responsible for wear related material and energy loss. If superlubricity can be applied properly in industry, it can save almost 5% of GDP (gross national products) of most of the nations on the world [24].

One of the main pillars in superlubricity is atomic scale mismatch on sliding surfaces. Actually it is called as incommensurate where two sliding surfaces are ideally misaligned or misfit each other, then the frictional forces vanish during sliding. Actually this theory belongs to Hirano and Sokoloff and experimentally verified during 1990s [7]. Under superlubricity sliding conditions there is little or no direct registry or interactions between atoms of touching surfaces.

DLC coatings are promising candidate for superlubricity because of their extraordinary low coefficient of friction values. Moreover, since DLC have amorphous structure, surfaces which are coated with DLC are natural incommensurate.

Depending on the fractions of sp^3, sp^2 and H (as mentioned earlier, hydrogen will participate to DLC film either by sp^3 bonds with carbon or go into structure as interstitial as atoms or molecules) level of friction and superlubricity changes [25]. Hence it is possible to engineer versatile films to meet requirements.

Hydrogen bonding on the surface of DLC film has a positive effect on superlubricity. They can occupy σ-bonds in a way that leaving no dangling bonds on the surface. Since C-H bonds are covalent and it is even stronger than C-C bonds, it increases passivation level of the surface reducing adhesion. Furthermore interstitial hydrogen immersed in the film can serve as reservoir in case of any hydrogen or carbon atom lost on the surface, hence it keeps surface from any adhesive attack, and hence it can be called self passivative.

Superflow friction is defined that the threshold for superflow friction coefficient is 0.01 [7]. In other words when the coefficient of friction is less than 0.01, it is called as superflow friction. Furthermore between DLC coated surfaces there is an opportunity to enhance superflow friction thanks to electrical dipole created by C-H σ-bonds on the surface of DLC films. In the C-H bond, carbon atoms attract electrons and leaves hydrogen nucleus nearer to the surface. Hence creation of such a dipole configuration at sliding interface can give rise to repulsion rather than attraction between hydrogen terminated sliding surfaces of the DLC films (Figure 2.22).

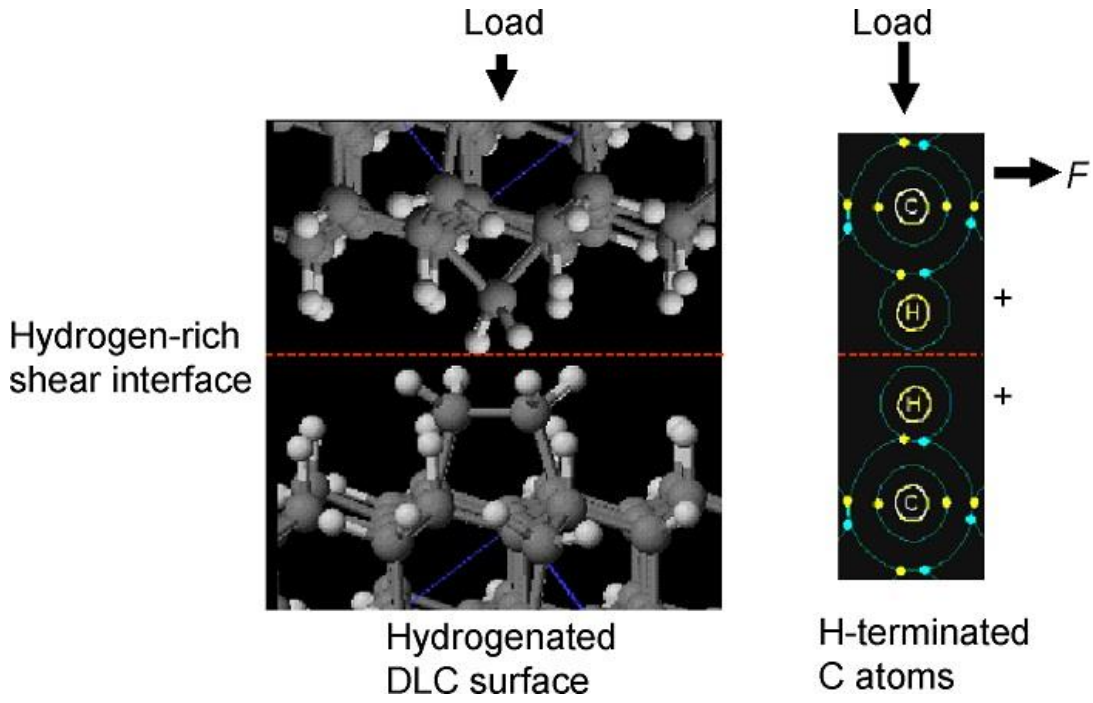

Figure 2.22 A model explaining hydrogenated surface superflow friction phenomena [7]

2.7 Coating Technique: (PE)CVD

CVD coatings are used extensively in applications requiring resistance to wear, often over a wide range of temperature. Actually, coatings and their substrates can be considered as composites which provide unique combinations of properties.

For most cases, achieving the best possible solution with a bare substrate/bulk material is very hard if it is not completely impossible. For example, the coating of a cutting tool such as a twist drill, the drill must be made of a tough and strong material, such as high speed-tool steel, that is able to withstand the stresses associated with drilling, at the same time its surface must be very hard and chemically resistant to withstand abrasion and corrosion. However, hardness and toughness are inverse properties and occasionally no single material can have both. A solution is to coat the steel body with a refractory metal carbide or nitride, or any other appropriate hard coating material

which protects the steel substrate from high temperature oxidation and reaction with the material to be cut and provide the necessary hardness and wear resistance.

2.7.1 General Information on Different Application Methods of CVD

Speaking generally, chemical vapor deposition (CVD) involves the formation of a thin solid film on a substrate material by a chemical reaction of vapor phase precursors [26]. It can be distinguished from the physical vapor deposition (PVD) processes like evaporation and reactive sputtering, which involve the adsorption of atomic or molecular species on the substrate in mostly physical way (physisorption). The chemical reactions of precursor species occur both in the gas phase and on the substrate. Reactions can be promoted or initiated by heat (thermal CVD), higher frequency radiation such as UV (photo-assisted CVD), and lower frequency radiation such as RF (radio frequency). No matter the specific sub method, the surface reaction occurs mostly under the category of chemisorption [27].

There are many different acronyms of different type of CVD techniques [27]. The most commonly used ones are given below.

MOCVD; metal-organic chemical vapor deposition which uses metal-organic precursors or it can be broaden to include the precursors containing metal-oxygen or metal-nitrogen bonds, and even metal-hydrides.

There are also MOCVD processes called as MOVPE: metal-organic vapor phase epitaxy, or OMVPE: organometallic vapor phase epitaxy, in all these methods single crystal (epitaxial) films are produced on single crystal substrates from metal-organic precursors [27].

Plasma-assisted or plasma-enhanced CVD (PECVD) is a technique in which electrical energy rather than thermal energy is used to initiate homogeneous reactions for the production of chemically active ions and radicals that can participate in heterogeneous reactions, which, in turn, lead to layer formation on the substrate. A major advantage of PECVD over thermal CVD processes is that deposition can occur at very low

temperatures, even close to ambient which allow temperature sensitive substrates to be used.

Another derivative of CVD process is atomic layer deposition (ALD) or atomic layer epitaxy (ALE). Sometimes it is also called as pulsed CVD or atomic layer chemical vapor deposition (ALCVD). In ALD, gaseous precursors are introduced sequentially to the substrate surface and the reactor is purged with an inert gas, or evacuated, between the precursor pulses. The chemical reactions leading to film deposition in ALD occur exclusively on the substrate at temperatures below the thermal decomposition temperature of the metal-containing precursor and gas-phase reactions are unimportant [27].

There are other derivatives of CVD, like chemical beam epitaxy (CBE) in which volatile metal-organic precursors and gaseous co-precursors are used. Another closely related technique of metal-organic molecular beam epitaxy (MOMBE) uses volatile metal-organic precursors and co-precursor vapor derived from the solid element. In both CBE and MOMBE the chemical reactions take place only on the substrate leading to single crystal films, so gas phase reactions play no significant role in the film growth.

These are some main types of CVD techniques. In this study DLC (diamond-like carbon) coating as a coating material is introduced. Although there may be different alternatives plasma-assisted or plasma-enhanced CVD (PECVD) technique in which electrical energy or electrical potential difference is used to generate plasma is one of the suitable techniques for DLC.

In a conventional CVD process, the steps are summarized as:

1- Evaporation and transportation of reagents (i.e. precursors) in the bulk gas flow region into the reactor;
2- Gas phase reactions of precursors in the reaction zone to produce reactive intermediates and gaseous by-products;
3- Mass transport of reactants to the substrate surface;
4- Adsorption of the reactants on the substrate surface;

5- Surface diffusion to growth sites, nucleation and surface chemical reactions leading to film formation;
6- Desorption and mass transfer of remaining fragments of the decomposition away from the reaction zone [27].

2.7.2 Comparison of CVD with Other Applied Techniques

Wear and corrosion protection can be provided by the well-established techniques of hard-facing and plating or by surface-modification processes such as boriding, nitriding, carburizing, and ion implantation. The protection these techniques afford is adequate in most environments but may fail over a period of time if the conditions are too severe.

Another useful and common technique is plasma spraying, which has the drawback of requiring thick deposits to ensure adequate protection. Often extensive grinding and polishing are needed. Other techniques, such as sputtering, provide excellent protection but are limited by their line of sight characteristics, such as line-of-sight deposition characteristic which makes the coating of deep holes and trenches difficult, low deposition rates, although the use of magnetron sputtering with multiple targets partially offsets this limitation.

CVD suffers these limitations to a lesser degree and, as a result, is being used increasingly in many industrial applications, particularly those operating in extreme conditions. It is often the best solution to severe problems of erosion friction, or hot corrosion. Moreover, CVD is one of the most conformal coating method in which coatings obey and match the surface morphology and complexities very well. Various CVD coated films are introduced in Table 2.6

Table 2.6 The properties of films (at 25°C) coated by CVD [4]

Material	Hardness kg/mm^2	Thermal conductivity W/cm.K	Coefficient of thermal expansion $m/m.°C\ 10^{-6}$	Notes/Comments
TiC	3200	0.17	7.6	high wear and abrasion resistance low friction
TiN	2100	0.33	9.5	high lubricity stable and inert
Ti(CN)	2500 - 3000	0.2 - 0.3	0.8	stable lubricant
Cr_7C_3	2250	0.11	10	resist oxidation to 900°C
SiC	2800	1.25	3.9	high conductivity shock resistance
TiB_2	3370	0.25	6.6	high hardness and wear resistance
Al_2O_3	1910	0.34	8.3	oxidation resistant high stability
DLC	3000 - 5000	2.0	9.0	high hardness high thermal conductivity

CHAPTER 3

EXPERIMENTAL PROCEDURE

For all experiments in the study, (a-DLC) amorphous Diamond-Like Carbon thin films were deposited on aluminum substrates. The composition is amorphous (mostly sp^3 and sp^2) and depends on the energy given to the chamber, precursor gases, temperature and hydrogen content. The coating chamber runs on Plasma Assisted Chemical Vapor Deposition (PECVD) technique. In this set up, the energy used to create plasma is attained by means of radio frequency (RF).

3.1 Coating System

In this research, a standard PECVD coating system was used in which DLC films can be deposited. It is mainly consisting of 3 main subsections: 1- Coating chamber, 2- Process gases, 3- RF generator and match box (Figure 3.1). The coating system used in the thesis is Leybold DLCcs (Figure 3.2).

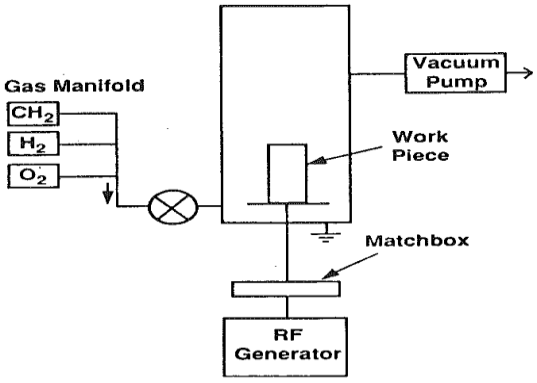

Figure 3.1 Schematic of the PECVD coating system

Figure 3.2 The PECVD coating system

3.1.1 Coating Chamber with Mechanical Subassemblies

Interior volume of the coating chamber is about 850 cm^3. There is a rotating circular plate (diameter: 521mm) at the bottom. The sample to be coated is placed on the plate 150 mm away from the center. The surface that is to be coated always should face up. The plate is rotating at a constant speed. There is no heating unit. However there is always circulating warm water at the periphery to keep the temperature constant

during the process. The only heat created is due to plasma generation and film deposition on the substrate. Temperature measurement is done via a thermocouple facing above the sample in the vacuum chamber. Furthermore, there is a vacuum line consisting of rough pumps (two pumps) and a turbo molecular pump directly connected to the chamber.

3.1.2 Process Gas Supplies

Plasma is created inside the chamber directly from the process gases. These are namely; Ar, H_2, C_2H_2. Argon plasma is used for pre-etching/cleaning purposes, the other gases hydrogen and acetylene are gases from which thin film is created. There are manifolds to control gas flow rates just before entering the chamber. All gases used in the experiments are extra pure, Ar: 99.999%, H_2: 99.9999%, C_2H_2: 99.5%. There is also O_2 used to plasma cleaning and purity of oxygen is 99.999%.

3.1.3 RF Generator and Match Box

One of the most critical units is the assembly of RF generator and respective match box. As an international standard this generator creates 13.56 mHz RF [28]. This is the internationally defined wavelength for most of the PECVD machines in the world and there is not any technical reason to choose this 13.56 mHz but the governmental regulations. The energy to create plasma inside the chamber is passing through a properly designed feedthrough. The second element in the assembly, matchbox, is used to balance the true frequency with respect to ongoing process conditions. All the equipment that needs to be cooled in the machine is cooled by circulating cold water.

3.2 Preparation and Initial Conditions

All the substrates are the same kind of bare aluminum. Although there were observed some impurity-like materials (e.g. Mg), they are accepted as measurement errors of SEM (Figure 3.3).

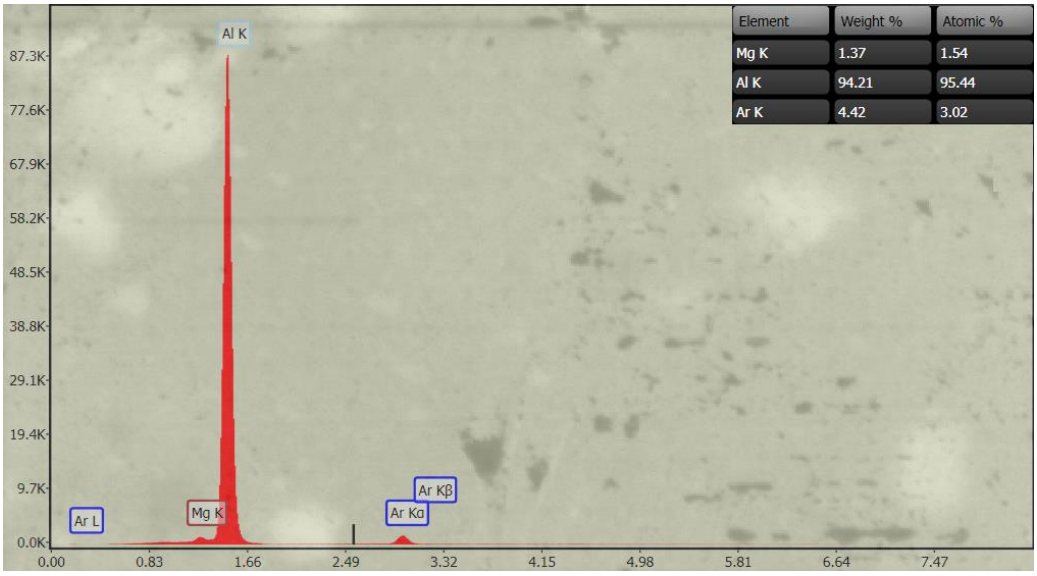

Figure 3.3 SEM (EDS) analysis of a bare (uncoated) aluminum substrate taken on polished side

Samples are cylindrical and have diameter of 25.4 mm (1”) and height (or thickness) of 1 mm (Figure 3.4).

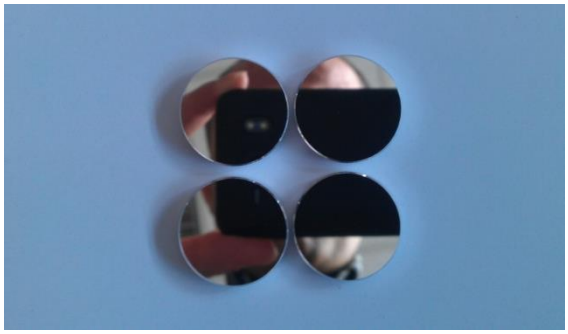

Figure 3.4 Aluminum substrates

Samples are masked (about 3-4 mm from a side to center) by a vacuum tape before coating. Hence after coating, measurements like thickness can be done by aid of this opening (uncoated region).

For each sample, one side is polished to optical grade. Furthermore, both surfaces are fairly flat and parallel. Surfaces of aluminum samples were scanned under a red (633 nm) light interferometer (Zygo) before coating. The aim is to see and analyze the effect of DLC coating on topology after coating.

Just before placing into the chamber all samples are cleaned with alcohol and dried with pressurized nitrogen (N_2). Since the bare aluminum surface is very soft and can be easily scratched, in any step, aluminum surface is not touched by any object including soft tissues.

3.3 Characterization Devices and Methods

At this point, it is better to mention about devices which were used and their related parameters.

3.3.1 Zygo (Redligth-633 nm) Interferometer

In Figure 3.5 schematic diagram which symbolizes the surface is geometrically execrated in order to show topography better. Although deviations from an ideal flat surface are on the order of a few hundred nanometers, it seems as if it has a bowl like noticeable geometry.

PV (Peak to valley): Difference between maximum (highest) and minimum (lowest) points on total surface.

Power: Deviation from pre-assumed theoretical radius. It is not a direct measure but a mean value symbolizing how much your surface deviate from pre-assumed surface geometry. Concave values are represented by [+] sign, while [-] denotes a convex surface.

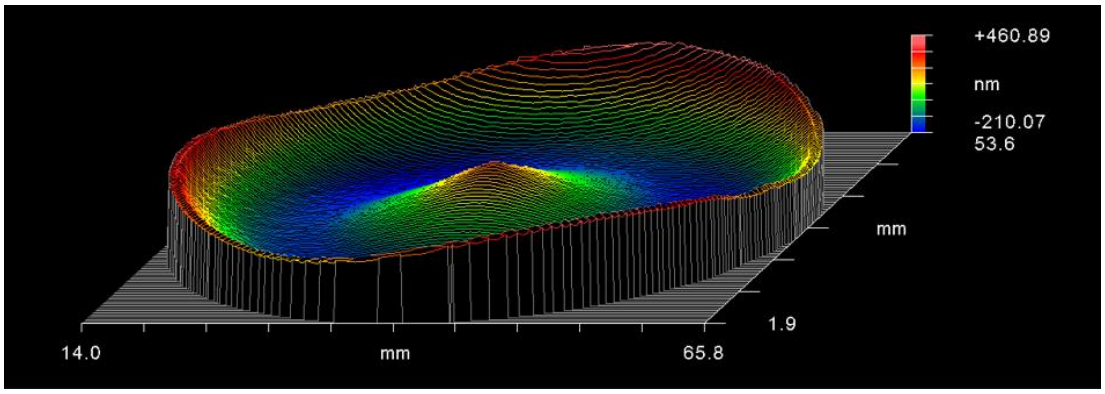

Figure 3.5 Sample surface measured by Zygo interferometer

3.3.2 Profilometer (Ambios^{TM} XP-200 Profilometer)

Prior to coating, vacuum tape is covered over a small area near any side. Hence only this small region stays uncoated and thickness measurement can be done using this difference.

3.3.3 FTIR Spectrometer (Perkin Elmer Frontier^{TM} Optica FT-IR Spectrometer)

All samples' reflectance measurements are done before and after coating in IR (Infrared) band. Analysis is done in the IR band of 8000-12000 nm and almost all uncoated-polished samples have about 98-99% reflectance. Reflectance of coated sample depends on the film thickness (i.e. multiple of λ/4). A sample measurement is shown in Figure 3.6.

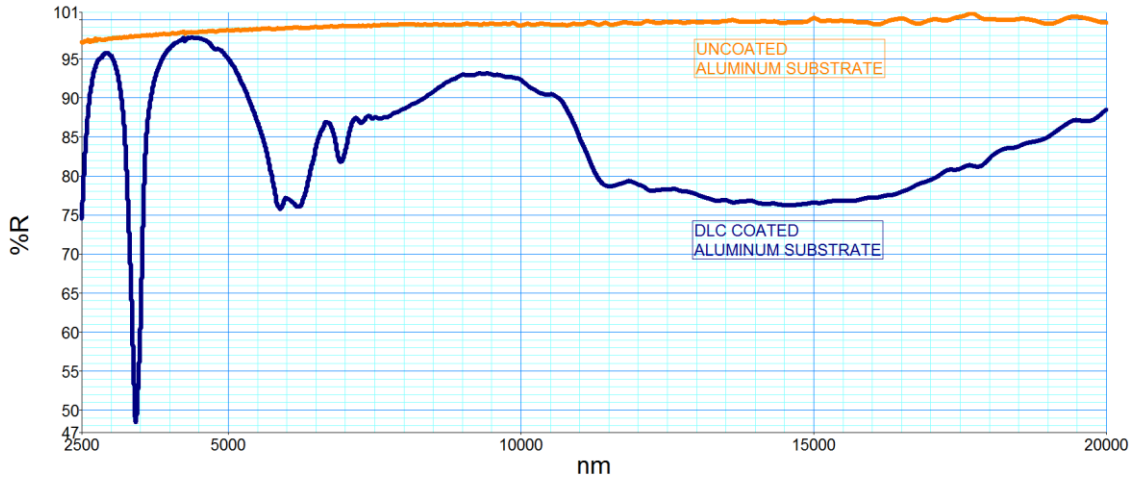

Figure 3.6 Typical FTIR reflection measurement results (uncoated [orange]-DLC coated [dark blue] aluminum sample)

3.3.4 Nano Indentation Measuring Machine (CSM Instruments)

Since DLC thin film is very brittle and it is virtually impossible to maintain the rigidity of the film and make indentation test without a substrate under it, it is hard to know characteristics like modulus of elasticity and hardness easily. Keeping this in mind, both hardness and elasticity of the system are measured by using a nano-indentor (CSM Instrument) with the substrate under the film. This testing machine can apply forces from 0.03 N to 20 N and can penetrate 180 micrometer. The indenter type is Vickers.

DLC is one of the hardest coatings; however the key word here is the thickness. Nevertheless substrate, aluminum, is a relatively soft material hence as the thickness increases hardness of the coated sample surface also increases. Measured hardness of the thin film is generally on the order of 13 GPa.

In literature aluminum has 69 GPa modulus of elasticity. Measurements show that aluminum substrate together DLC film on it has 84-92 GPa. Although it is expected that DLC should have extremely higher modulus of elasticity values, since the thin film and substrate were thought together in the study, all measurement were done

noting that there is a system consisting of a aluminum sample and DLC thin film on it rather than evaluating thin film alone.

3.3.5 Scratch Tester (CSM Instruments)

A scratch tester is used in order to measure friction coefficient and related tribological features. Properties or limits of the testing machine can listed as: the loading interval is between 30 mN – 25 N, maximum scratching force is 25 N, maximum scratch length is 12 mm, scratch speed can be varied from 0.4 to 500 mm/min and maximum depth is 1 mm.

In this study scratching length is 6 mm, frictional force reaches maximum 2.5 N and the normal force applied is increased from 0.05 N to 5 N linearly, the loading rate is 2.48 N/min [29]. The speed of the tip is 3 mm/min and it is constant. The maximum depth measured during the test is about 16 micrometers. [30]

3.3.6 X-ray Photoelectron Spectrometer (PHI 5000 Versa Probe)

X-ray Photoelectron Spectroscopy (XPS), also known as Electron Spectroscopy for chemical Analysis (ESCA) is a widely used technique to investigate the elemental and chemical composition (i.e. concentration of the elements and their chemical states) of surfaces based on the photoelectric effect [31].

Because the samples are exposed to air for days after the runs, in this study before the XPS tests, all DLC samples are first exposed to an argon plasma in order to get rid of possible oxidation on the surface. Then about on an area of 0.2 mm x 0.2 mm which is an arbitrary selected region on the sample surface, X-rays are exposed and data is gathered from this region.

The data extracted first is raw data and it should be processed to get meaningful results. In our case a sample's spectrum of raw output is given in Figure 3.7. Processed graph show sp^2, sp^3 and C-O rates in the film clearly as in Figure 3.8.

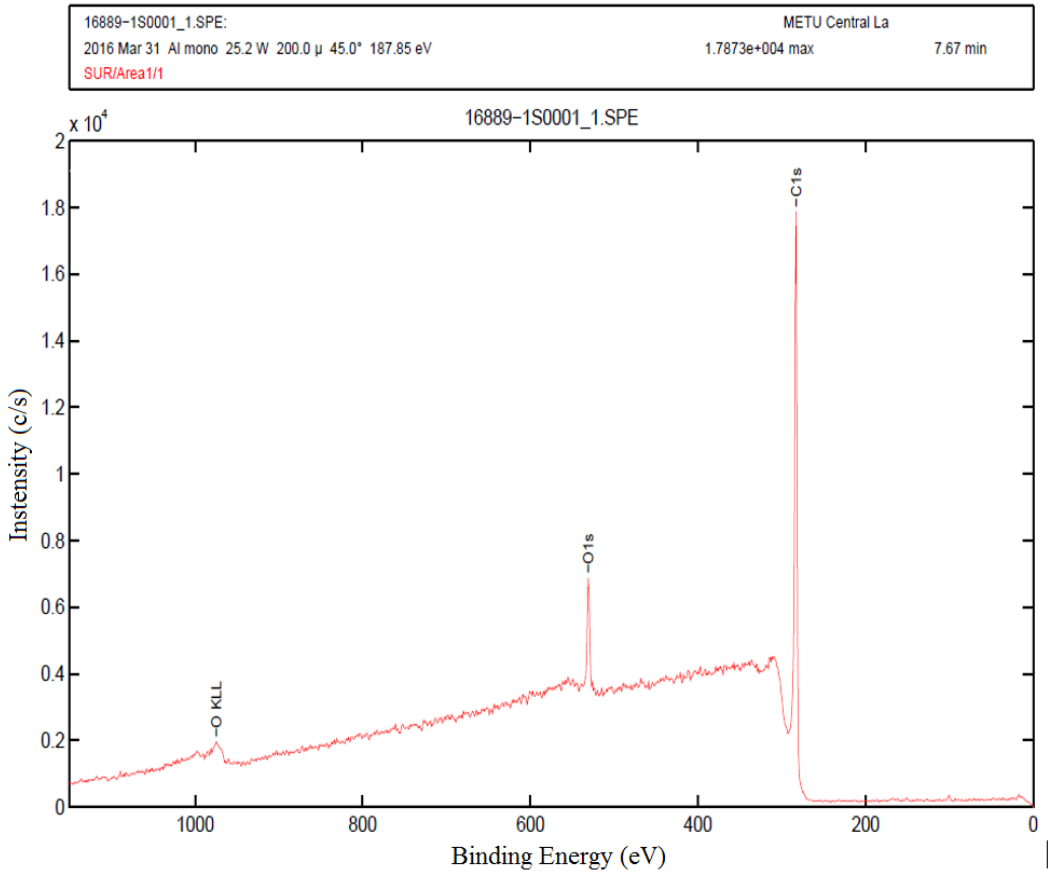

Figure 3.7 A sample spectrum of raw output measured in METU Central Lab by the XPS

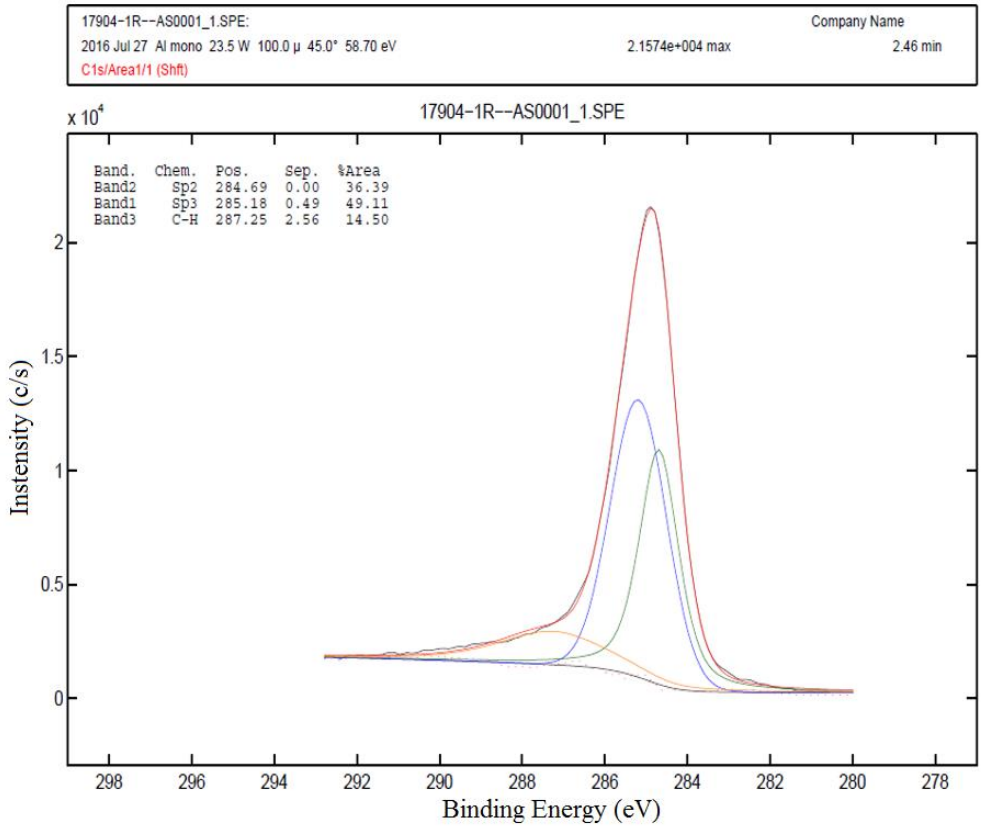

Figure 3.8 A sample XPS processed (de-convoluted) results with DLC on aluminum measured in METU Central Lab

3.3.7 XRD (Rigaku-Smartlab)

In XRD, analysis of the angular position and intensity of the diffracted x-ray beam gives information on the crystal structure. Since XRD detects certain structures in the material or film, there should be a structure in the sample, otherwise the XRD cannot detect any thing. In other words, if the material or film is amorphous, XRD cannot detect any structure and shows only the structure of substrate graphically if it has any. There is an internationally accepted standard called as Joint Committee on Powder Diffraction Standards (JCPDS) database, it is a database of standard XRD reference patterns for various materials. When one examines a material using X - ray diffraction, a XRD spectra is obtained. One then compares the spectra with respect to the JCPDS

reference pattern for the material and determines the crystal structure, indexes the various planes etc [32]. For pure aluminum the JCPDS number is 04-0787.

3.3.8 Humidity Test

For humidity test, a test chamber which can supply stable 95% relative humidity and temperature oscillates in a band of 20 - 60°C is used. In order to supply controllable test condition, the chamber should be tightly closed and isolated from the environment. The test lasts ten days without any interruption and composed of five times repeating two day long routines (5x2 days) as seen in Figure 3.9. [33].

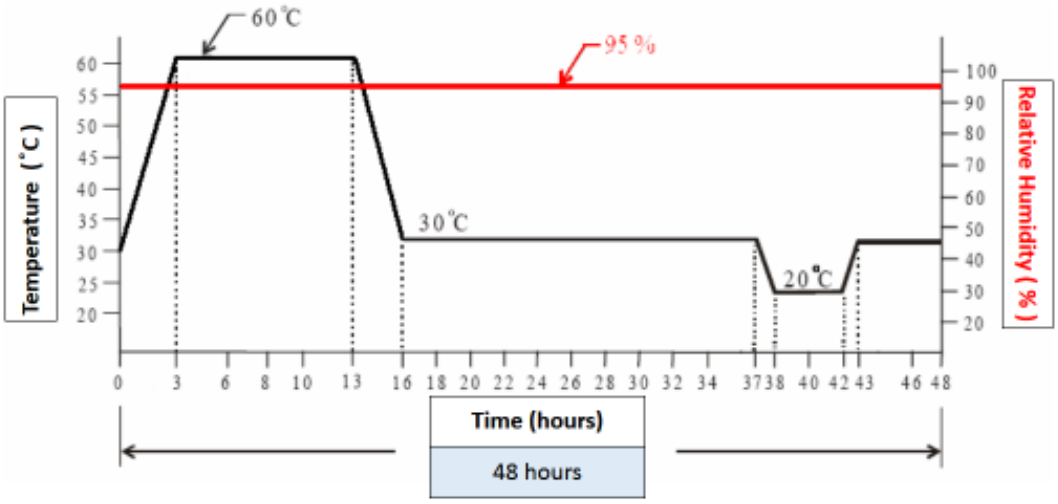

Figure 3.9 The 2 days humidity test routine applied in this study

3.3.9 Salt Fog Test

For salt fog, test chamber's temperature should be kept at 35°C and at relative humidity of 85%. The salt solution which is sprayed to create the fog should contain 5% NaCl in weight. pH value for the solution sprayed is to be 6.5 – 7.2. The test lasts five days without any interruption.

3.4 Coating Process Parameters and Strategy

Coating process is typically consisting of 4 distinct and continuous steps. A complete coating cycle is called as a run. For a standard run, coating table is rotating about 12 rev/min. These steps are given below.

3.4.1 Argon Plasma Step

This is the first step and aim of the step is to make pre-cleaning on surface which is facing up (to be coated). Besides cleaning, Argon plasma makes the tiny sharp entities smother. As a rule of thumb, sharp entities/edges always keen on creating weak coatings.

Argon plasma starts to be created when vacuum level reaches high vacuum (i.e. 1.5 x 10^{-5}mbar) and lasts a few hundred seconds. Gas feed rates (Argon) is just below 100 sccm (centimeter cube per minute) during the step. RF power is on the order of 500 W. Temperature starts to increase from 33-40°C and reaches about 100 -110°C during the step inside the chamber.

3.4.2 Crossing Step

This is the second step and the aim of this step is to make a smooth pass to the next coating step.

This step lasts 70 s. Argon flow rates gradually decreases to 0 sccm, meanwhile H_2 and C_2H_2 flowrates increases to target values at the end of step. RF power depends on the final flow rates if elsewhere set any other value. Speaking roughly, temperature starts to increase from about 100°C and can go higher during the step inside the chamber.

3.4.3 Coating Step

This is the third and the main step.

Step time can be changed and depends on the desired final film thickness. Argon flow rates set to 0 sccm, meanwhile H_2 and C_2H_2 flowrates increase and reach the target values to the end of step. RF power is absolutely depends on the gas flow rates. Temperature, after a while, is quite stable to the end.

3.4.4 Waiting Step

This is the last step in which gas feed stops, only vacuum is active. Temperature decreased slowly without any extra effort. The chamber opens when the temperature drops below 70°C.

As mentioned before process gases are H_2, C_2H_2 and Ar. Further in the study, flow rates of H_2 and C_2H_2 to be adjusted in order to get desired films.

Furthermore there is also plasma cleaning. This cleaning process creates and uses oxygen plasma, feed gas is O_2. Cleaning procedure repeats once or more (depends on coating thickness) after and for each run.

CHAPTER 4

RUNS, RESULTS and DISCUSSIONS

A run is a whole coating cycle which starts with the placement of the substrate on the coating table, continues with coating steps and ends with breaking the vacuum of the chamber. All coating parameters are adjusted to get desired optimum results on DLC coated aluminum samples, that is to say highest reflectivity (or in other words minimum loss in reflectance) with maximum durability. Hence coating time, precursor flow rates, RF power and/or bias voltages are engineered in a controlled manner to get the desired optimum results.

DLC films are the hardest films ever known which can only be compared with diamond. On the other hand aluminum is a soft material which can easily be corroded or oxidized also. Besides, aluminum is found in nature abundantly and comparatively cheap. Furthermore, it is among the lightest metals and this makes it a promising candidate for many different applications from industry to space applications. Hence, as protective layers, DLC films have high potentials if it is collaborated with aluminum.

The aim of this research is to find out optimum practical conditions in a PECVD run in order to synthesize hydrogenated amorphous diamond-like carbon films on aluminum substrates with optimum optical, mechanical and tribological properties. The study is mainly composed of three stages. First stage is to decide on the thickness. Since surface of aluminum is soft and vulnerable to environmental effects, the film

should be thick enough. Furthermore maximum reflectance should be obtained and thickness is the parameter to define the reflectance of the surface according to quarter-wave rule. On the other hand, stress level in the film is another defining factor to survive as a rigid body on the substrate, hence film thickness cannot go beyond critical levels.

In the second stage, the effects of hydrogen content in the film are explored. Hydrogen content determines lots of properties of the film including the structure (sp^3/sp^3 ratio), intrinsic stress level, durability and optical properties. The basic and simple method is to change the precursor gas flow rates (H_2/C_2H_2).

After choosing optimum thickness and hydrogen content, the last and third stage focuses on the RF power. RF power is the defining factor for atomic bonding types and structure. Moreover, intrinsic stress level is highly depended on RF power.

4.1 Runs (Coating Cycles)

As mentioned in section 3.4 there are four main steps in a run. These are namely 1- Argon plasma step, 2- Crossing step, 3- Coating step and 4- Waiting step. Apart from 3rd step, in all steps all parameters are kept as they are just at first run. On the other hand, in 3rd step (coating step) critical parameters are re-setted before the run to find out the optimum process conditions.

In total, 37 runs are done and critical initial parameters and some results are listed in Appendices.

4.2 Phase 1: Deciding on Thickness

In this phase mechanical, tribological and optical effects of thickness variations are explored in order to decide true thickness or the true working range of thickness for the next studies.

4.2.1 Thickness and Coating Time

For the first run, flow rates of precursor gases are set to 150 cm^3/s for H_2 and C_2H_2 is kept constant, 700 V of bias voltage is selected to create and control RF power. Coating time of the coating step is selected as 1800 s.

As the part of the strategy, first trials are done based on varying coating time. Hence a series of coating runs were conducted with different coating time values keeping all other parameters constant. Increasing coating time also increases thickness, this is the first presumption. Following 17 successive runs showed that as the coating time (the coating step time) increases, the thickness of the film also increases and the correlation between them is almost linear as shown in Figure 4.1.

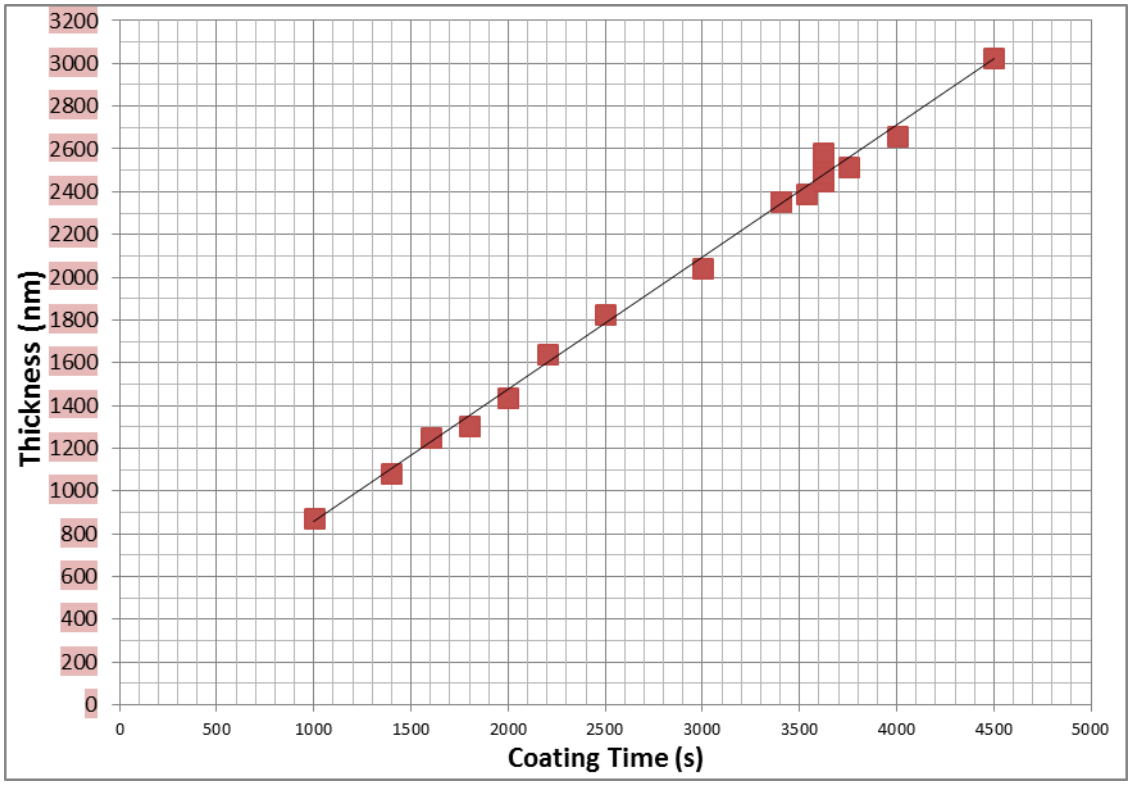

Figure 4.1 Thickness variations vs. coating time for constant precursor gases rates of H_2: 150cm^3/s and C_2H_2: "constant" cm^3/s

4.2.2 Interferometer Measurements: Surface Topography

As mentioned in Chapter 3, interferometer is used in order to reveal surface topography both before and after coatings. Hence it is possible to see and explore the effects of coating on surface topography of the aluminum samples.

First of all the general shape of the aluminum surfaces are preserved, that means a few micron thick coatings can never add an extra shape or change morphology drastically. On the other hand depending on the thickness of the film coated, concaveness or convexness of the surfaces or optical power of the surfaces can change. Actually as the film thickness increases the optical power of surface of the film decreases for our cases (please remember that compressive stress creates negative power values). Namely, power differences (ΔP) between the uncoated and coated surfaces are getting higher as the thicknesses increase. Figure 4.2 and Figure 4.3 show the change in topography of the surfaces, as it can be easily seen degree of concaveness is decreasing after the coatings, in other words surface goes convex side more. Furthermore Figure 4.4 shows in a broadened view that DLC films have a tendency to make the surface more convex, those are all because of the intrinsic compressive stresses developed in the film.

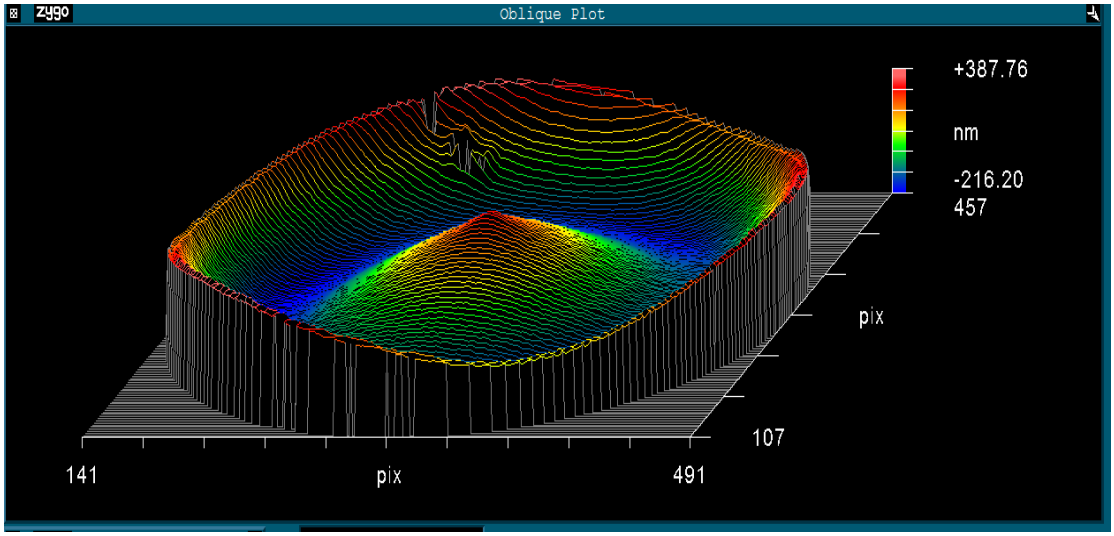

2583 nm DLC coated

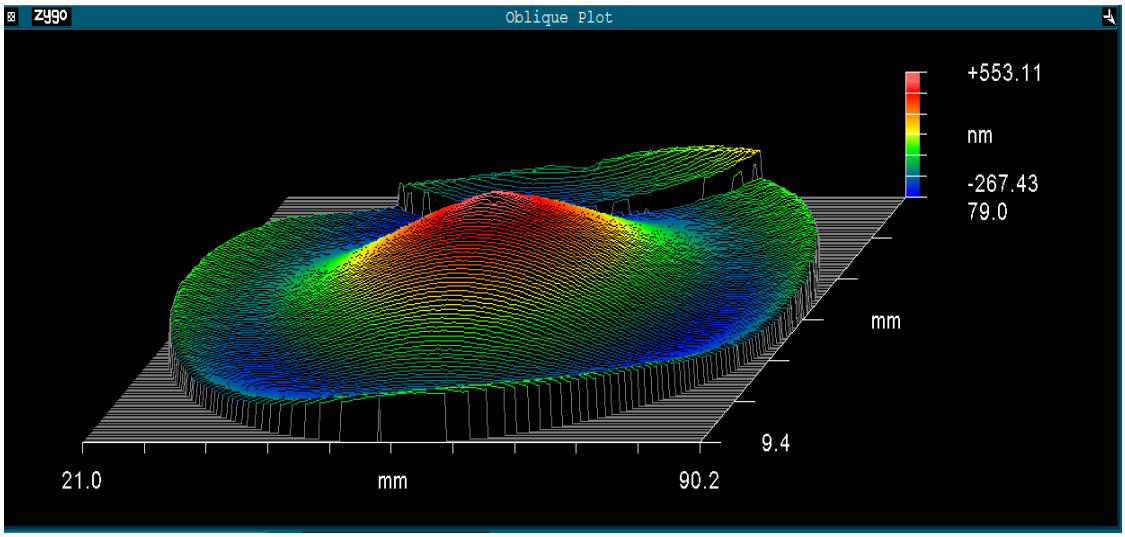

Figure 4.2 Surface of aluminum sample 12 measured before and after coating by Zygo red light (600 nm) interferometer

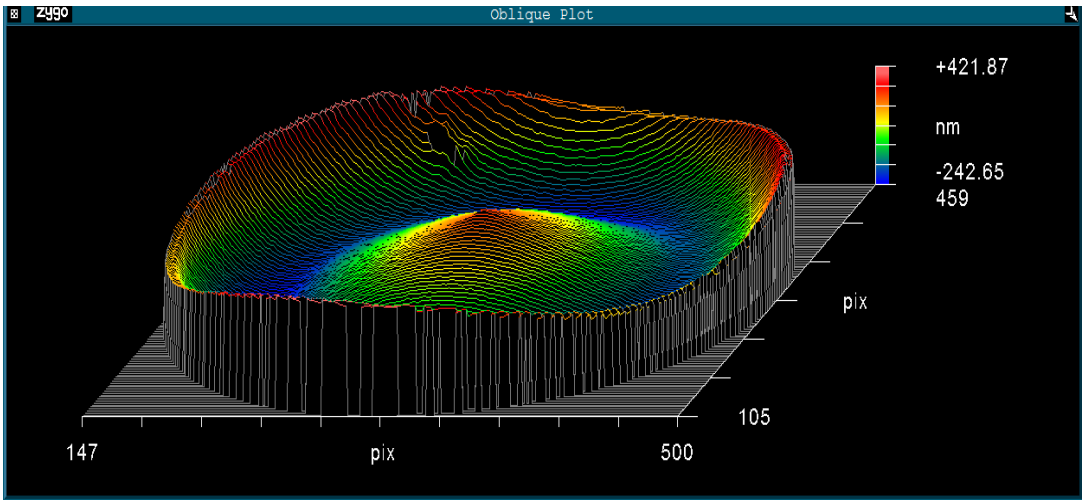

2515 nm DLC coated

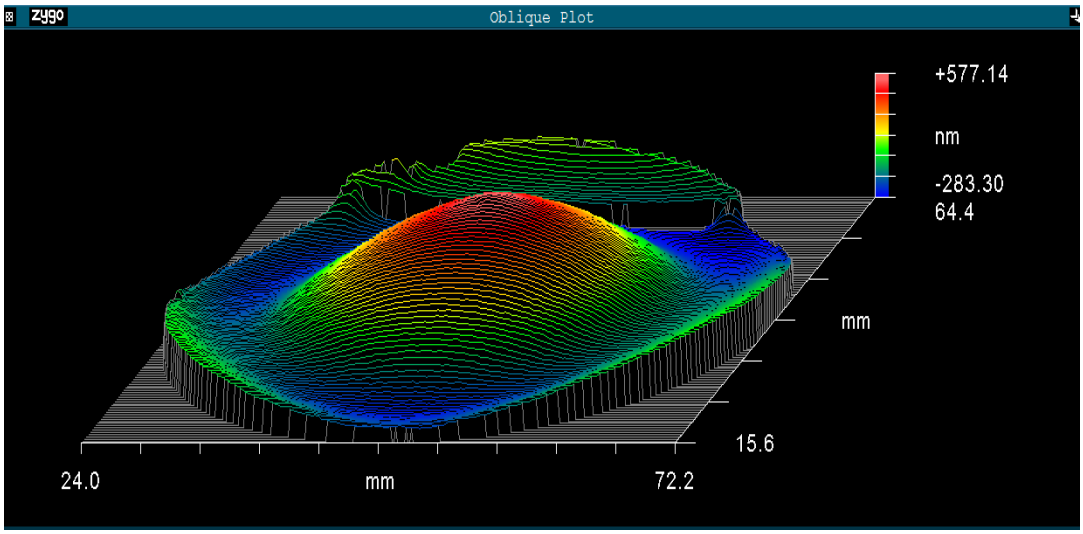

Figure 4.3 Surface of aluminum sample 15 measured before and after coating by Zygo red light (600 nm) interferometer

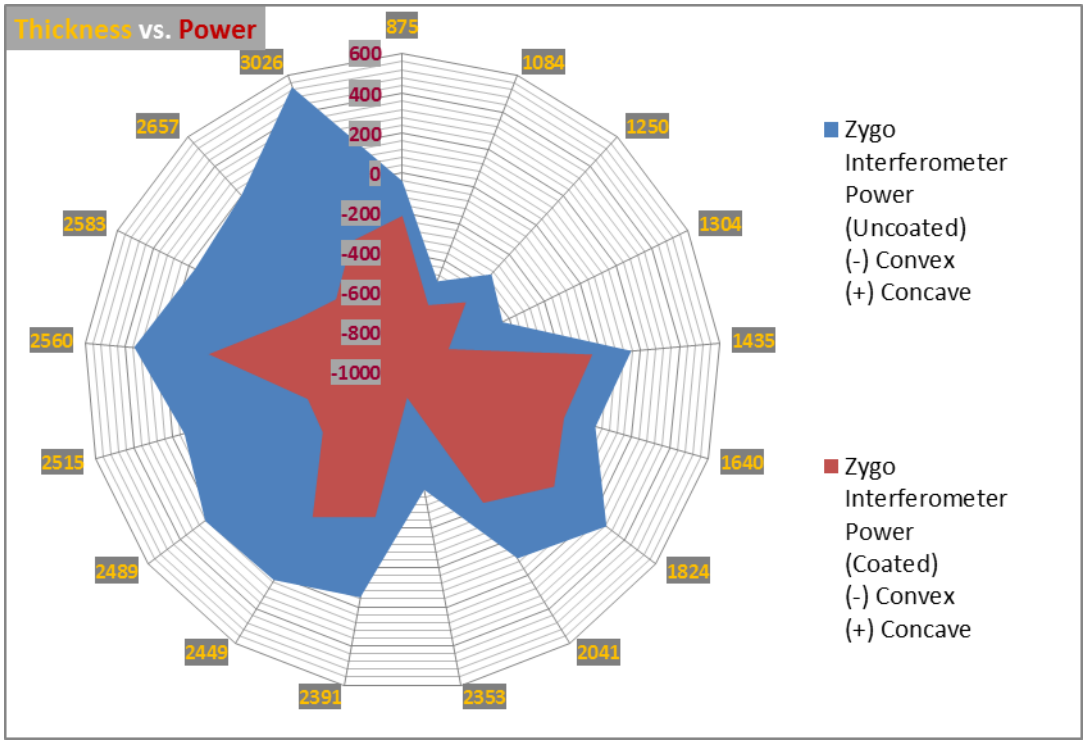

Figure 4.4 Power vs. thickness variations measured by a Zygo red light (600 nm) interferometer

Another result is that the gradual increase of convexness can be seen as the film thickness increases. As it can be tracked in the Figure 4.5, power values slide into negative side more as the thickness of the film increases. For example, the power difference (P_{coated} - $P_{uncoated}$) for the first sample, which is 875 nm thick, ΔP: -175, while ΔP: -831 for the thickest sample, which has thickness of 3026 nm.

It is expected that there is a limit for the thickness, beyond this limit the film cannot conserve its rigidity because excessive intrinsic compressive stress overcomes the adhesive stress (please refer to section 2.4). As the film thickness exceeds a few micron, the probability of delamination increases [[5] and [34]]. On the other hand there are other parameters like impurities, characteristics of substrate, coating method and hydrogen content which affect endurance of film. Hence in our case, as our experiments show (in Figure 4.5), the sample which is 3026 nm thick is failed after a little time passed and there is no reason but violation of the upper limit of thickness.

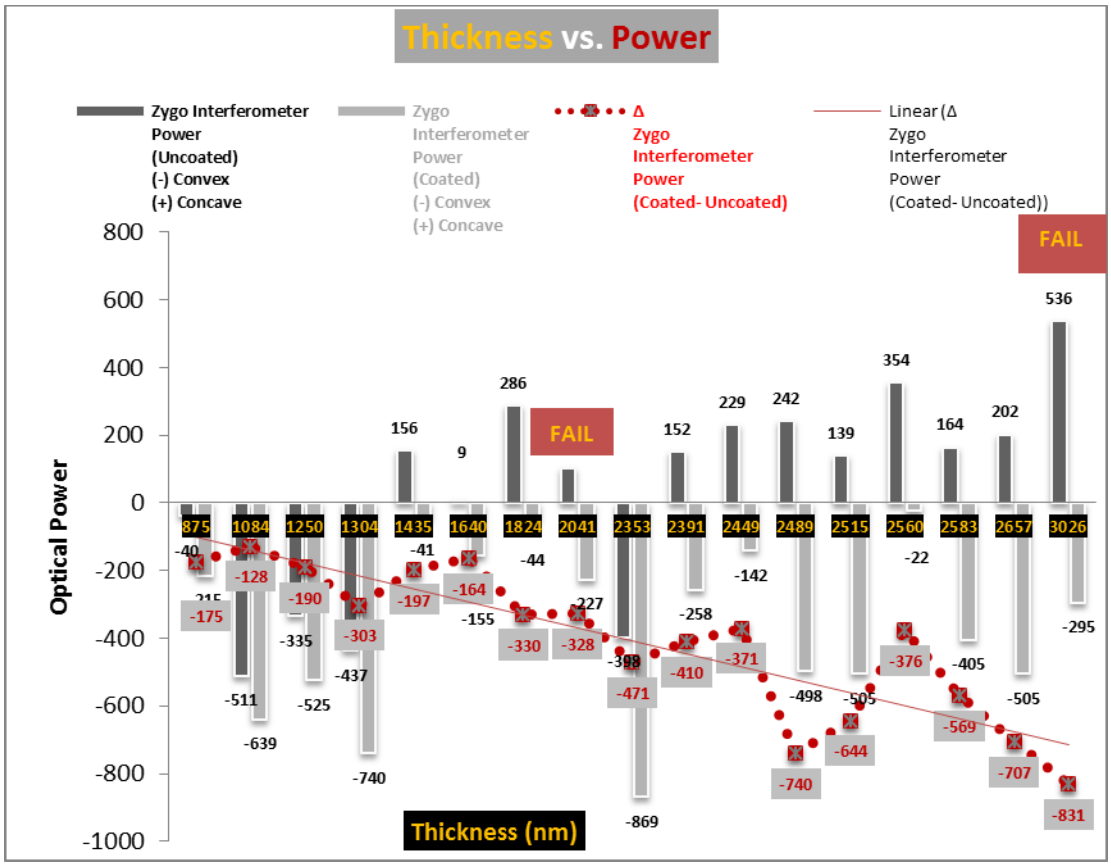

Figure 4.5 Power vs. thickness variations measured by a Zygo red light (600 nm) interferometer

4.2.3 FTIR Measurements: Reflection

If one of the crucial parameters to decide on the thickness is durability or ability to withstand without delamination, the other decisive factor is the reflectance. As mentioned in Chapter 2, the maximum reflectance can be obtained with a thickness of half wavelength optical thickness of target wavelength. In our case 8 000 - 12 000 nanometers in IR region is the range to maximize the reflectance; hence the middle value, namely 10 000 nm is going to be the target wavelength. At this wavelength mean refractive index can be accepted as 1.931 [35]. It is expected that at half wavelength optical thickness (nd/λ_0), namely at 2500 nm, reflectance should be

maximum. A software (Essential Mcleod®) used to calculate optical performance of a design also shows the nearly same route (Figure 4.6).

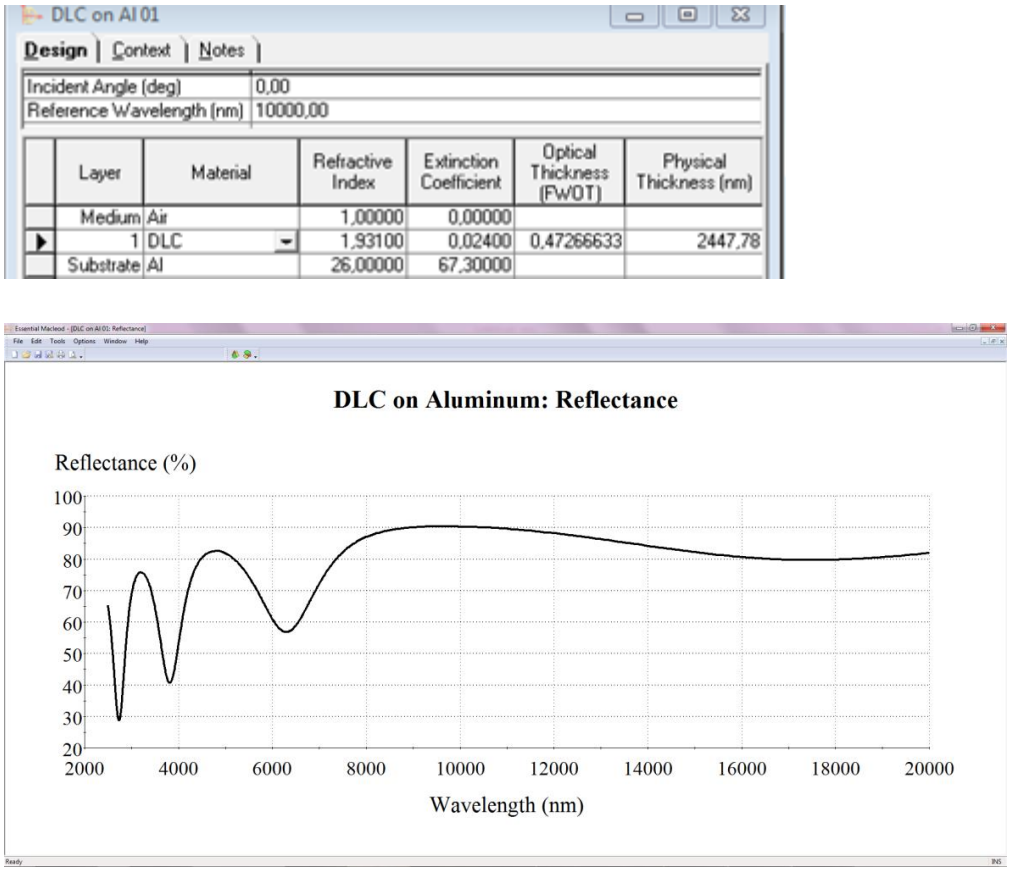

Figure 4.6 Software (Essential Mcleod®) design forecast for 10 000 nm target wavelength for a single layer of DLC film on aluminum

The measurements prove that for the coated thin films with near 2500 nm thicknesses, the reflectance values veritably at maximum (Figure 4.8). The real coated thin films' reflectance measurement of sample 12, sample 13 and sample 18 are shown in Figure 4.7. Common property of these samples is that they are all coated with the same process coating time of 3620 s. Thickness variations are due to unpredictable process deviations, but these cannot create noticeable differences.

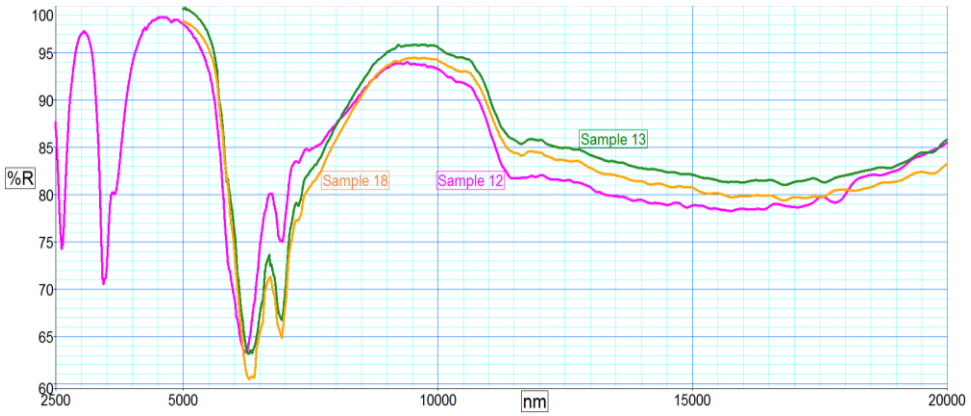

Figure 4.7 FTIR reflectance measurements of aluminum samples (sample 13, 18, 12 coating times are the same for all: 3620 s) coated thicknesses vary between 2263 – 2583 nm

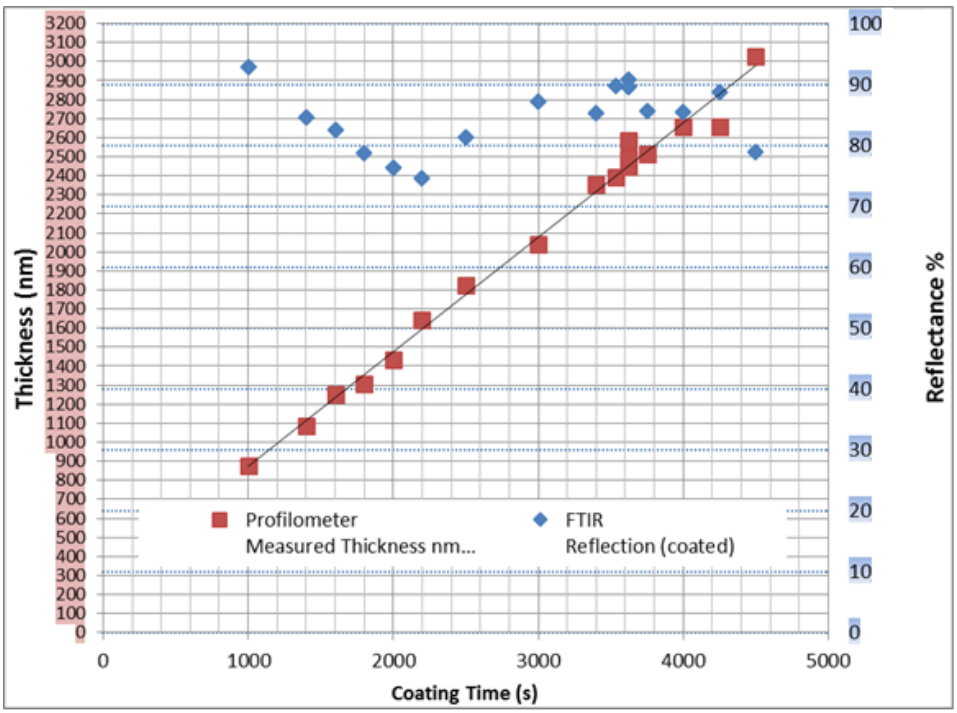

Figure 4.8 Thickness vs. Reflectance (average) with changing coating time (from 1000 s to 4500 s)

Although Figure 4.7 shows that measured values of reflectance fits the calculated design, please note that the peaks do not exactly occur at the target wavelength. It should be kept in mind that it is not the prime importance where the peak value occurs; but rather, the mean reflectance value constitutes the core consideration. Hence as the measurements suggest (Figure 4.8) maximum mean reflectance at the band of 8000 – 12000 nm can be obtained at about 2500 nm film thickness, remember that it was 2444 nm in the design.

As it can be traced from Figure 4.8, maximum reflectance can be obtained at about 850 nm and at about 2600 nm (as the quarter wave rule suggests). However there is another problem about thickness, if it is too thin (<1000 nm) the film becomes too soft. Namely the softness is inherited from aluminum substrate, please see section 4.2.4. Hence for the maximum reflectance, about 2600 nm thick film is the decided thickness and corresponding coating time for this thickness is about 3620 s for our process.

4.2.4 Hardness and Elasticity

Hardness (H) is another parameter to decide on the film thickness. All the runs in this phase are done by keeping flow rates of precursor gas constants as it is and also RF power is also kept in a band by fixing the bias voltage to V = 700 V throughout the coating step. Please keep in mind that the only changing parameter is the coating time and resultantly film thickness. There are 6 samples having different film thicknesses which go under test by a nano-indenter in order to measure the hardness.

Furthermore elasticity (E) of the films is also measured. As mentioned in literature survey section of this study (section 2.6) hardness (H) and elastic modulus (E) are fundamental parameters for the tribological behavior of the film. For a wear resistant hard coating, plastic work of indentation or in other words the ratio of hardness (H) to Young's modulus (E) namely H/E defines how the film is strain tolerant. High H/E ratios bring also high elastic recovery rates. Hence high H/E rates make the film more robust and increases the durability of it. In Table 4.2 and Figure 4.9 nano-indentation test results including H/E rates are listed.

Table 4.2 Tabulated values of hardness (H) and elasticity (E) values measured by nano-indenter of the 6 samples

Al Sample No	Coating Time (s)	Thickness (nm)	Hardness - HIT (GPa)	Elasticity - EIT (GPa)	H / E Rates
5	1000	875	10,5	83,6	0,13
2	1600	1250	12,7	90,1	0,14
8	2500	1824	14,1	91,9	0,15
11	3536	2391	13,4	89,2	0,15
15	3750	2515	13,4	88,2	0,15
17	4000	2657	13	90,3	0,14

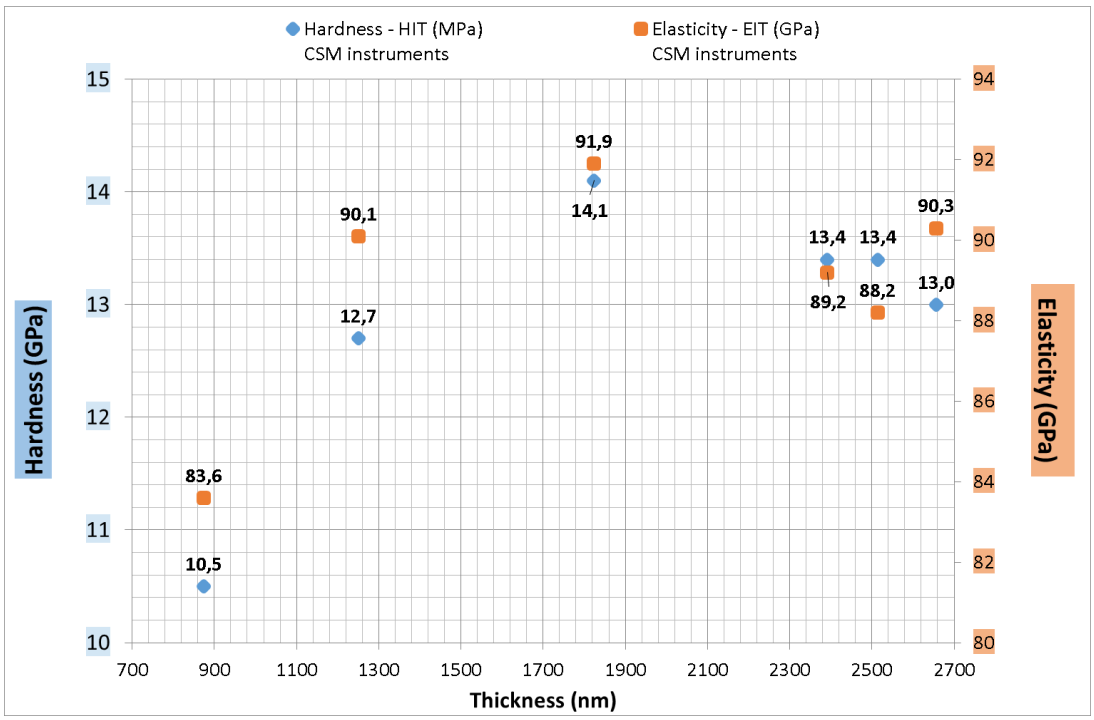

Figure 4.9 Hardness (H) and elasticity (E) values measured by nano-indenter of the six samples

As it can easily be seen from the results, H/E ratios and hardness values are not good for the films thinner than 1500 nm. This is an expected result because below a value of thickness, substrate (aluminum) surface gets into play and the "total" surface is going to be softer. On the other hand, the ratio H/E cannot be increased beyond a point; this point captured in this study is about 2500 nm.

As mentioned earlier in literature survey, the threshold for a hard coating is 10 GPa and if the hardness is above 10 GPa the coating is accepted as hard. These results also showed that the hydrogenated amorphous DLC films that are constructed in this study have 10-14 GPa hardness (as expected in the literature Table 2.5) and this can exceed this threshold (10 GPa) to be accepted as "hard". Also the measured elastic modulus of the samples are in the range of 84 – 92 GPa, this also suits the literature expectations for hydrogenated amorphous DLC films (60-210 GPa, Table 2.5). Furthermore, the measured H/E rates of samples are between 0.13 - 0.15 which falls again in the class of hydrogenated amorphous DLC films those have a range of 0.1 – 0.16 as defined in the literature (Table 2.5).

Although there is a good match between what is expected according to literature and the results obtained in the current study, the mismatch in elastic modulus needs to be improved.

4.2.5 Frictional Analyses

In addition to hardness, friction and friction coefficient are the core subjects in tribology [36]. Three samples, namely sample 5, sample 7, sample 18 are selected whose thicknesses are 875 nm, 1640 nm and 2489 nm respectively. The scratching tip touch first point on the surface and travel a linear route with a linearly increasing load and leave the surface after 6 mm as mentioned in section 3.3.5. All the tests are done under normal room conditions. Penetration depth, residual depth and acoustic emission are recorded and analyzed. Hence system gives frictional forces and resultantly friction coefficients are calculated.

4.2.5.1.Frictional Analyses for Sample 5

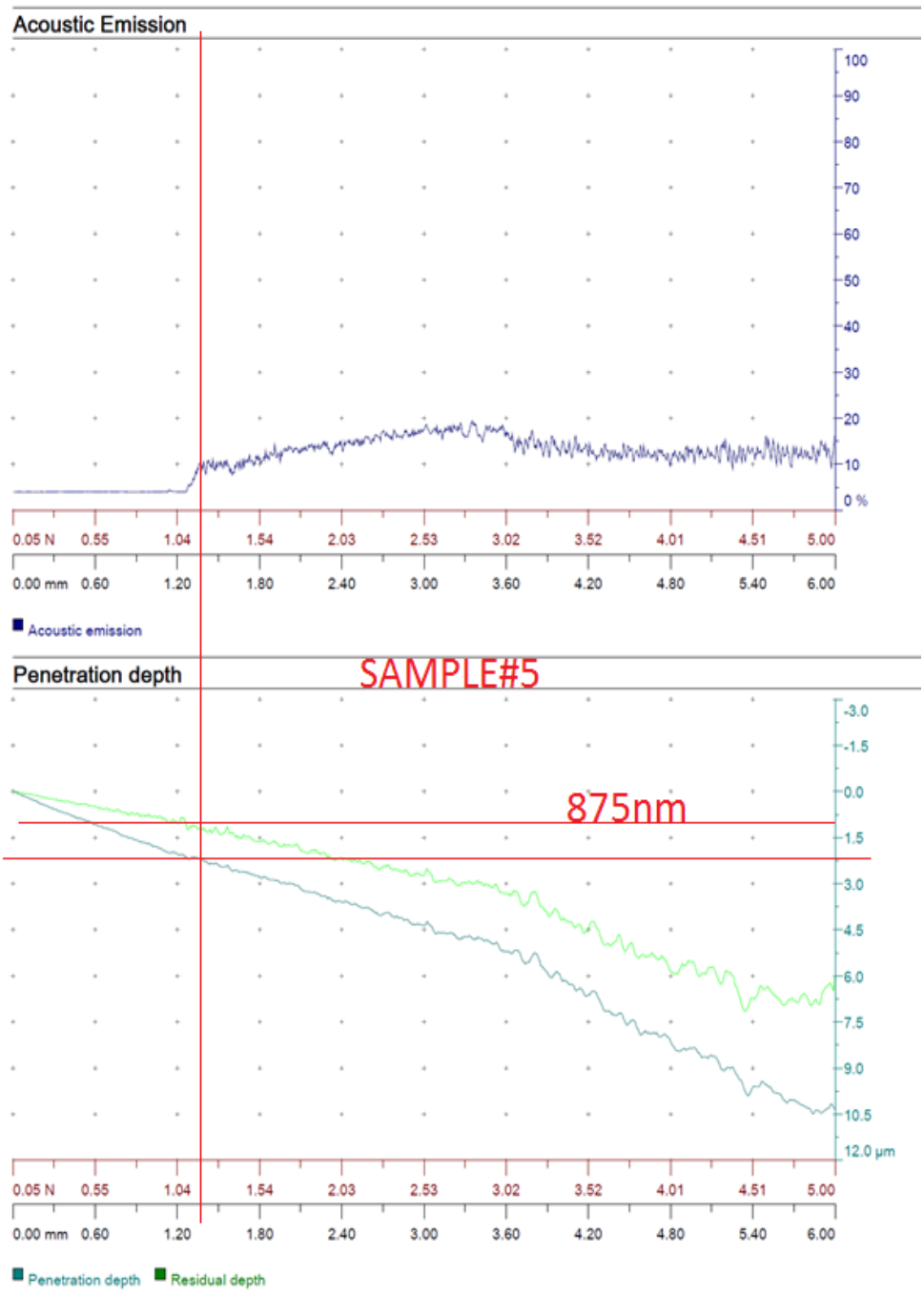

Figure 4.10 Change of acoustic emission and penetration depth vs normal load and scratch length (Sample 5)

Sample 5 has 875 nm DLC film thickness. Penetration depth (Figure 4.10) reaches 875 nm at about 0.60 mm from the point of first touch. On the other hand residual depth of 875 nm registered at 1.30 mm, and to reach this residual depth, the tip must penetrate about 2 microns which is then so called as the penetration depth. Although 2 micron is much greater than the film thickness, at the corresponding travel distance (1.3 mm), the film keeps its integrity as it can be seen below (Figure 4.11). This also means that when the film is indented, both film and substrate yawn or deflect together. Furthermore at this point (Penetration depth – Residual depth) / Film thickness ratio is about 1.29. This is the ratio that can be accepted as the restoration power of the film together with the substrate, and it is going to be calculated each time as a reference for the rest of the measured samples. As far as film does not delaminate, this ratio can give fairly meaningful and valuable information. The term and definition of "restoration power" is unique to this thesis and used very first time here.

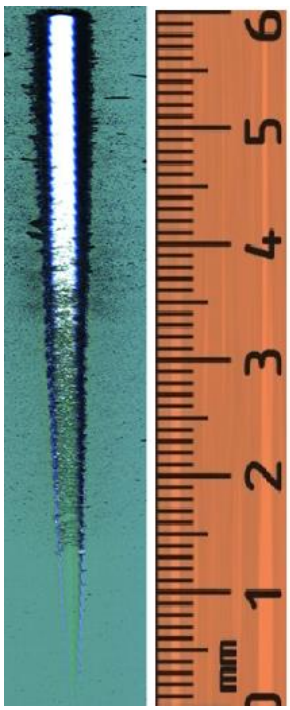

Figure 4.11 Scratch print after the scratch test for sample 5

Figure 4.11 shows that film starts to lose its integrity at about 1.4 mm, after this point aluminum substrate is starting to be seen as very small white circles on Figure 4.11. Hence location just before this point can be accepted as optimum point where friction coefficient of the DLC film can be measured and defined. Then friction coefficient of the film is 0.18 at 1.4 mm from the point of start (Figure 4.12).

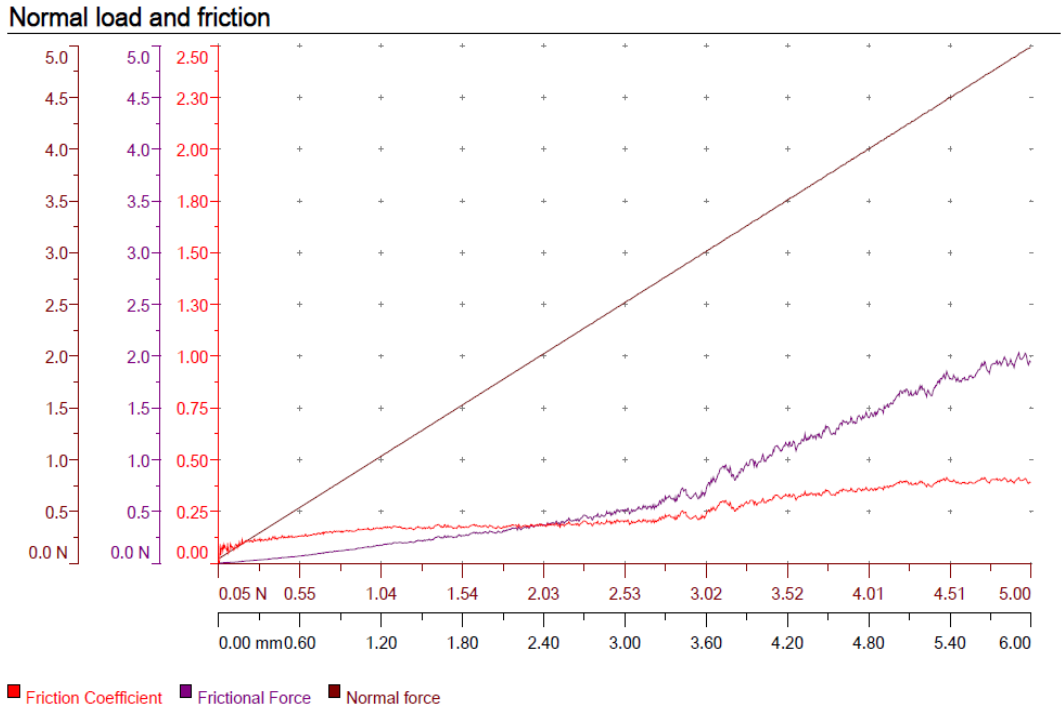

Figure 4.12 Normal load and scratch length vs friction coefficient/frictional force/normal force (Sample 5)

After this point friction coefficient increase and does not represent only the film because bare aluminum surface is taking into the place. Furthermore, after about 3.7 mm (Figure 4.11) film goes almost total destruction and it not possible to talk about a film after this point.

4.2.5.2. Frictional Analyses for Sample 7

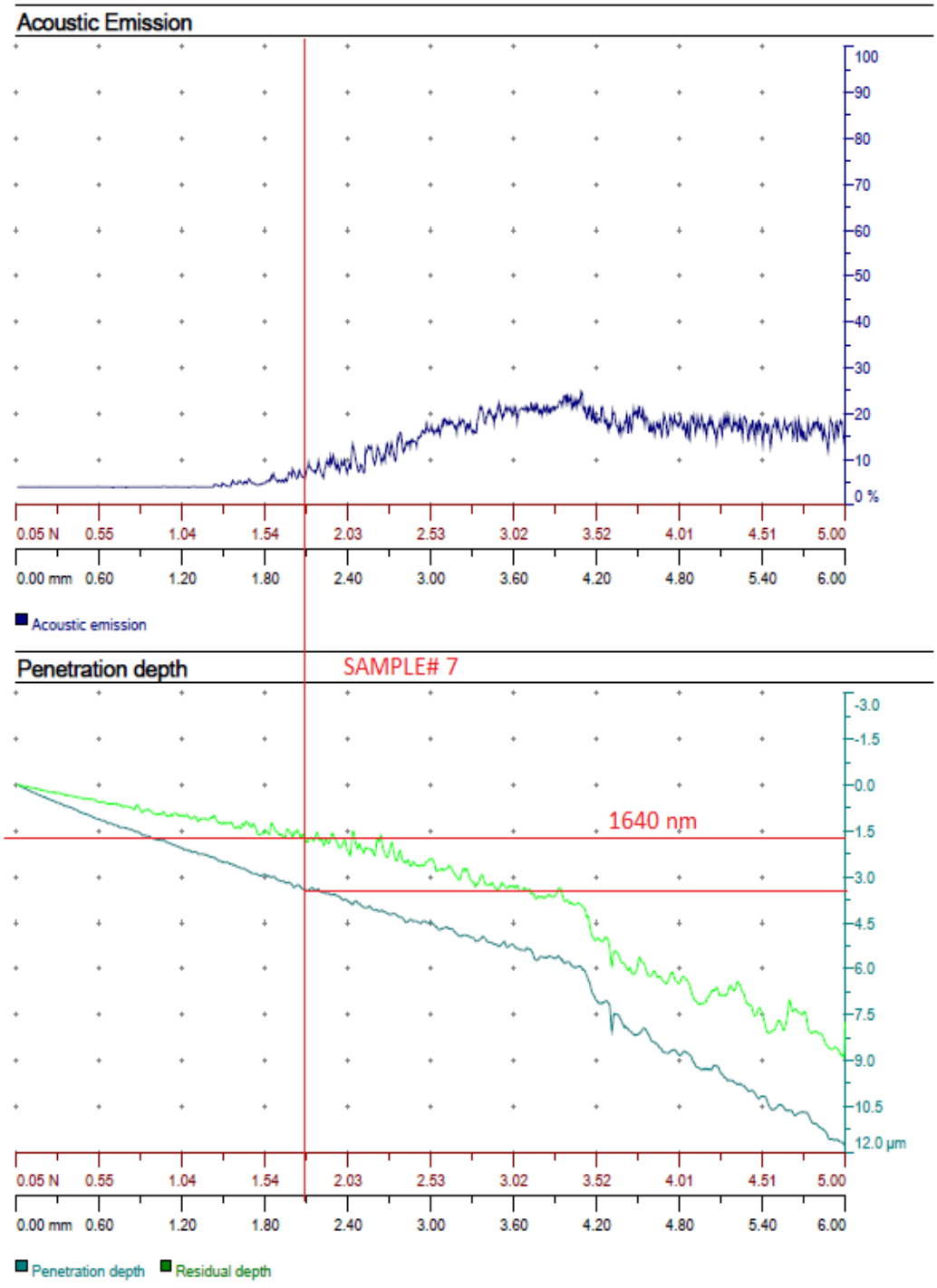

Figure 4.13 Change of acoustic emission and penetration depth vs normal load and scratch length (Sample 7)

Sample 7 has 1640 nm DLC film thickness. Penetration depth (Figure 4.13) reaches 1640 nm at about 1.00 mm from the point of first touch. On the other hand residual depth of 1640 nm registered at 2.10 mm, and to reach this residual the tip must penetrate about 3.5 microns which is then so called as the penetration depth. Although 3.5 micron is much greater than the film thickness, at the corresponding travel distance (2.1 mm) the film keeps its integrity as it can be seen below (Figure 4.14). This also again means that when the film is indented, both film and substrate yawn or deflect together. Furthermore at this point (Penetration depth – Residual depth) / Film thickness ratio is about 1.13. This is the ratio that can be accepted as the restoration power of the film on and with the substrate.

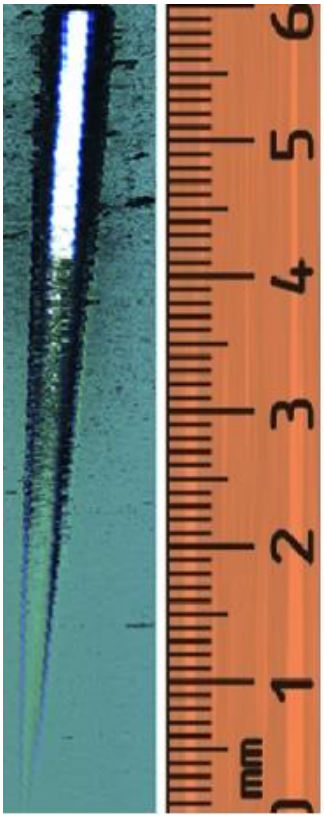

Figure 4.14 Scratch print after the scratch test for sample 7

Figure 4.14 shows that film starts to lose its rigidity at about 2.4 mm. This point can be accepted as optimum point where friction coefficient of the DLC film can be defined. Hence friction coefficient of the film is 0.18. Furthermore beyond this point at about 4.2 mm frictional force curve on Figure 4.15 change its slope (actually the slope increased drastically), this increase is certainly because of confrontation with aluminum surface.

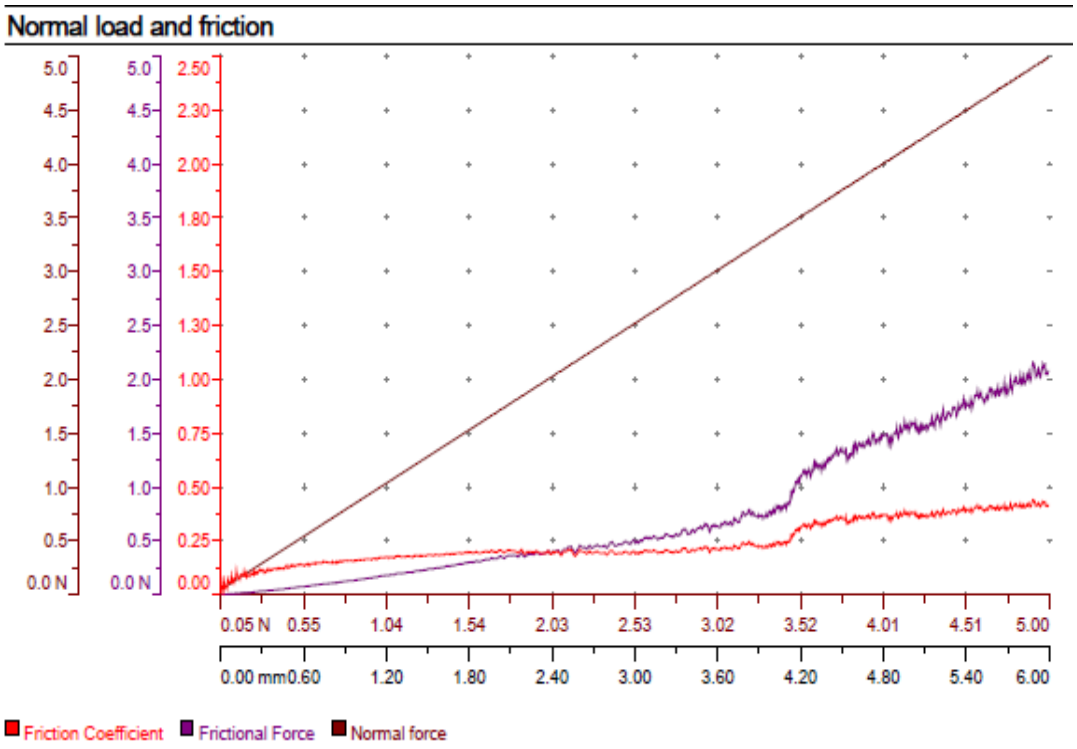

Figure 4.15 Normal load and scratch length vs friction coefficient/frictional force/normal force (Sample 7)

Furthermore, after about 4.2 mm film goes almost total destruction, and it is not possible to talk about a film after this point. Although restoration power decreased, since the film thickness increased about twice, the total destruction takes place at 4.2 mm which is beyond the value recorded for the sample 5 which was 3.7 mm.

4.2.5.3. Frictional Analyses for Sample 18

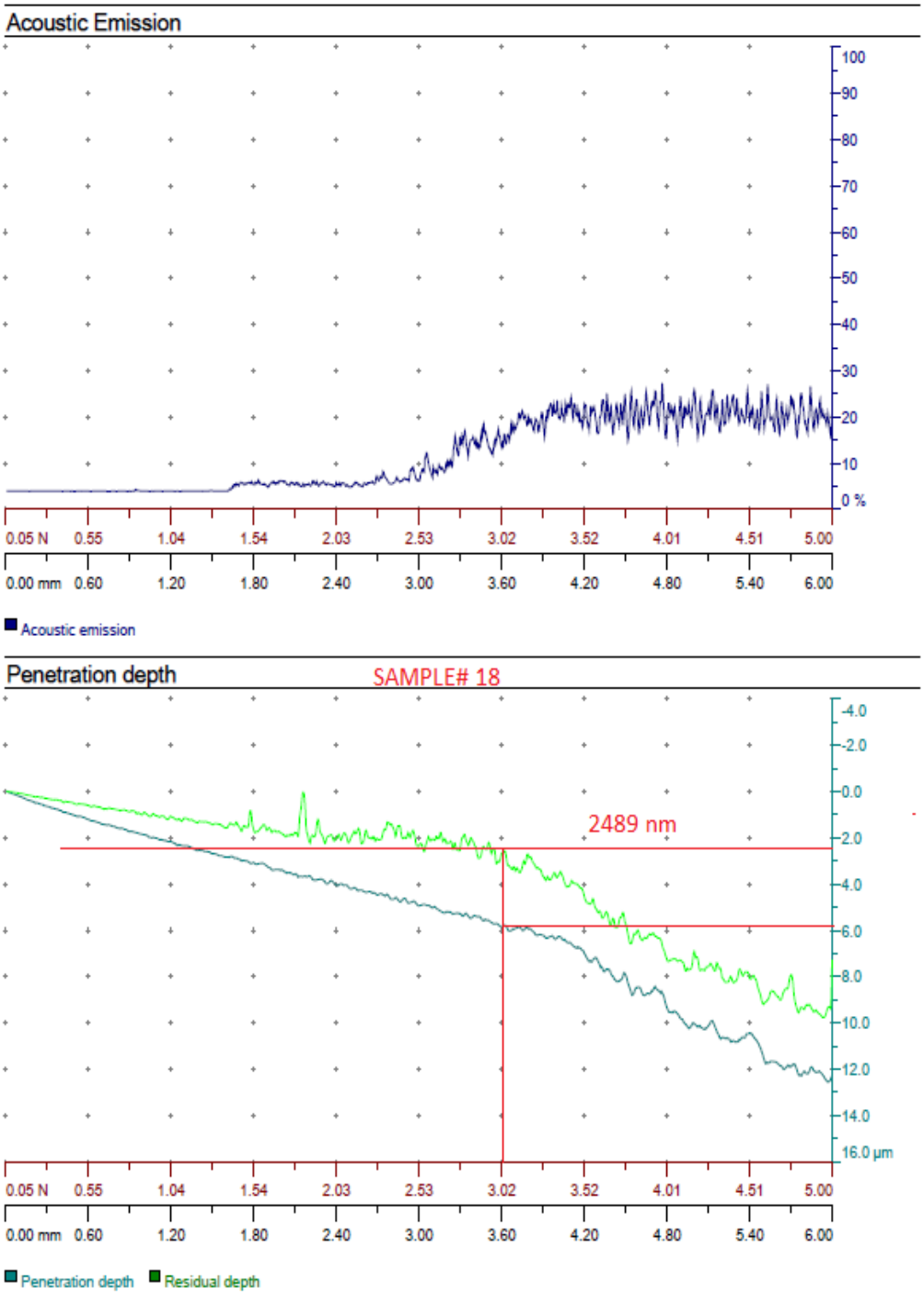

Figure 4.16 Change of acoustic emission and penetration depth vs normal load and scratch length (Sample 18)

Sample 18 has 2489 nm DLC film thickness. Penetration depth (Figure 4.16) reaches 2489 nm at about 1.40 mm from the point of first touch. On the other hand residual depth of 2489 nm registered at 3.05 mm, and to reach this residual depth, the tip must penetrate about 5.8 micron which is then so called as the penetration depth. Although 5.8 micron is much greater than the film thickness, at the corresponding travel distance (3.05 mm) the film almost keeps its integrity as it can be seen below (Figure 4.17). This also again means that when the film is indented, both film and substrate yawn or deflect together. Furthermore at this point (Penetration depth – Residual depth) / Film thickness ratio is about 1.33. This is the ratio that can be accepted as the restoration power of the film on and with the substrate.

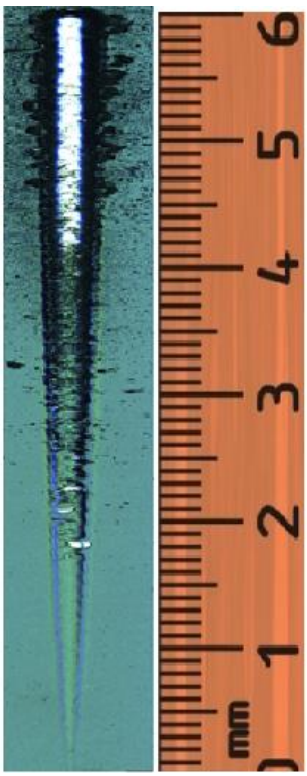

Figure 4.17 Scratch print after the scratch test for sample 18

Figure 4.17 shows that film starts to lose its rigidity at about 1.7 mm. Small white openings (aluminum substrate surfaces) seen on Figure 4.17 between 1.7 mm and 2.3

mm are most probably due to other reasons but scratch. Whether or not it is due to scratch, they are affecting friction coefficient, hence it is meaningful to look at just before 1.7 mm where there is no substrate surface seen, then friction coefficient of the DLC film is about (Figure 4.18) 0.18.

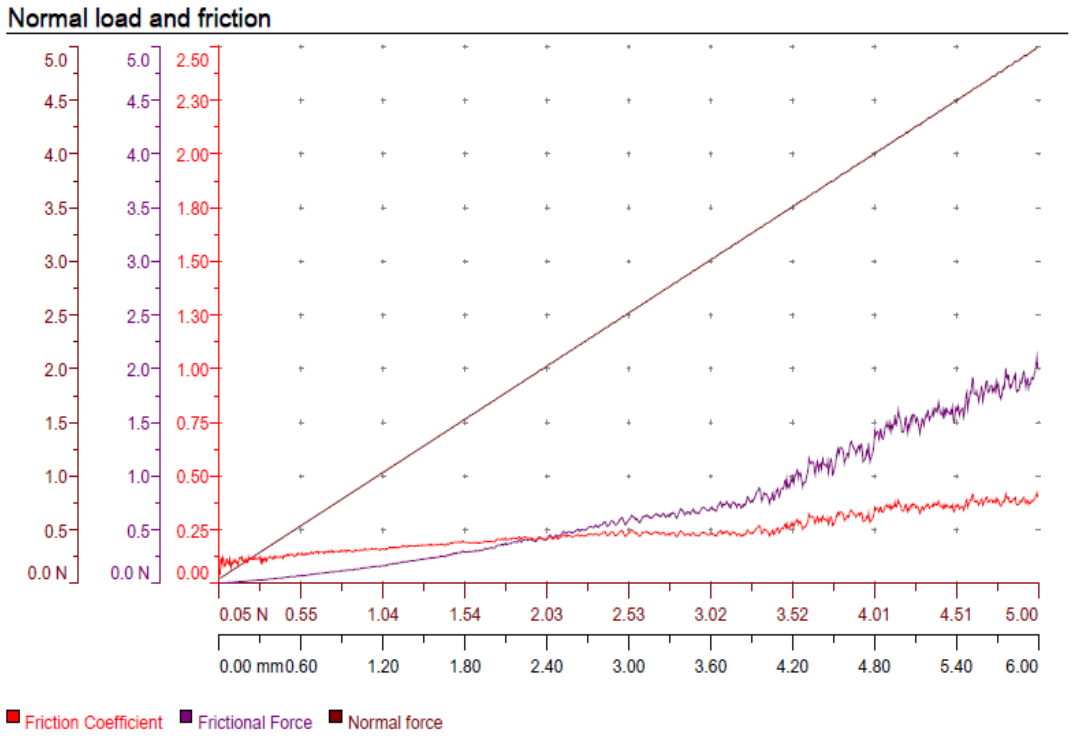

Figure 4.18 Normal load and scratch length vs friction coefficient/frictional force/normal force (Sample 18)

Furthermore, although there is not a perfect clean substrate surface, after about 4.2 mm it not possible to talk about a film.

To sum up, some critical results are tabulated in Table 4.3. Although it is difficult to deduce certain conclusion from only three samples, it is clear that total destruction length is increased as the thickness increases, which is meaningful, because as the thickness increases we are going away from the aluminum surface. Furthermore there

is no significant change neither in restoration power nor for friction coefficient (Table 4.3).

Table 4.3 Scratch test results for sample numbers of 5, 7, 18

Al Sample No	Thickness (nm)	Penetration Depth (nm)	Residual Depth (nm)	Restoration Power	Friction Coefficient	Total Destruction Length (mm)
5	875	2000	875	1.29	0.18	3.7
7	1640	3500	1640	1.13	0.18	4.2
18	2489	5800	2489	1.33	0.18	4.2

4.2.6 Structural Analysis (XPS)

Hydrogenated amorphous DLC films mainly consist of sp^2 and sp^3 carbonaceous compounds. As mentioned in literature survey section sp^3 is responsible for diamond properties, whereas sp^2 is a base structure for graphite. DLC benefits both structural properties of them. Moreover there can be also trace amount of sp^1 compounds in the film, but this amount can be neglected for our structural analysis. It is also possible to add other element apart from carbon into the film. If this element is hydrogen then the film take a pro name as hydrogenated. Hydrogen can either replace carbon atoms in the compound or it can go into film as an interstitial element.

At this point without disturbing or damaging the structure a XPS analysis can be done to differentiate the structure. Hence sample 5, sample 7, sample 15 and sample 18 are measured by XPS. All the measurements are taken on a spot size of 200 μm and each spot is placed arbitrarily on the surface, in other words measurements are taken from different locations for each sample. Mean energy levels for sp^3, sp^2 and C-O bonds are accepted as 285.20 eV, 284.55 eV and 287 eV respectively as defined in the literature. Although there is no input to add any oxygen into the film, results show that there are C-O bonds and we deduced that C-O bonds are due to oxidation after the runs because they are all exposed to atmosphere [37]. Although 3-6 min argon

sputtering process is applied before each measurement, it is not possible to remove oxygen totally.

Almost all results verify that the films are in the class of hydrogenated amorphous DLC films defined by literature (Table 2.1). However it is not observed a correlation between thicknesses and bonding structures. Besides, it seems that distribution of sp^3/sp^2 in the films is random. In order to make the situation clear, sample 5 is re-measured and analyzed by re-choosing a different place for the spot where XPS measurement is taken. The new percentages are different than the ones obtained before (Table 4.4). Especially sp^3 and sp^2 percentages are not similar at all. Rethinking all the results obtained up to now, it is possible to conclude that sp^3, sp^2 distribution is not uniform throughout the film. Besides by looking the increase in C-O it is possible to deduce that the film oxidation level increase, hence it is also an indication or proof of time based oxidation in a normal room environment. Moreover sp^3/sp^2 ratios for all 4 samples also change between 1.35 and 2.37 hence they shows no correlation.

Table 4.4 XPS results for samples 5, 7, 15, 18

Al Sample No	H_2 - C_2H_2 Flow Rates (cm^3/s)	RF Coating Step Control Bias Voltage (V)	Coating Time (s)	Profilometer Measured Thickness (nm)	sp^3 ~@285.20 eV (%)	sp^2 ~@284.55 eV (%)	C-O ~@287 eV (%)	sp^3/sp^2
5	150-100	700	1000	875	55.09	37.59	7.33	1.47
5 (Re-measured)					61.88	28.06	10.06	2.21
7	150-100	700	2200	1640	49.11	36.39	14.50	1.35
15	150-100	700	3750	2515	54.78	37.55	7.67	1.46
18	150-100	700	3620	2489	63.15	26.66	10.18	2.37

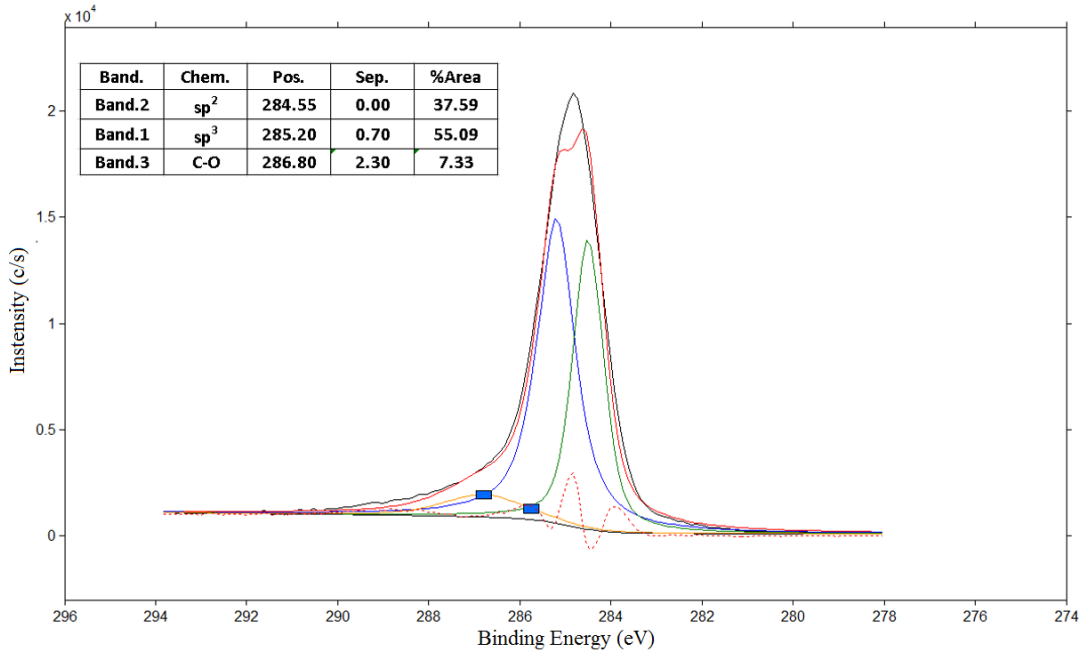

Figure 4.19 First processed XPS measurement results of sample 5

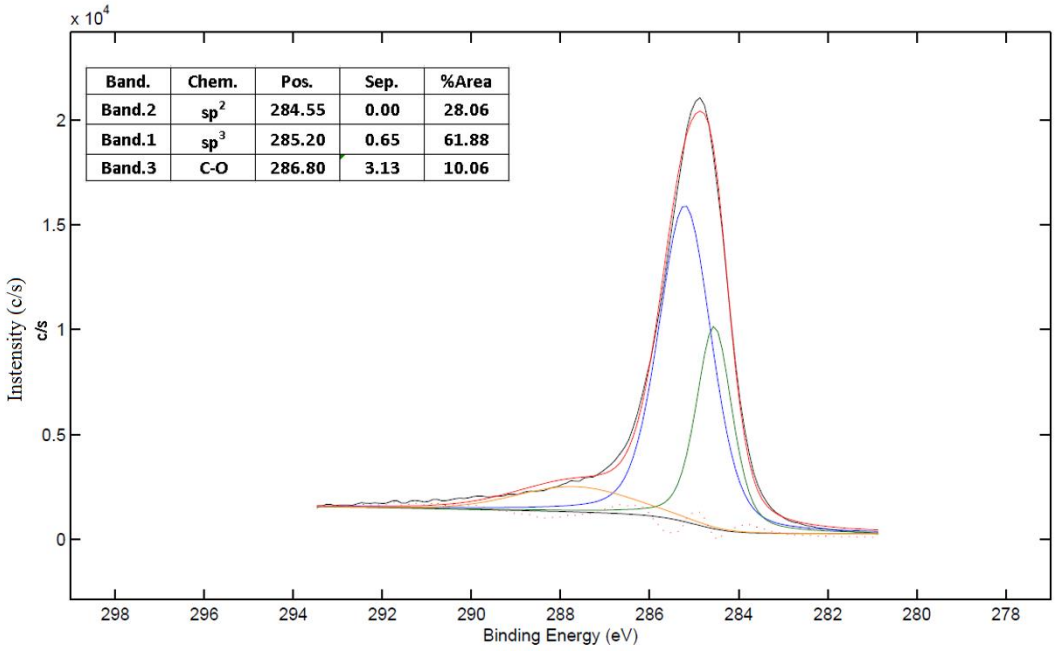

Figure 4.20 Second processed XPS measurement results of sample 5

Although results show that sp^3/sp^2 percentages are uncorrelated with thickness, it is clear that in terms of sp^3/sp^2 percentages almost all films can be accepted as in the family of hydrogenated amorphous diamond like carbon (Table 4.4, Figure 4.19 Figure 4.20).

4.2.7 Environmental Tests: Humidity + Salt Fog

Because the environmental tests are totally destructive, these tests should be carried on after completing all coatings and characterization tests. The first environmental test is 10 days humidity test. It is composed of 2 days cycle which is repeated 5 times during the whole test. Temperature is not constant and altered between minimum and maximum temperatures of 20 °C and 60 °C, respectively as seen on Figure 3.9. Besides, 95% relative humidity is conserved throughout the 10 days test in the test chamber.

The second test is the salt fog test. In salt fog test, there is temperature constraint that temperature should be kept constant at 35 °C in a closed test chamber throughout the test run. The total duration is 5 days without any interruption. There is a nozzle spraying a solution of 5% NaCl in weight (in other words 5% NaCl and 95% deionized water). The pH of the salty solution should be kept between 6.5 and 7.2. The spray should never face directly to the film surfaces; the only effect that should be is the salty fog on the film. Furthermore the speed of solution drop should be kept between 0.0125-0.0375 ml/(cm^3*hour) on the base of the chamber. Moreover in order not to accumulate solution or salt on the films, the samples placed perpendicularly on an inert (not reacting with the samples during and under the test conditions) holder (this is the same method also applied in humidity test).

All samples are tested together on a sample holder.

Environmental test results show that increase in thickness decreases durability, especially over the film thickness about 1600 nm, films get start to fail beginning from the edges. Especially films on samples 18 and 29 are totally destructed, their thicknesses are 2489 nm and 2655 nm, respectively (Figure 4.22). On the other hand

thinner films (<1640 nm) on aluminum samples are not destructively affected. The most probable reason for destruction is the intrinsic compressive stress and tension (T) that is also increases with increasing thickness (Figure 4.5). Temperature variations in humidity test creates stress variations in the film, this is thought to be the main cause of destruction.

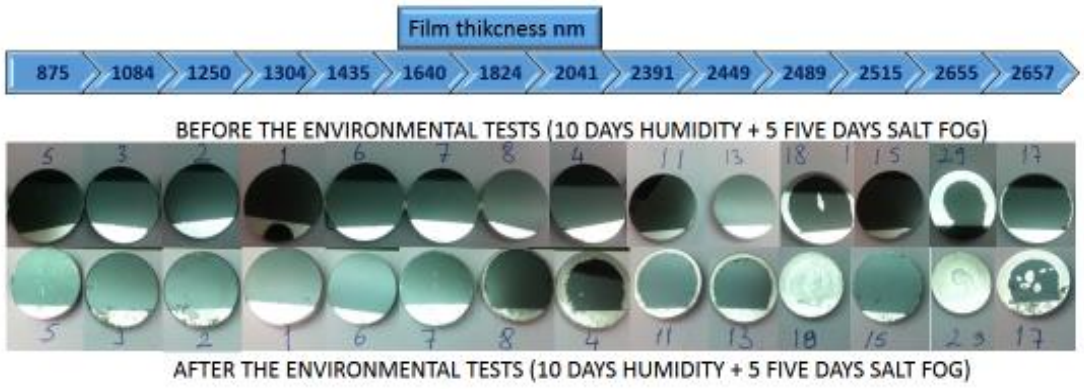

Figure 4.22 Thickness variation phase samples after environmental tests

To sum up considering all the characterization studies and test results, 2500 nm can be taken as the optimum thickness and corresponding process time is defined as 3620 s. For the rest of the study and runs this is the pivot point that other trials are going to be done respectively.

4.3 Phase 2: Effect of Hydrogen Content

In order to investigate the effect of hydrogen content on film properties, flow rates of precursor hydrogen gas is selected as the parameter to be tuned at this second phase. In other words the aim is to change the hydrogen content in the film by changing H_2 flow rate and to see what properties are affected. Hence flow rate of C_2H_2 are set at a certain value and kept constant throughout the coating step, but H_2 flow rates are set to a value between 0 cm^3/s and 200 cm^3/s and changed before each run. Moreover 700

V of bias voltage is again kept constant to create and control RF power throughout the coating step. Coating time of the coating step is again selected as 3620 s as the experiments up to now suggest.

4.3.1 Thickness and Hydrogen Content

As the part of the strategy mentioned, second phase trials are done based on varying hydrogen flow rate and it is expected that varying flow rate of hydrogen also changes hydrogen content of the film. In other words, it is expected that increasing/decreasing hydrogen flow rate should increase/decrease hydrogen content. Hence a series of coating runs were conducted with different flow rates. Throughout the runs, all other parameters are conserved as they are at this very beginning. As a first assumption it is expected that changing hydrogen content changes thickness slightly, because some bonds and bonding types are supposed to be changed. Moreover hydrogen atoms which participated as interstitial elements can also add some distortive effects on the structure and consequently on the total volume occupied in space by the film. These are the presumptions. Following 12 successive runs showed that as the hydrogen flow rate increases, the thickness of the film is getting higher. Furthermore the correlation between them is almost linear as shown in Figure 4.23.

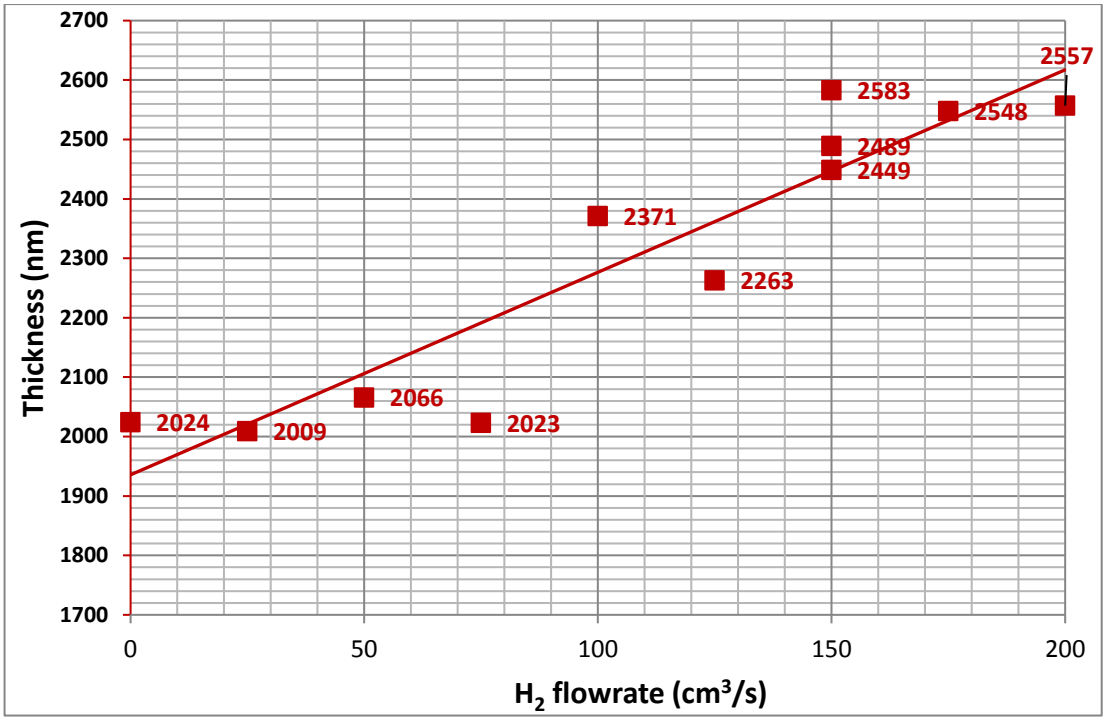

Figure 4.23 Thickness variations vs. hydrogen flow rate for constant coating time (3620 s)

For zero flow rate of hydrogen the thickness is 2024 nm, whereas it is 2557 nm at maximum (200 cm^3/s) H_2 flow rate and the increase is almost gradual.

4.3.2 Interferometer Measurements: Surface Topography

Like in the former coatings, general morphology was not changed drastically. On the other hand depending on the hydrogen content of the film, concaveness or convexness of the surfaces or in other words power of the surfaces are changed. Actually the more hydrogen means the less power difference (ΔP). Since DLC films have a tendency to create internal, intrinsic compressive stress and as the tension (T) due to compressive stress increases, the film gets more convex (Figure 2.9).

However increasing hydrogen content reduces power difference and tension, this can easily followed via Figure 4.24 and Figure 4.25. We can deduce that hydrogen in DLC

can relax intrinsic stresses in the film. We also know that increasing H_2 can add polymeric characteristics to the film. Although too much compressive stress is detrimental, a level of compressive stress is essential to keep the film rigid, otherwise below a point film cannot keep its coherence. As it can be traced from the Figure 4.25, films coated with hydrogen flow rates of 200 cm^3/s peel off or fail, the most meaningful explanation is that it is due to too low compressive stress.

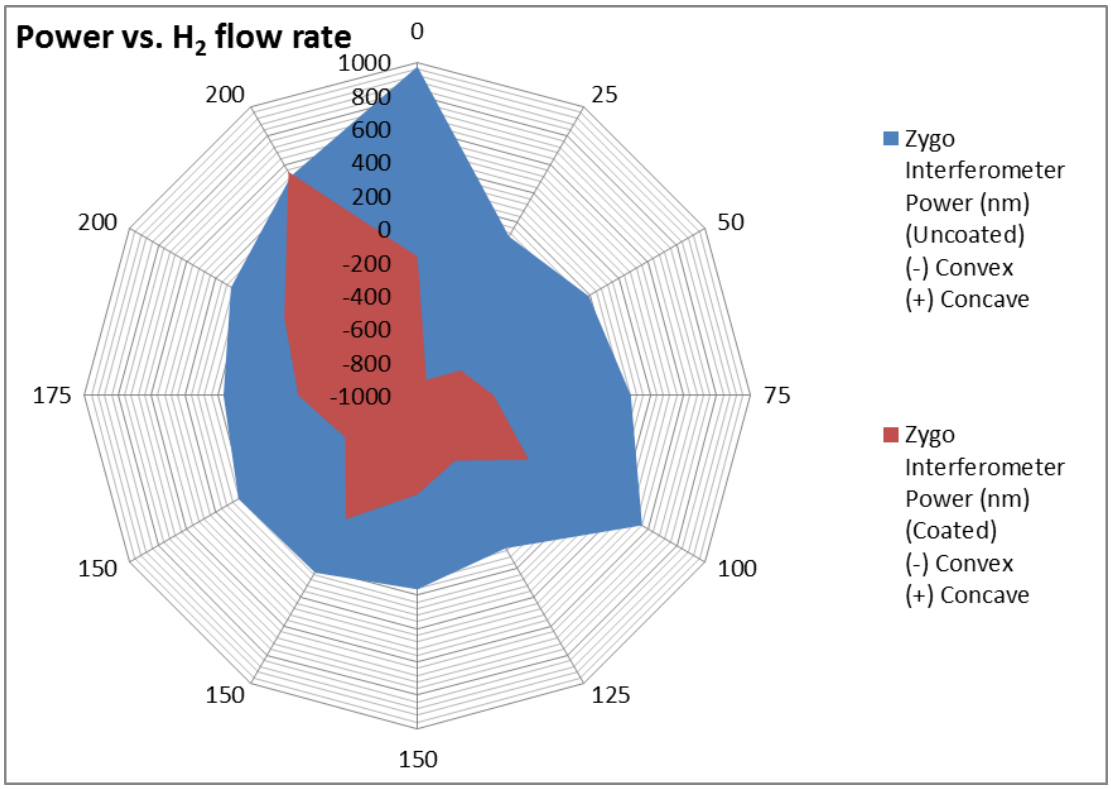

Figure 4.24 Power vs. thickness variations measured by a Zygo red light (600 nm) interferometer

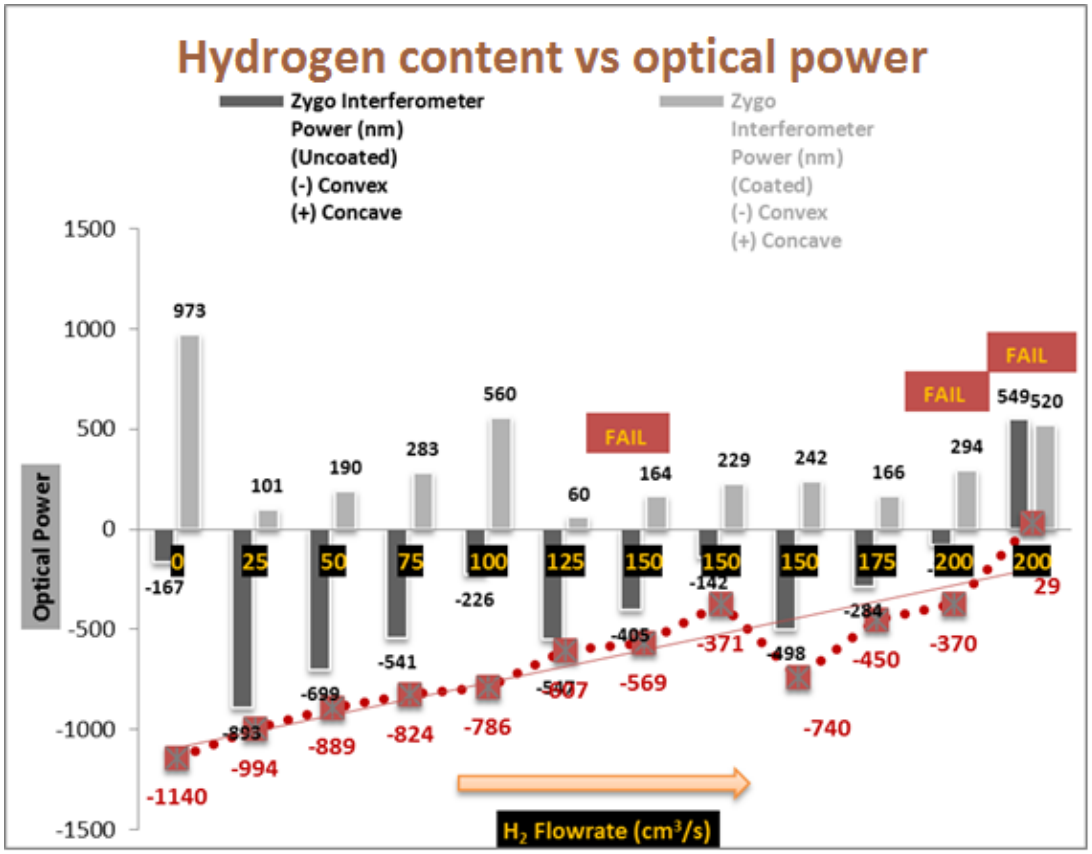

Figure 4.25 Power vs. thickness variations measured by a Zygo red light (600 nm) interferometer

4.3.3 FTIR Measurements: Reflection

As mentioned before, near 2500 nm thicknesses, the reflectance values are veritably at maximum. The films with different hydrogen content but the same coating durations have different film thicknesses and the reflection values follow "Quarter Wave Rule" as mentioned before. Furthermore, since increasing hydrogen content increases transparency in IR region. Hence it is quite meaningful to expect a decrease in refractive index as the hydrogen content increases, this decrease in refractive index means also a decrease in optical thickness (n*d) assuming physical thickness stays fairly the same or does not decreases at all. Consequently, Figure 4.27 suggests that the optimum optical thickness is attained by hydrogen flow rate of 150 cm^3/s and the maximum reflectance is also observed near this point (Figure 4.27). In other words,

maximum average reflectance can be obtained at H_2 flow rate of 150 cm^3/s. These results show nothing but a consistency with what was obtained in the thickness determination phase.

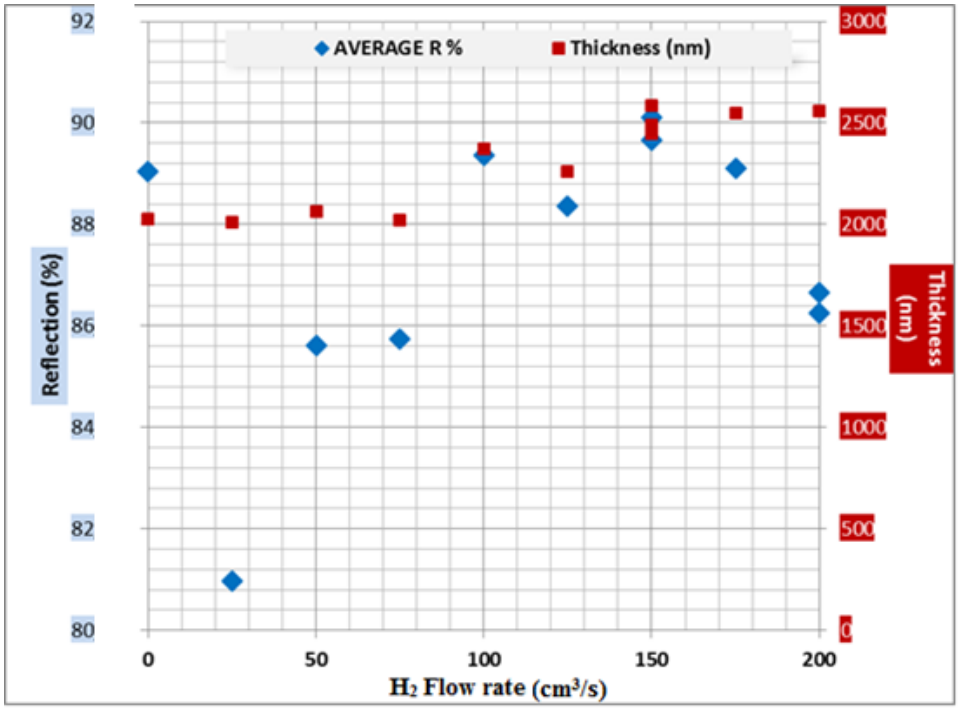

Figure 4.27 H_2 Flow rates vs. reflectance (mean values at the band of 8-12 μm) with varying coating time

4.3.4 Hardness and Elasticity

Hardness (H) is the other parameter to decide on the film thickness. This time the only changing parameter is the hydrogen flow rate. It has been changed between 0-200 cm^3/s in a controllable manner for each of single run. Then four runs are conducted with hydrogen (H_2) flow rates of 0, 50, 100 and 150 cm^3/s, respectively and these samples were tested by the CSM instruments in order to measure the hardness and elasticity. Unfortunately, the samples of 200 cm^3/s cannot be tested because these coatings, as mentioned before, peeled off shortly after the run.

It is better to remember that hardness (H) and elastic modulus (E) are fundamental parameters on the tribological behavior of the film. For a wear resistant hard coating, plastic work of indentation or in other words the ratio of hardness (H) to Young's modulus (E), namely H/E defines how the film is strain tolerant. It is better to remember that high H/E ratios bring also high elastic recovery rates. Hence high H/E rates make the film more robust and increases the durability of it. In Table 4.5 CSM instruments test results including H/E rates are listed.

Table 4.5 Tabulated hardness (H) and elasticity (E) values measured by CSM instruments for the four samples

Al Sample No	H_2 Flow Rates (cm^3/s)	Hardness - HIT (GPa)	Elasticity - EIT (GPa)	H / E rates (Recovery Power)
27	0	23.6	161.5	0.15
26	50	24.4	179.8	0.14
20	100	19.5	131.8	0.15
18	150	14.9	95.0	0.16

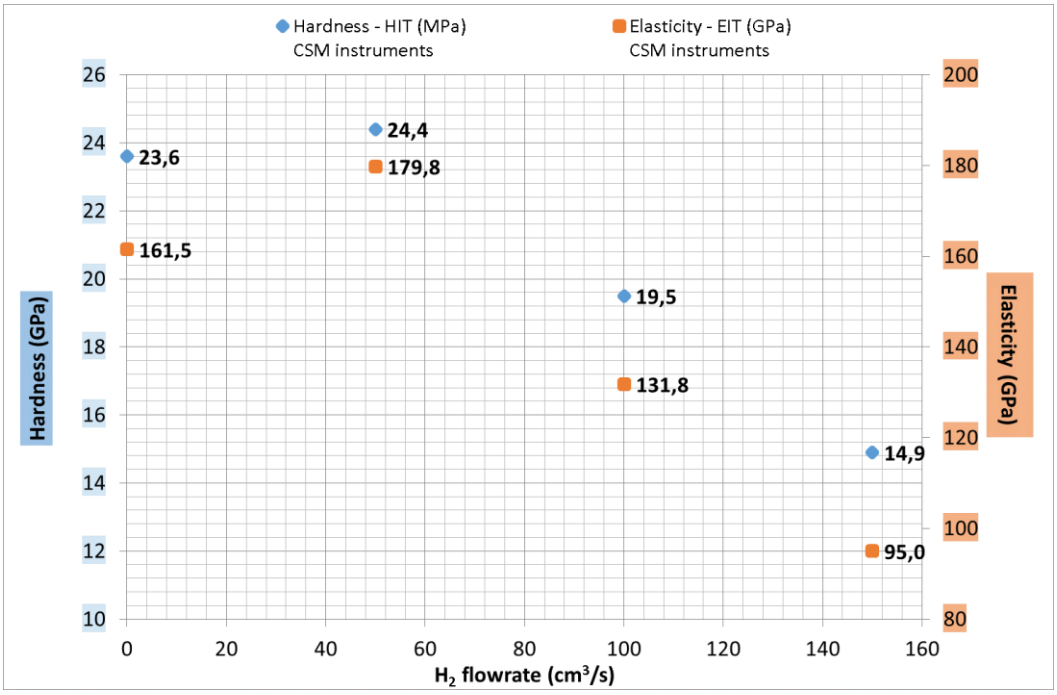

Figure 4.28 Hardness (H) and elasticity (E) values measured by nano-indenter of the four samples

Increasing hydrogen content has tendency to reduce both the hardness and Young's modulus [8]. The results (Figure 4.28) are consistent with this rule. It can easily be traced that with increasing the hydrogen flow rate (consequently hydrogen content) both hardness and elasticity decrease. On the other hand the "recovery power" stays fairly the same.

Please remember that the threshold for a hard coating is 10 GPa and if the hardness is above 10 GPa the coating is accepted as hard. All the samples are harder than the samples in thickness determination phase, hence they exceed the threshold (10 GPa) hence can be accepted as hard also. Furthermore the measured elastic modulus of the samples are in the range of 95 – 180 GPa, this also conforms the literature expectations for hydrogenated amorphous DLC films (60-210 GPa, Table 2.5). The measured H/E rates of samples are between 0.14 - 0.16 which fall again in the class of hydrogenated amorphous DLC films, those range is defined as 0.1 – 0.16 in literature (Table 2.5).

4.3.5 Frictional Analyses

Four coated samples are chosen, namely sample 18, sample 20, sample 26 and sample 27 from different runs whose hydrogen flow rates are different. Coating times of coating step for these four samples are the same (tc=3620 s). Hydrogen flow rates of these four samples (sample 18, sample 20, sample 26, and sample 27) are 150 cm^3/s, 100 cm^3/s, 50 cm^3/s and 0 cm^3/s, respectively. All the tests are done under normal room conditions and with the same parameters as before.

4.3.5.1.Frictional Analyses for Sample 18

Since frictional analysis is argued in 4.2.5.3 it will not be repeated here. Please refer the section of Frictional Analyses for Sample 18.

4.3.5.2.Frictional Analyses for Sample 20

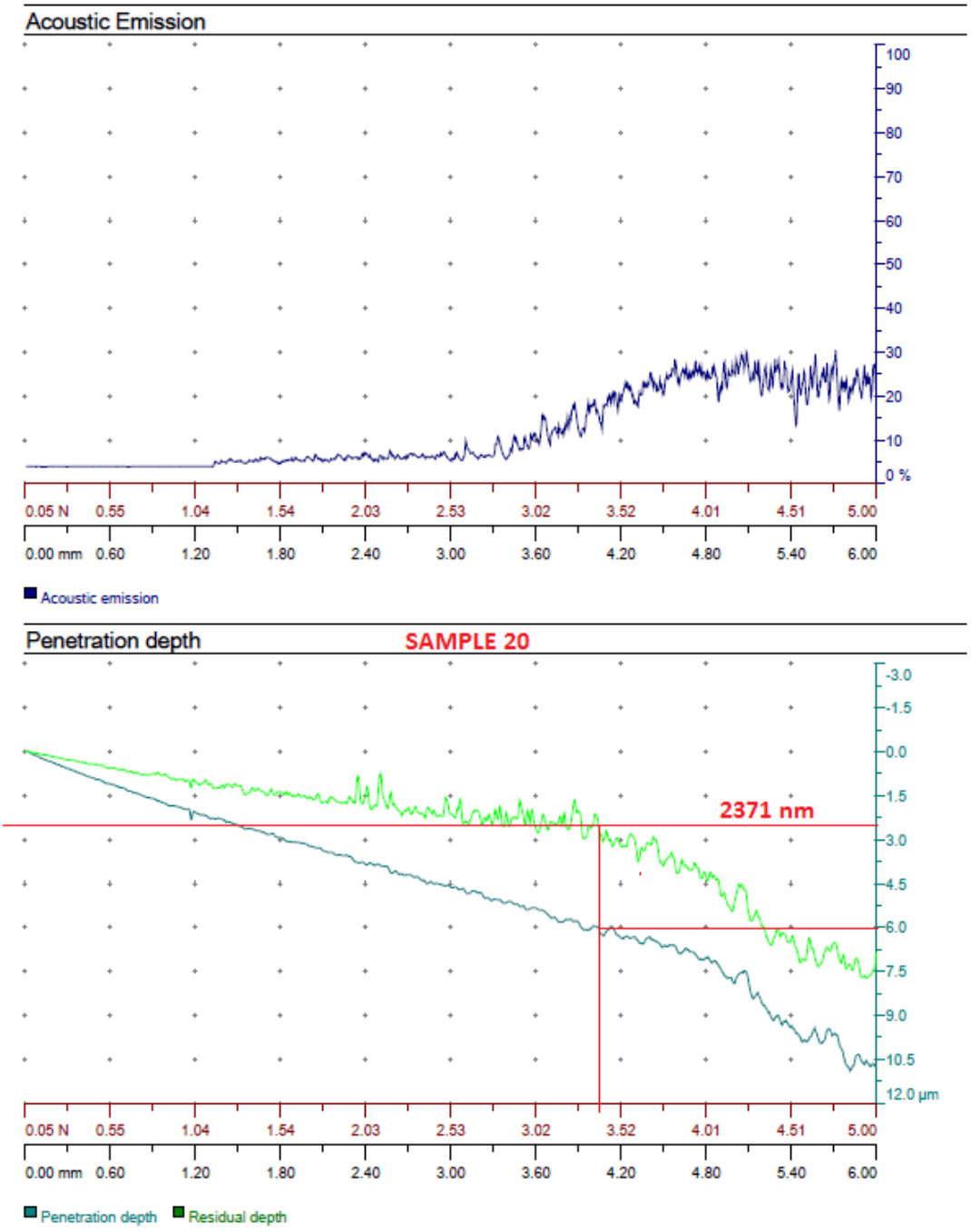

Figure 4.29 Change of acoustic emission and penetration depth vs normal load and scratch length (Sample 20)

Sample 20 has 2371 nm DLC film thickness, besides it has the second highest hydrogen content (H_2 flow rate in its run is 100 cm^3/s) among the 4 samples. Penetration depth (Figure 4.29) reaches 2371nm at about 1.50 mm from the point of first touch. On the other hand residual depth of 2371 nm registered at about 4.05 mm, and to reach this residual the tip must penetrate about 6.05 micron which is then so called as the penetration depth. Although 6.05 micron is much greater than the film thickness, at the corresponding travel distance (4.05 mm) the film keeps its integrity as it can be seen below (Figure 4.30). This also means that when the film is indented, both film and substrate yawn or deflect together. Furthermore at this point the (Penetration depth – Residual depth) / Film thickness ratio is about 1.55. This is the ratio that can be accepted as the restoration power of the film on and with the substrate, and it is the highest restoration power among the results obtained up to now. As far as film does not delaminate, this ratio can give fairly meaningful and valuable information.

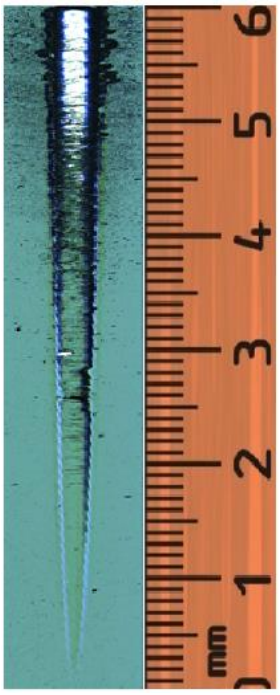

Figure 4.30 Scratch print after the scratch test for sample 20

Figure 4.30 shows that film starts to lose its integrity at about 1.5 mm starting with a dark region (tiny ruptures). Hence location just before this point can be accepted as optimum point where friction coefficient of the DLC film can be measured and defined. Then friction coefficient of the film is 0.15 at 1.5 mm from the point of start (Figure 4.31).

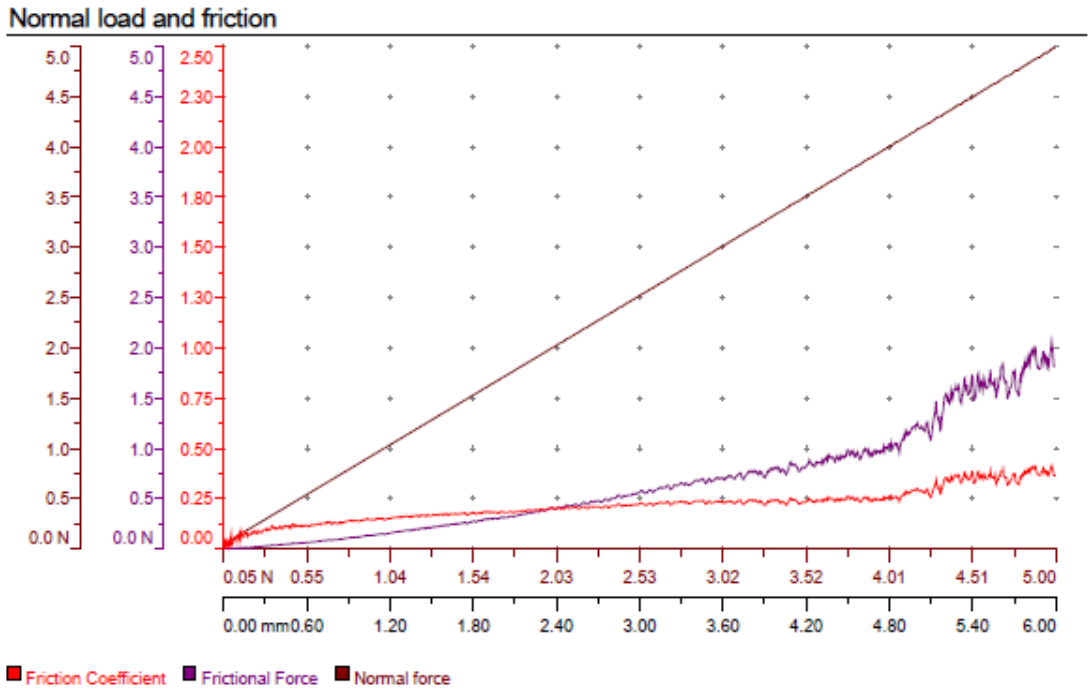

Figure 4.31 Normal load and scratch length vs friction coefficient/frictional force/normal force (Sample 20)

Furthermore, after about 5.2 mm (Figure 4.30) film goes almost total destruction and it not possible to talk about a film after this point. 5.2 mm is the second longest travel that any DLC film stands up in this thesis.

4.3.5.3. Frictional Analyses for Sample 26

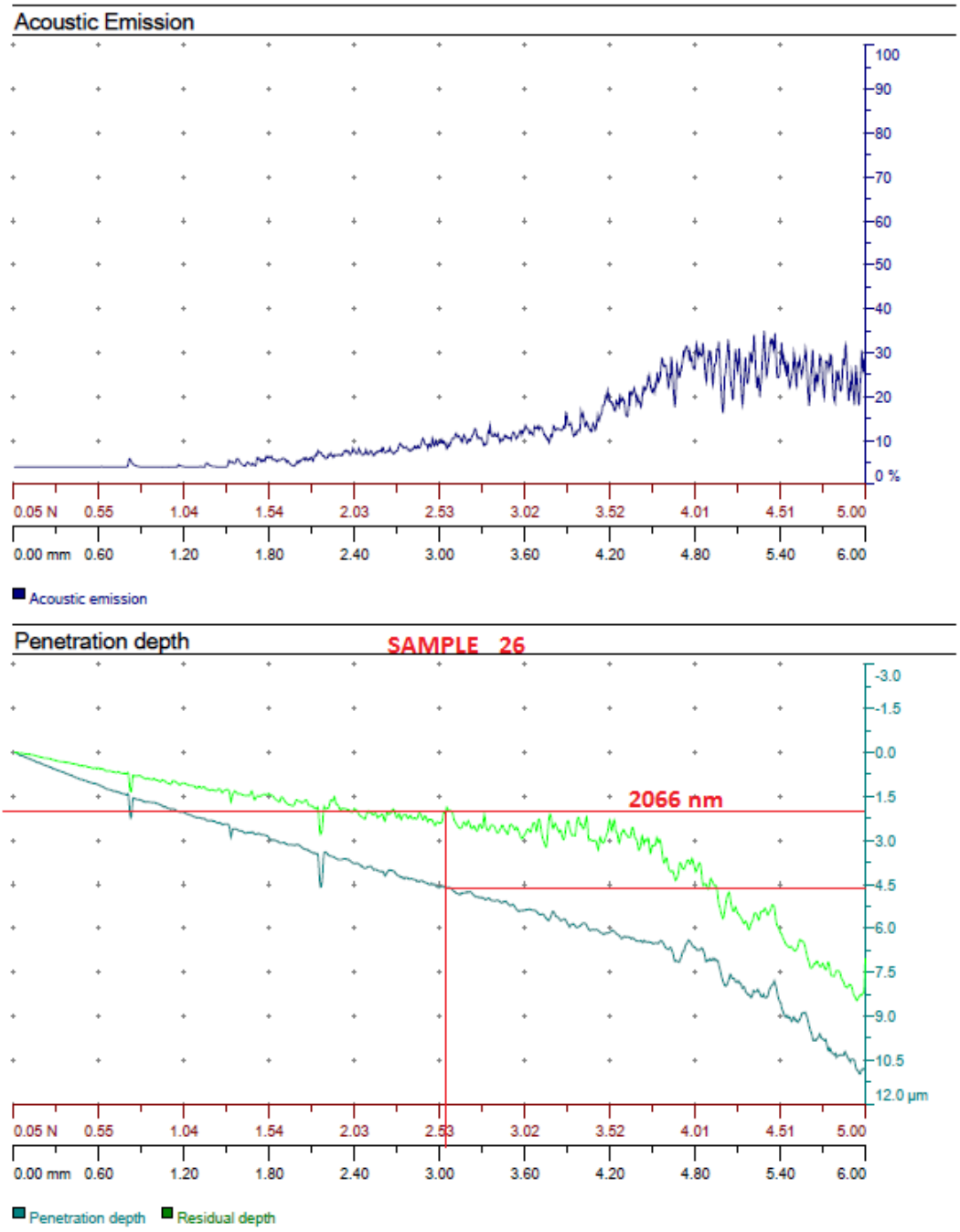

Figure 4.32 Change of acoustic emission and penetration depth vs normal load and scratch length (Sample 26)

Sample 26 has 2066 nm DLC film thickness, besides it is supposed to have lower hydrogen content than the sample 20 (H_2 flow rate in the run that sample 26 coated is 50 cm^3/s). Penetration depth (Figure 4.32) reaches 2066 nm at about 1.20 mm from the point of first touch. On the other hand residual depth of 2066 nm registered at about 3.05 mm, and to reach this residual the tip must penetrate about 4.6 micron which is then so called as the penetration depth. Although 4.6 micron is much greater than the film thickness, at the corresponding travel distance (3.05 mm) the film keeps its integrity as it can be seen below (Figure 4.33). This also means that when the film is indented, both film and substrate yawn or deflect together. Furthermore at this point the (Penetration depth – Residual depth) / Film thickness ratio is about 1.25. This is ratio lower than restoration power of sample 20 and it is also in agreement with recovery power obtained H/E (hardness/elasticity) of these two samples. In other words H/E for sample 26 is 0.14, on the other hand the same ratio was 0.15 for sample 20.

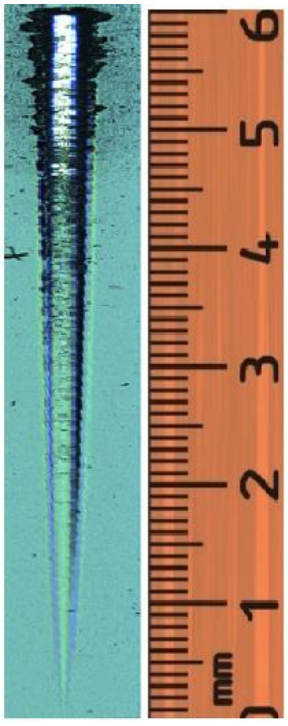

Figure 4.33 Scratch print after the scratch test for sample 26

Figure 4.33 shows that film starts to lose its integrity at about 1.5 mm starting with a dark region (tiny ruptures) on the right side. Hence location just before this point can be accepted as optimum point where friction coefficient of the DLC film can be measured and defined. Then friction coefficient of the film is 0.17 at 1.5 mm from the point of start (Figure 4.34).

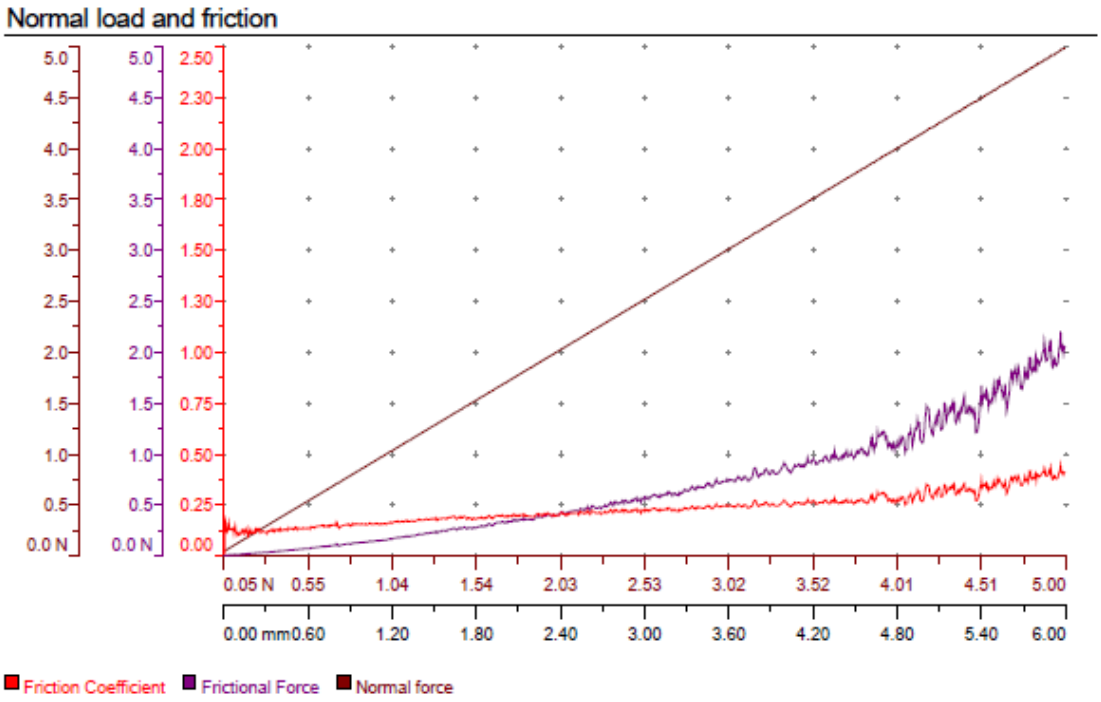

Figure 4.34 Normal load and scratch length vs friction coefficient/frictional force/normal force (Sample 26)

Furthermore, after about 4.9 mm (Figure 4.33) film goes almost total destruction, and it not possible to talk about a film after this point. 4.9 mm is the third longest travel that any DLC film stand up to now.

4.3.5.4.Frictional Analyses for Sample 27

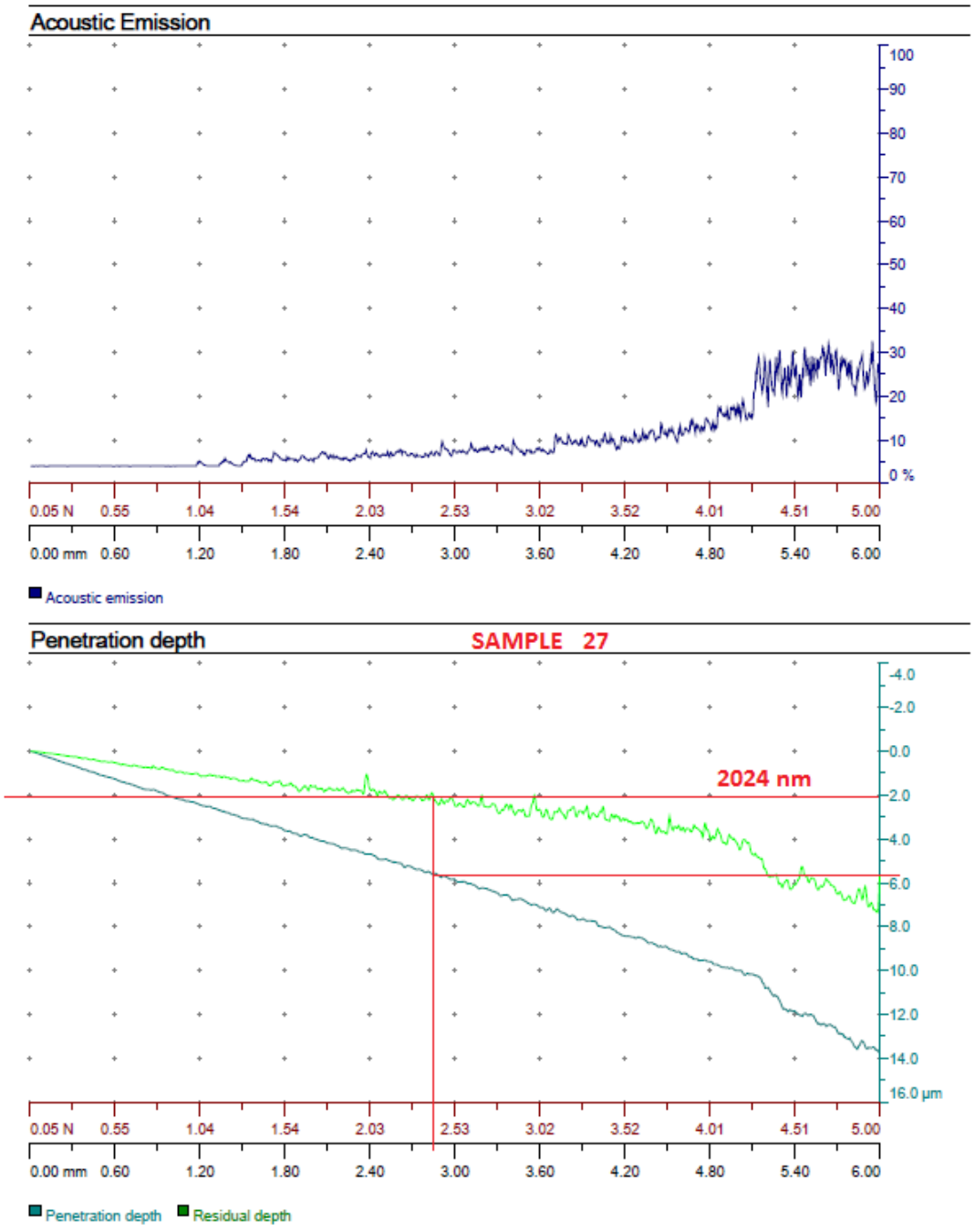

Figure 4.35 Change of acoustic emission and penetration depth vs normal load and scratch length (Sample 27)

Sample 27 has 2024 nm DLC film thickness, besides it has to be lowest hydrogen content (H_2 flow rate in the run that sample 27 coated is 0 cm^3/s). Penetration depth (Figure 4.35) reaches 2024 nm at about 1.00 mm from the point of first touch. On the other hand residual depth of 2024 nm registered at about 2.82 mm, and to reach this residual the tip must penetrate about 5.6 micron which is then so called as the penetration depth. Although 5.6 micron is much greater than the film thickness, at the corresponding travel distance (2.82 mm) the film keeps its integrity as it can be seen below (Figure 4.36). This also means that when the film is indented, both film and substrate yawn or deflect together. Furthermore at this point the (Penetration depth – Residual depth) / Film thickness ratio is about 1.77. This is the highest ratio measured up to now and that can be accepted as the highest restoration power of the film on and with the substrate.

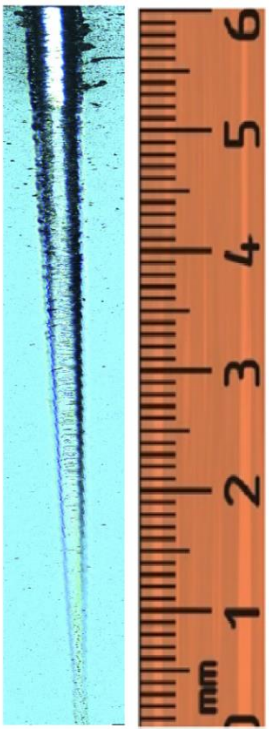

Figure 4.36 Scratch print after the scratch test for sample 27

Figure 4.36 shows that film starts to lose its integrity at about 1.6 mm starting with a dark region (tiny ruptures) on the right side. Hence location just before this point can be accepted as optimum point where friction coefficient of the DLC film can be measured and defined. Then friction coefficient of the film is 0.17 at 1.6 mm from the point of start (Figure 4.37).

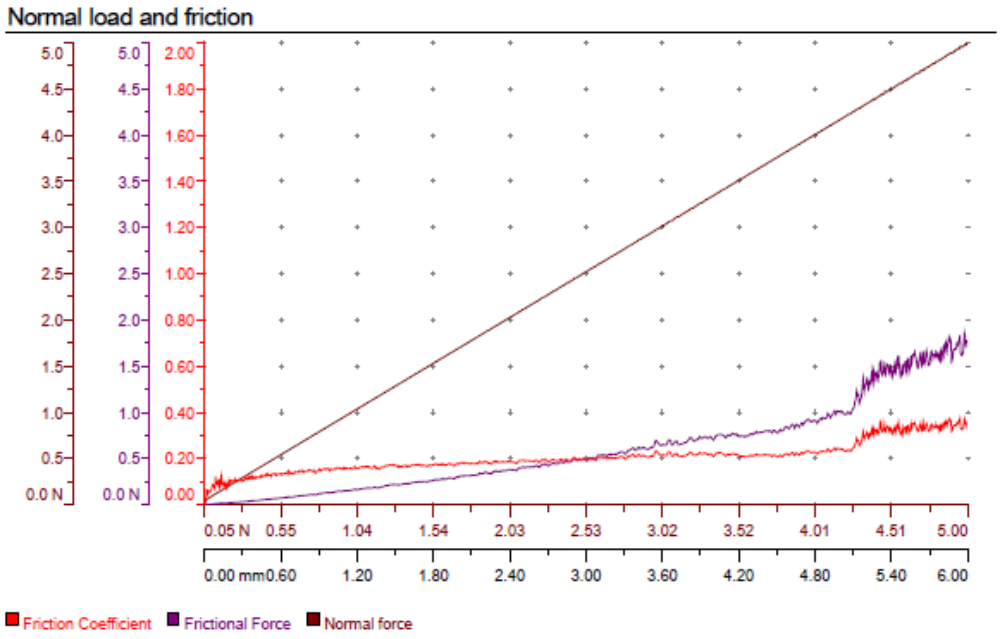

Figure 4.37 Normal load and scratch length vs friction coefficient/frictional force/normal force (Sample 27)

Furthermore, after about 5.7 mm (Figure 4.36) film goes almost total destruction, and it not possible to talk about a film after this point. 5.7 mm is the longest travel in this thesis. It seems lowering hydrogen content is increasing film durability.

At a first glance it seems that there is not an outstanding relation between hydrogen content and restoration power. However the highest restoration power is recorded at lowest hydrogen flow rate (or in other words lowest hydrogen content) for sample 27 which has virtually zero hydrogen flow rate. Furthermore longest total destruction length is observed for lowest flow rate and shortest one is recorded for highest

hydrogen flow rate (Table 4.6). Besides the friction coefficients also generally lower for lower hydrogen content, hence this also supports the idea that decreasing hydrogen content creates more durable and robust films.

Table 4.6 Scratch test results for sample numbers of 18, 20, 26, 27

Al Sample No	Thickness (nm)	H_2 Flow Rate (Precursor)	Penetration Depth (nm)	Residual Depth (nm)	Restoration Power	Friction Coefficient	Total Destruction Length (mm)
18	2489	150	5800	2489	1.33	0.18	4.2
20	2371	100	6000	2371	1.55	0.15	5.2
26	2066	50	4650	2066	1.25	0.17	4.9
27	2024	0	5600	2024	1.77	0.17	5.7

4.3.6 Structure Analysis (XPS)

As in the thickness determination phase, at this point without disturbing or damaging the structure XPS analyses are done to differentiate the structure. This time sample 18, sample 20, sample 26, sample 27 are measured by XPS. All the measurements are taken on a spot size of 200 μm and each spot is selected arbitrarily on the surface, in other words measurements are taken from different locations for each sample. Mean energy levels for sp^3, sp^2 and C-O bonds are 285.20 eV, 284.55 eV and 287.00 eV, respectively and although there is no input to add any oxygen, results show that there are C-O bonds and we deduced that C-O bonds are due to oxidation after the runs result of exposing the samples to atmosphere. Although 3-6 min argon sputtering process is applied before each measurement, it is not possible to remove oxygen totally.

Table 4.7 XPS results for samples 18, 20, 26, 27

Al Sample No	H_2 - C_2H_2 Flow Rates (cm^3/s)	RF Coating Step Control Bias Voltage (V)	Coating Time (s)	Profilometer Measured Thickness (nm)	sp^3 ~@285.20 (eV) (%)	sp^2 ~@284.55 (eV) (%)	C-O ~@287 (eV) (%)	sp^3/sp^2
18	150-100	700	3620	2489	63.15	26.66	10.18	2.37
20	100-100	700	3620	2371	48.76	36.99	14.25	1.32
26	50-100	700	3620	2066	58.43	30.04	11.53	1.95
27	0-100	700	3620	2024	50.72	33.24	16.04	1.53

Almost all results verify that the films are in the class of hydrogenated amorphous DLC films defined by literature (able 2.1). Like in the thickness determination phase there cannot be observed a correlation between hydrogen content and sp^3/ sp^2 ratios. Besides, it seems that distribution of sp^3/sp^2 is random in other words sp^3, sp^2 distribution is not uniform throughout the film. Moreover sp^3/sp^2 ratios also change between 1.32 and 2.37 and although non-uniform distribution makes it difficult to see, there is a tendency to decrease in sp^3 percentages with decreasing H_2 flow rates or contents (Table 4.7) as expected in literature which is given in Figure 2.7.

4.3.7 Environmental Tests: Humidity + Salt Fog

As mentioned before, because the environmental tests are totally destructive, these tests should be carried on after completing all coatings and characterization tests. It is worth to remember that the first environmental test is 10 days humidity test. It is composed of 2 days cycles which repeats 5 times during the whole test. Temperature is not constant and altered between minimum and maximum temperatures of 20 °C and 60 °C, respectively as seen on Figure 3.9. Besides, 95% relative humidity is conserved throughout the 10 days test in the test chamber.

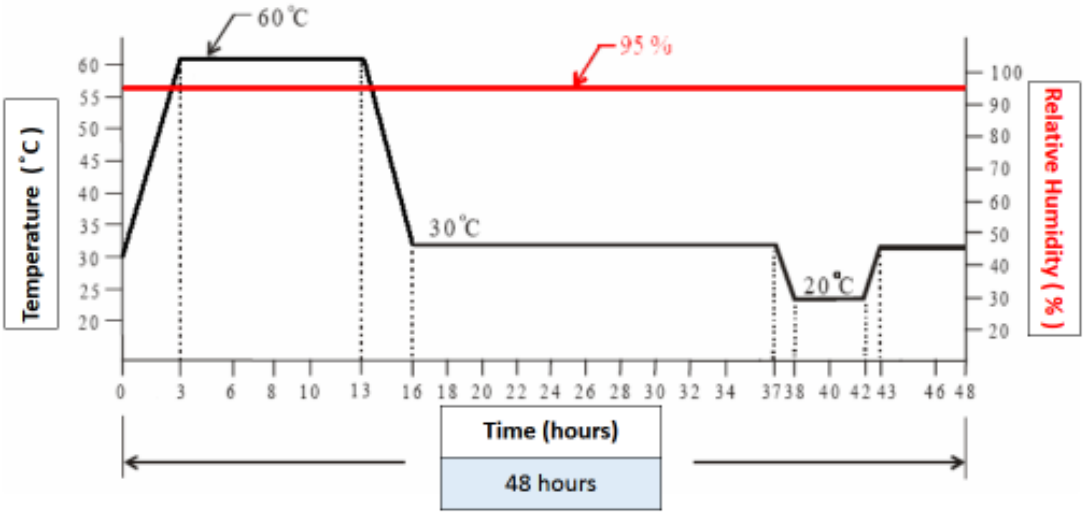

Figure 4.38 Humidity test temperature and humidity profile for a 48 hours (2 days) cycle

Please remember that the second test is the salt fog test. In salt fog test there is temperature constraint that temperature should be kept constant at 35 °C in a closed test chamber throughout the test run. Duration is 5 days without any interruption. There is a nozzle spraying a solution of 5% NaCl in weight (in other words 5% NaCl and 95% deionized water). The pH value of the salty solution should be kept between 6.5 and 7.2. The spray should never face directly with the film surfaces, the only effect must be the salty fog on the film. Furthermore the speed of solution drop should be kept between 0.0125-0.0375 ml/(cm^3*hour) on the base of the chamber. Moreover in order not to accumulate solution or salt on the films, the samples placed perpendicularly on an inert (not reacting with the samples during and under the test conditions) holder (this is the same method also applied in humidity test).

Again all samples are exposed to the tests simultaneously on a sample holder.

Environmental test results show that increase in hydrogen flow rate (assuming also an increase in hydrogen content) decreases durability, especially samples coated over the flow rates of 100 cm^3/s, failure on the films starts from the edges. Especially film on sample 18 (coated with H_2 flow rate of 150 cm^3/s) totally destructed after the

environmental tests (Figure 4.39). Furthermore sample 22 which is coated with a H_2 flow rate of 175 cm^3/s failed after 10 months and sample 21 and sample 24 those are coated with H_2 flow rate of 200 cm^3/s failed or destructed totally in only a month after the coating even without any environmental test applied.

There should be two powerful and probable reason for this destruction due to environmental tests; first, increasing hydrogen content decrease elasticity of the film drastically. Especially over 150 cm^3/s as can be observed on Table 4.5, elasticity of the sample 18 is 95 GPa but it is 161 GPa for the sample 27 (which is coated with zero H_2 flow rate). This proves that decrease in elasticity is a weakness considering oscillating temperatures during the humidity test. In other words, oscillating temperatures causes thermal expansion/contraction cycles and due to these cycles there occurs a thermal fatigue and resultantly the film failed.

The second reason for destruction is the intrinsic compressive stress. We stated before that too low and too high intrinsic stresses cause to lose rigidity of the film. Figure 4.25 shows that increasing hydrogen decreases compressive stress too much, this is powerful sign of weakness or instability for a film. Temperature variations in humidity test creates stress variations in the film, this is thought to be the main cause of destruction for such films.

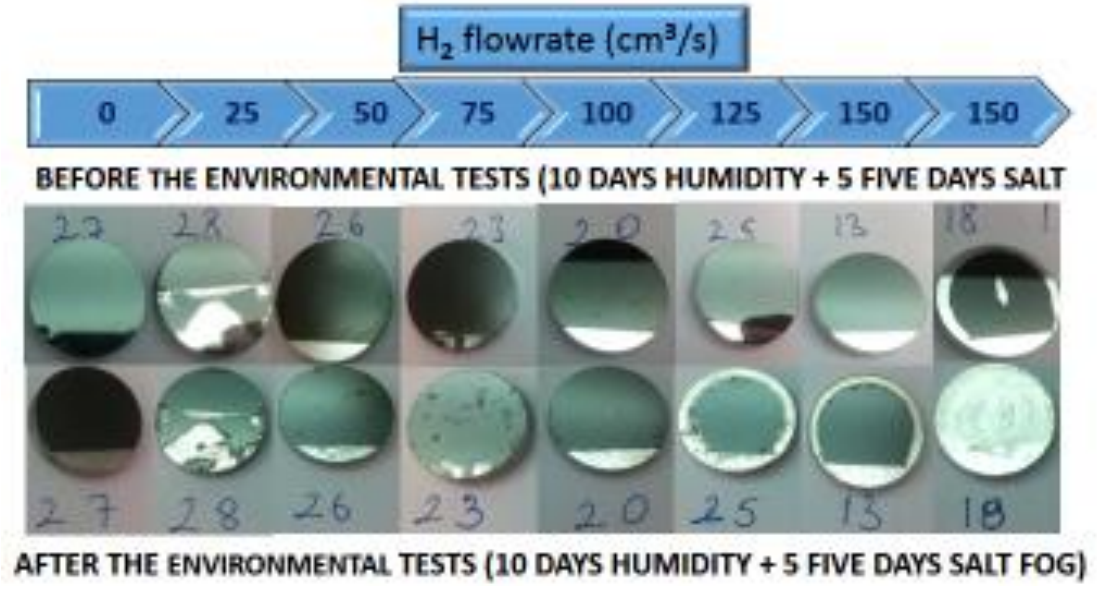

Figure 4.39 Effect of hydrogen content phase samples after environmental tests

To sum up considering all the characterization studies and test results, flow rates of precursor gases should be 150 cm^3/s for hydrogen with respect to a "constant" for acetylene in order to obtain optimum film properties. For the rest of the study and runs this is the pivot point that other trials are going to be done respectively.

4.4 Phase 3: Effect of RF Power

The last parameter for which a series of run and characterization procedure is going to be done is based on Radio Frequency (RF) power that is mainly responsible for the creation of plasma and energy levels of energetic coating agents. In order to investigate the effect of RF on film properties, supply power is to be altered for each run at this third phase. In other words, the aim is to change the RF power between extremities that is meaningful and allowed by machine, hence we set it before the each run and to see what properties are affected. The RF power is going to be controlled by controlling or defining the bias voltage. The bias voltage is then set between 300 V and 850 V and again kept constant to create and control RF power throughout the coating step. 850 V is the machine upper limit set, hence with the machine used it is

not possible to go beyond this voltage value virtually and practically. Coating time of the coating step is again selected as 3620 s as the experiments up to now suggest. Hydrogen flow rate is kept at 150 cm^3/s, acetylene flow rate is not changed also.

4.4.1 Thickness and RF Power

As the part of the strategy mentioned before, third phase trials are done based on bias voltage and it is expected that varying bias voltage also change the RF power. Consequently, it is expected that changing RF power should have effect on the characteristic of the film. Hence a series of coating runs were conducted with different bias voltage. Throughout the runs, all other parameters are conserved as they are at this very beginning. As a first assumption it is expected that changing RF power changes thickness slightly just because of deposition speed and some bonds and bonding types are supposed to be changed. In case of high RF power, there will be more atoms detached from molecules due to high energy they are exposed, hence atom density in plasma cloud will increase, this favors the increase in the speed of coating. However the number of atoms those bounce off from the substrate surface will also increase, on the contrary to energetic effect this will decrease the speed of coating. Then there must be a tradeoff between these presumptions, the thickness of the films will be different though their coating time is exactly the same. Based on these presumptions, following nine successive runs showed that as the RF power increases, the thickness of the films also increases. Furthermore the correlation between them is almost linear as shown in Figure 4.40. Hence energetic dense plasma cloud overwhelm the bounce off effect and this favors the increase in thickness.

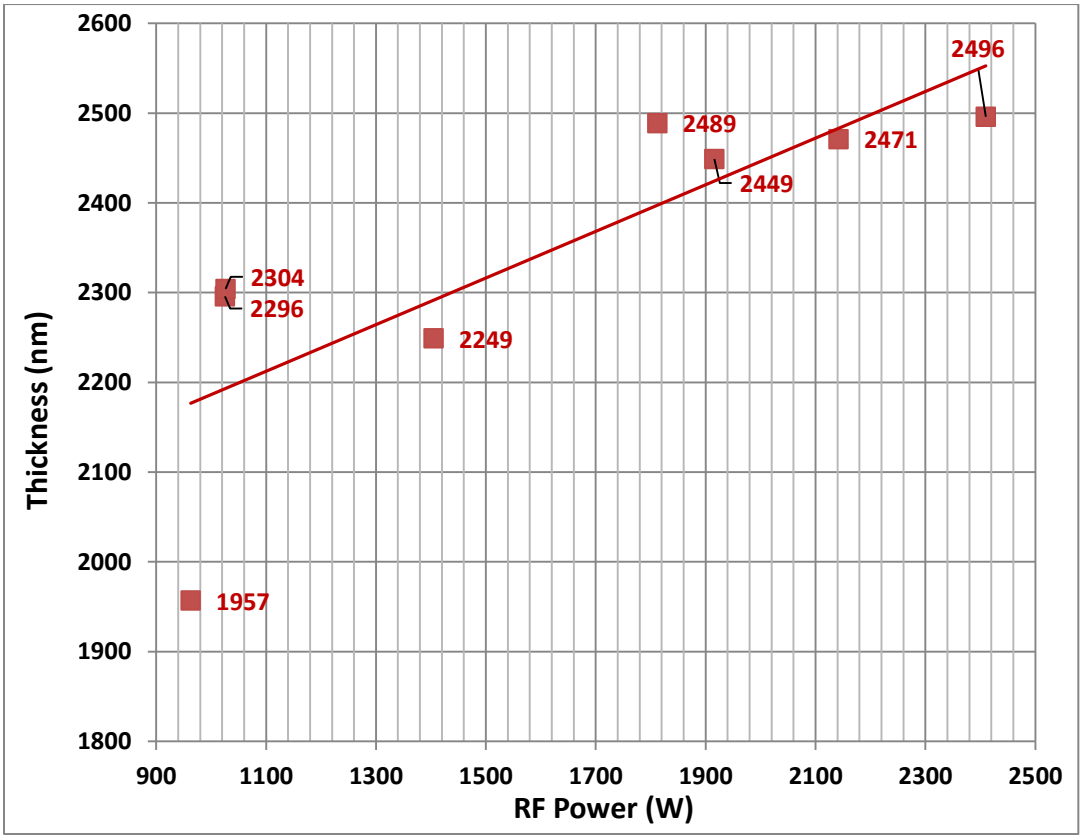

Figure 4.40 Thickness variations vs. RF power for the same period of coating time (3620 s)

4.4.2 Interferometer Measurements: Surface Topography

Like in the former coatings general morphology does not change drastically. On the other hand depending on the RF power applied, optical power of the surfaces are changed slightly. Actually the more RF power means the less optical power difference (ΔP). We know from the literature that DLC films have a tendency to create internal, intrinsic compressive stress and as the compressive stress increases the film gets more convex (Figure 2.9).

However increasing RF power reduces power difference. Decrease in power difference is a powerful indication of decrease in compressive stress, this can easily be followed by Figure 4.41 and Figure 4.42. Although too much compressive stress is detrimental, compressive stress is essential to keep the film rigid, otherwise film

cannot keep its coherence. As it can be read from the Figure 4.42, two films coated with higher RF power of 2142 W (i.e. over bias of 700V) peel off in a short period, one of the most probable explanation is too low compressive stress. We also know from literature (chapter 2.2) that high incident energy during the coating decreases hydrogen content and make the film unstable also.

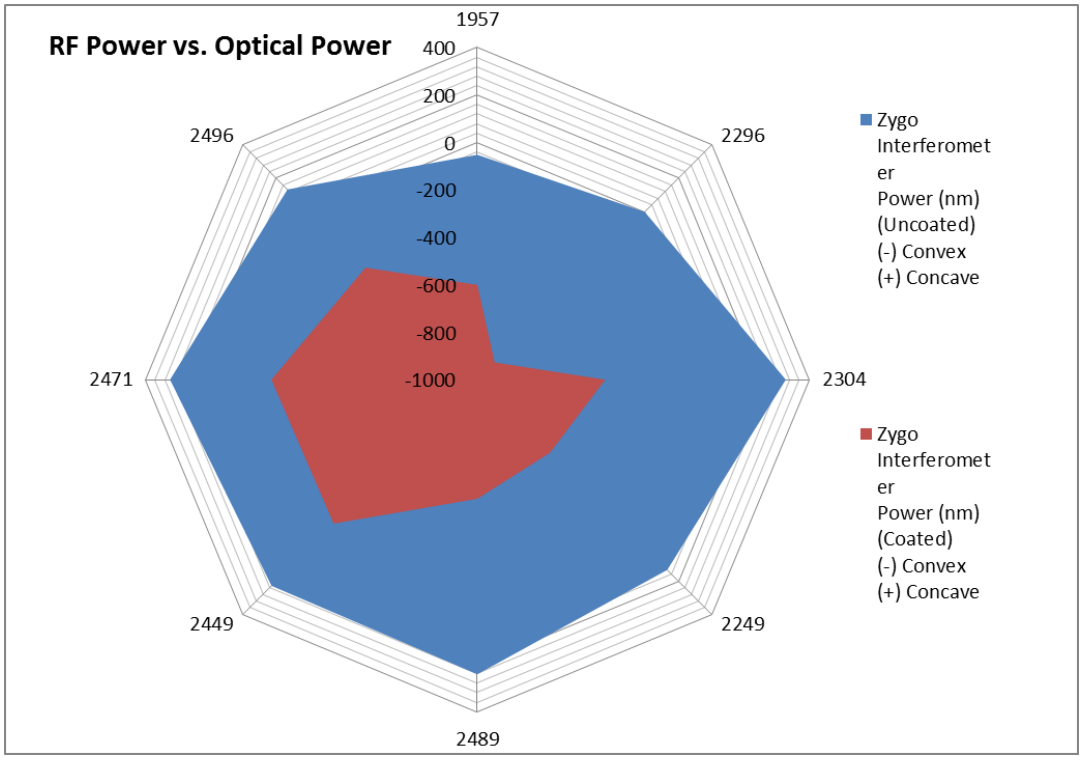

Figure 4.41 Power vs. thickness variations measured by a Zygo red light (600 nm) interferometer

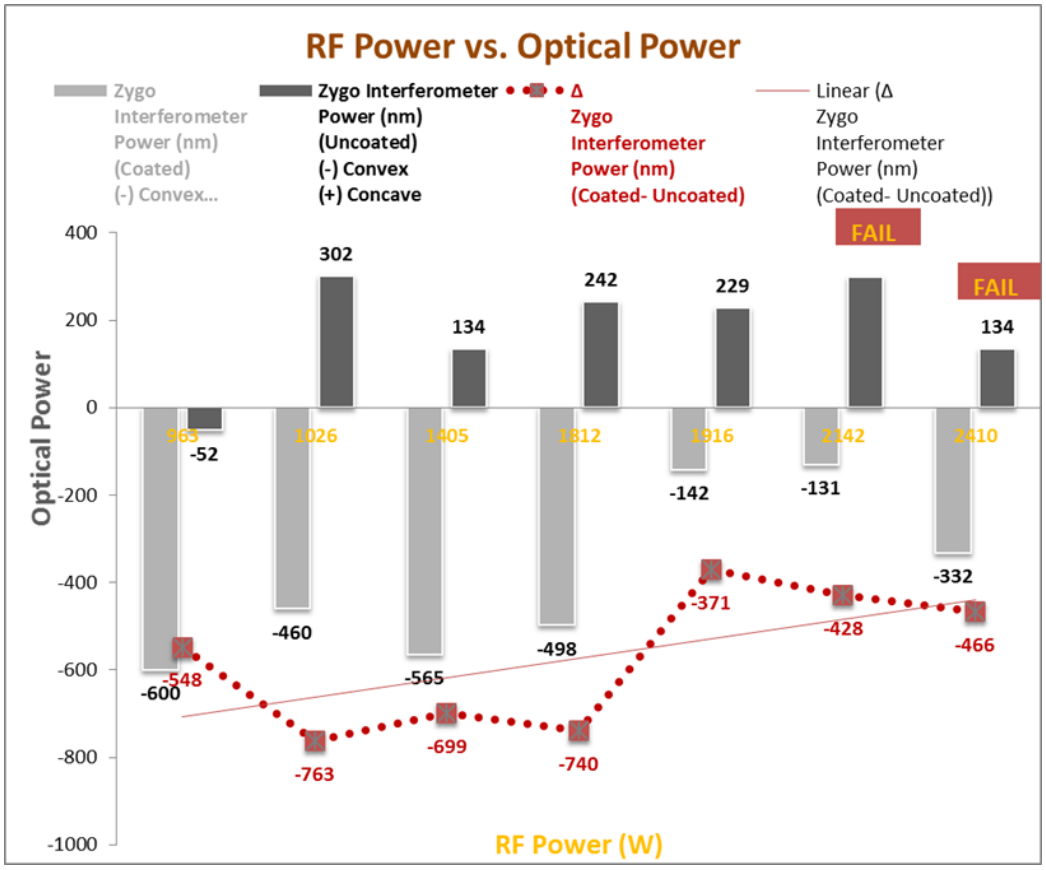

Figure 4.42 RF power vs. optical power measured by a Zygo red light (600 nm) interferometer.

4.4.3 FTIR Measurements: Reflection

As mentioned before near 2500nm thicknesses and for the H_2 flow rates of 150 cm^3/s, the reflectance values are veritably at maximum. The films with different RF power but the same coating durations have different film thicknesses. As mentioned before the reflection values must follow "Quarter Wave Rule". On the other hand since at low bias voltages the RF powers are also low. This condition makes the energy levels of atoms/ions lower. Hence atoms/ions can find enough time to settle down and this make the film more intense, as the intensity increases it is expected that the refractive index (n) also increases. Higher n value makes the optical thickness (nd/λ_0) virtually thicker. Although they are physically thinner, since optical thickness is the essential parameter in optical reflectance or transmittance they can show nearly the same

reflectance with thicker films as shown in Figure 4.44. To sum up changing RF power do not cause an essential shift in reflection behavior in the study.

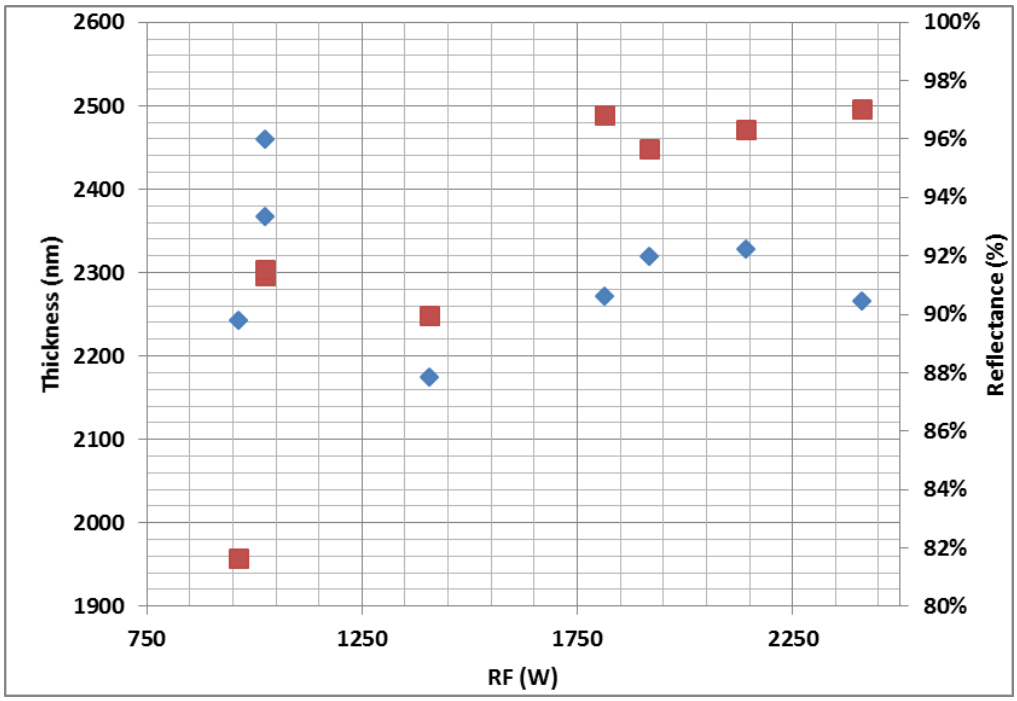

Figure 4.44 RF power (W) vs. reflectance and thickness (average reflectance values at the band of 8-12 μm)

4.4.4 Hardness and Elasticity

Three runs are conducted with bias voltages of 300, 700 and 800 V, respectively and these samples go under test by a nano-indenter in order to measure the hardness and elasticity. It is better to remember that hardness (H) and elastic modulus (E) are fundamental for the tribological characteristics of the film. For a wear resistant hard coating plastic work of indentation or in other words the ratio of hardness (H) to Young's modulus (E) namely H/E defines how the film strain tolerant. It is better to remember that high H/E ratios bring also high elastic recovery rates. Hence high H/E rates make the film more robust and increases the durability of it. Nano-indentation

test results including H/E rates are listed in Table 4.8 and in Figure 4.45 corresponding hardness and elasticity values are also plotted.

The results (Figure 4.45) show that increasing bias and consequently RF power decreases both hardness and elasticity at the same time. Furthermore, although there are only three samples measured, change or decrease can be accepted as linear. This decrease is a powerful sign of again a decrease in sp^3/sp^2 rate. Furthermore the "recovery power" or in other words hardness to elasticity ratio is 0.15 and it will slightly increase to 0.16 as the RF power increases and the hardness values decreases.

Table 4.8 Tabulated hardness (H) and elasticity (E) values measured by nano-indenter of the 3 samples

Al Sample No	Max. Temperature (°C)	Max. RF Power (W)	RF Coating Step Control Bias Voltage (V)	Hardness - HIT (GPa)	Elasticity - EIT (GPa)	H / E rates (Recovery power)
34	94	963	300	17.7	120.9	0.15
18	148	1812	700	14.9	95.0	0.16
35	166	2142	800	13.8	87.7	0.16

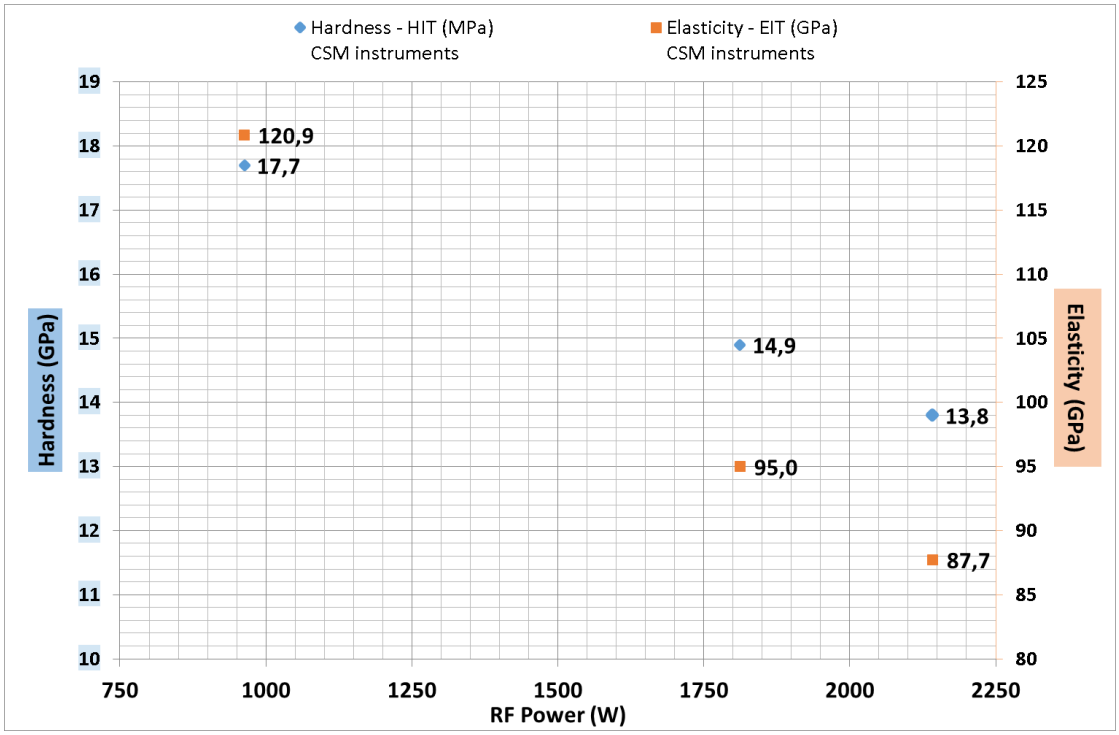

Figure 4.45 Hardness (H) and elasticity (E) values measured by nano-indenter for the three samples

The threshold for a hard coating is 10 GPa and if the hardness is above 10 GPa the coating is still accepted as hard. Furthermore the measured elastic modulus of the samples are in the range of 88 – 121 GPa, this also conforms the literature expectations for hydrogenated amorphous DLC films (60 - 210 GPa, Table 2.5). Furthermore, the measured H/E rates of samples are between 0.15-0.16 which falls again in the class of hydrogenated amorphous DLC films those in the range of 0.1 – 0.16 defined in literature (Table 2.5).

4.4.5 Frictional Analyses

Four coated samples namely sample 18, sample 34, sample 35, sample 37 from different runs with different mean RF powers are selected. Coating times of coating step for these three samples are the same (tc=3620 s). RF power of these four samples are tuned by changing bias voltage and bias voltages are 700 V, 300 V, 800 V and 850

V and maximum RF powers recorded during the runs are 1812 W, 963 W, 2142 W and 2410 W, respectively. The maximum allowable RF power is limited as 2500 W by the machine safety regulations, hence it is not possible to go beyond 2500 W practically. Unfortunately sample 37 with 850 V bias voltage peeled off after the run in a very short time. The test parameters are the same with scratch tests done before.

4.4.5.1. Frictional Analyses for Sample 18

Since frictional analysis is argued in section 4.2.5.3 it will not be repeated here. Please refer section 4.2.5.3.

4.4.5.2. Frictional Analyses for Sample 34

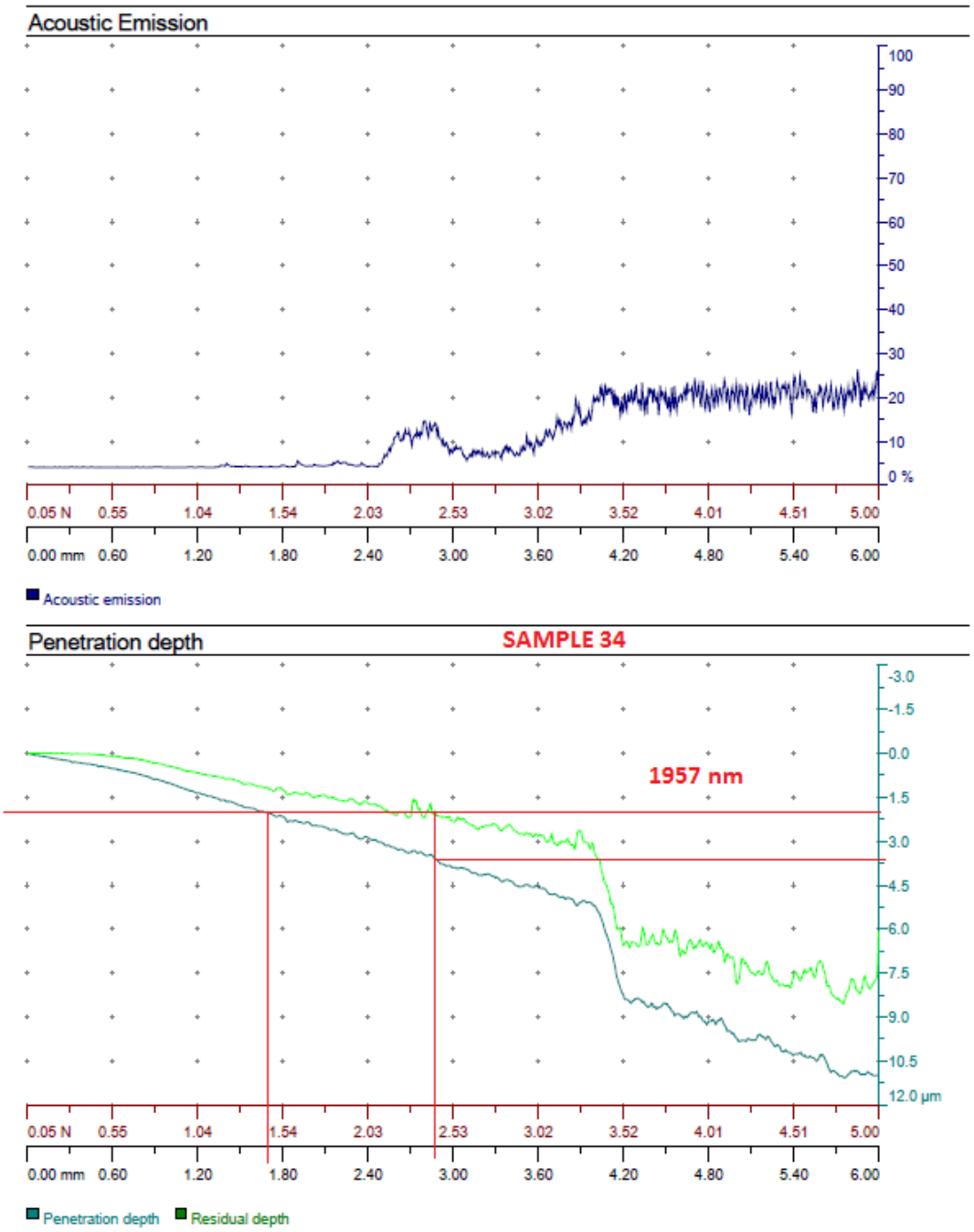

Figure 4.46 Change of acoustic emission and penetration depth vs normal load and scratch length (Sample 34)

Sample 34 has 1957 nm DLC film thickness, besides it is coated with the lowest bias voltage (300 V) and resultantly one of the lowest RF power (maximum RF power recorded during its run is 963 W). Penetration depth (Figure 4.46) reaches 1957 nm at about 1.70 mm from the point of first touch. On the other hand residual depth of 1957 nm registered at about 2.88 mm, and to reach this as residual, the tip must penetrate about 3.65 micron which is then so called as the penetration depth. Although 3.65 micron is much greater than the film thickness, at the corresponding travel distance (2.88 mm) the film still survives to exist on the substrate as it is seen below (Figure 4.47). Furthermore at this point the (Penetration depth – Residual depth) / Film thickness ratio is about 0.87. This is the lowest restoration ratio measured up to now. Hence the restoration ability under a destructive stress is fairly poor with respect to the films coated up to now. As Figure 4.47 also suggests that mechanical durability of the film is also fairly poor because total destruction is observed very early at about 4.4 mm. Furthermore aluminum substrate surface is seen on the sides of scratched region (starting from the initial touch point of scratch) at 1 mm seen below (Figure 4.47), that shows the film is very keen on to peel off under such a scratching stress effect.

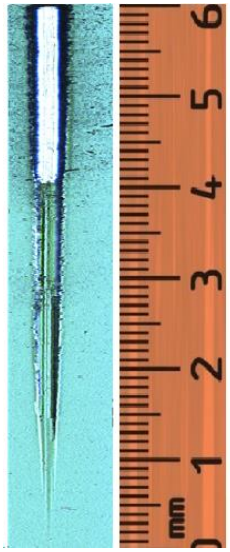

Figure 4.47 Scratch print after the scratch test for sample 34

Figure 4.47 shows that film starts to lose its integrity at about 1.3 mm starting with a dark region (tiny ruptures) on the right side in the Figure 4.47. Hence location just before this point can be accepted as optimum point where friction coefficient of the DLC film can be measured and defined. Then friction coefficient of the film is 0.17 at 1.3 mm from the point of start (Figure 4.48).

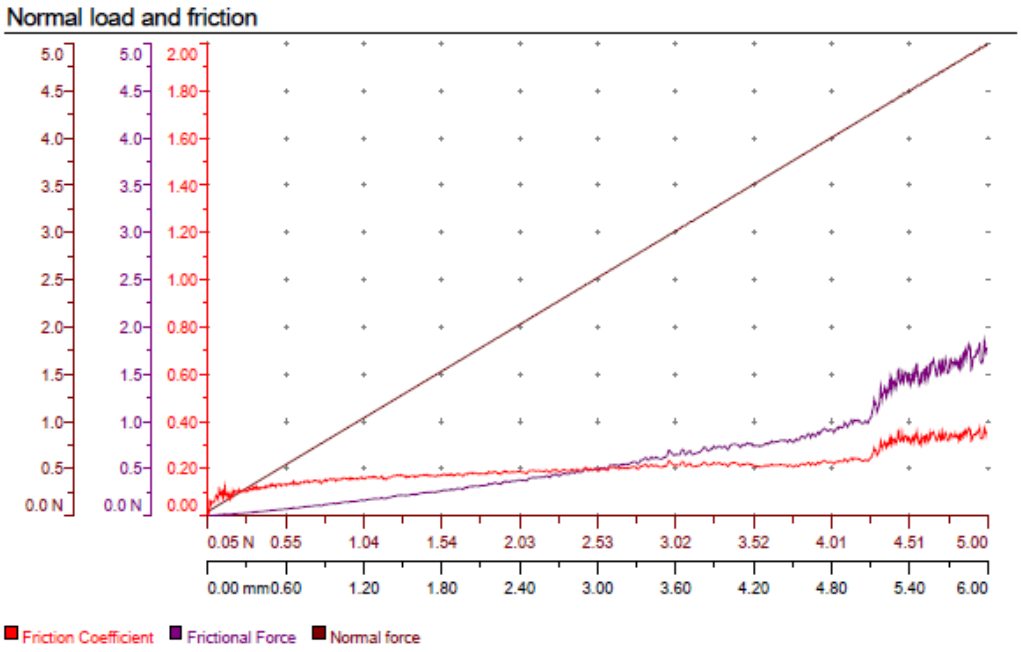

Figure 4.48 Normal load and scratch length vs friction coefficient/frictional force/normal force (Sample 34)

Furthermore, after about 4.1 mm (Figure 4.47) film goes almost total destruction, and it is not possible to talk about a film after this point. 4.1 mm is one of the shortest length up to now. It seems that low RF power is deadly decrease durability of the film in case of such destructive attack.

4.4.5.3.Frictional Analyses for Sample 35

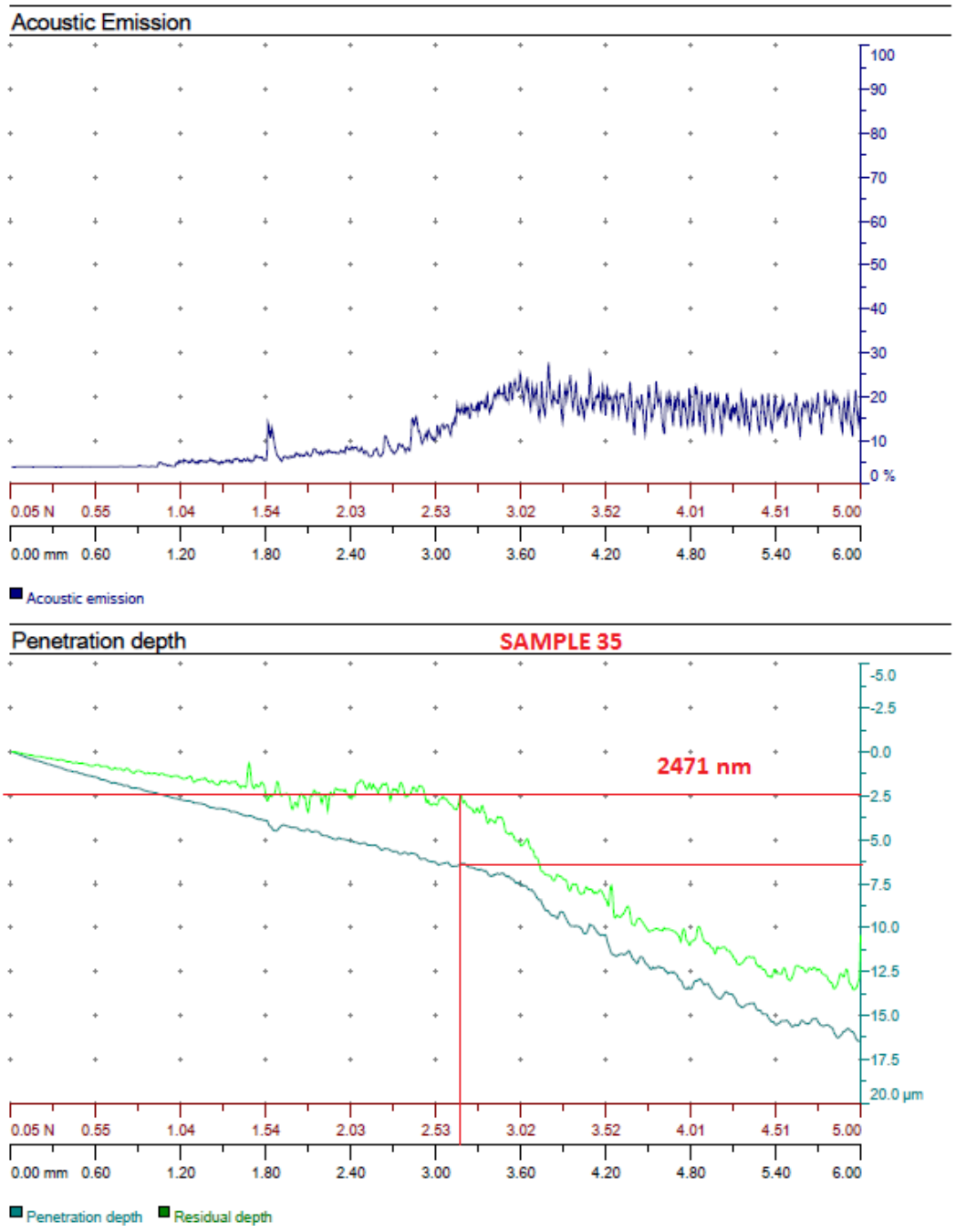

Figure 4.49 Change of acoustic emission and penetration depth vs normal load and scratch length (Sample 34)

Sample 35 has 2471 nm DLC film thickness, besides it is coated with one of the highest bias voltage (800 V that can stand more than a day) and resultantly almost the highest RF power (maximum RF power recorded during its run is 2142 W). Penetration depth (Figure 4.49) reaches 2471 nm at about 1.10 mm from the point of first touch. On the other hand residual depth of 2471 nm registered at about 3.20 mm, and to reach this residual the tip must penetrate about 6.5 micron which is then so called as the penetration depth. 6.5 micron is much greater than the film thickness, at the corresponding travel distance (3.20 mm) although the film is destructed totally there is still film on the substrate after from the this point (i.e. at 4 mm the tip penetrate the film more than 10 micron) as it is seen below (Figure 4.50). Hence although it is hard to designate where the total destruction point is, it is for sure that the film stability regarding the scratching effects is not the best. Furthermore the (Penetration depth – Residual depth) / Film thickness ratio is about 1.63. This is the one of the highest ratio measured up to now. However Figure 4.50 suggests destructed regions cannot be foreseen easily and that means mechanical durability of the film is fairly unstable (Figure 4.50), which shows the film is very keen on to peel off under such a scratching effect. We also know that 2 samples, namely Sample 36 and Sample 37 those are coated with highest bias voltages (800V) and RF power (2410 W) that the coating machine allows cannot stand more than a few minutes after the run. Hence integrity of the films coated with high RF powers are not good at all.

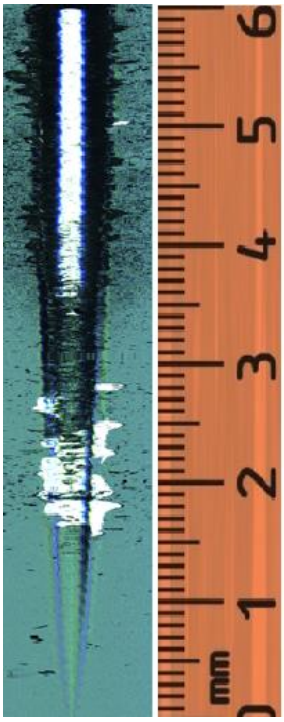

Figure 4.50 Scratch print after the scratch test for sample 35

Figure 4.50 shows that film starts to show unforeseen and unstable behaviors. There it peels off near 2 mm (Figure 4.50). Furthermore starting from 1.0 mm there can be seen dark sides. Hence this point just can be accepted as optimum point where friction coefficient of the DLC film can be measured and defined. Then friction coefficient of the film is 0.20 at 1.0 mm from the point of start (Figure 4.51). This is the highest friction coefficient, hence it is the worst sample and the film in terms of friction. To sum up we can conclude that increasing FR power also increases friction coefficient and decreases durability of the film.

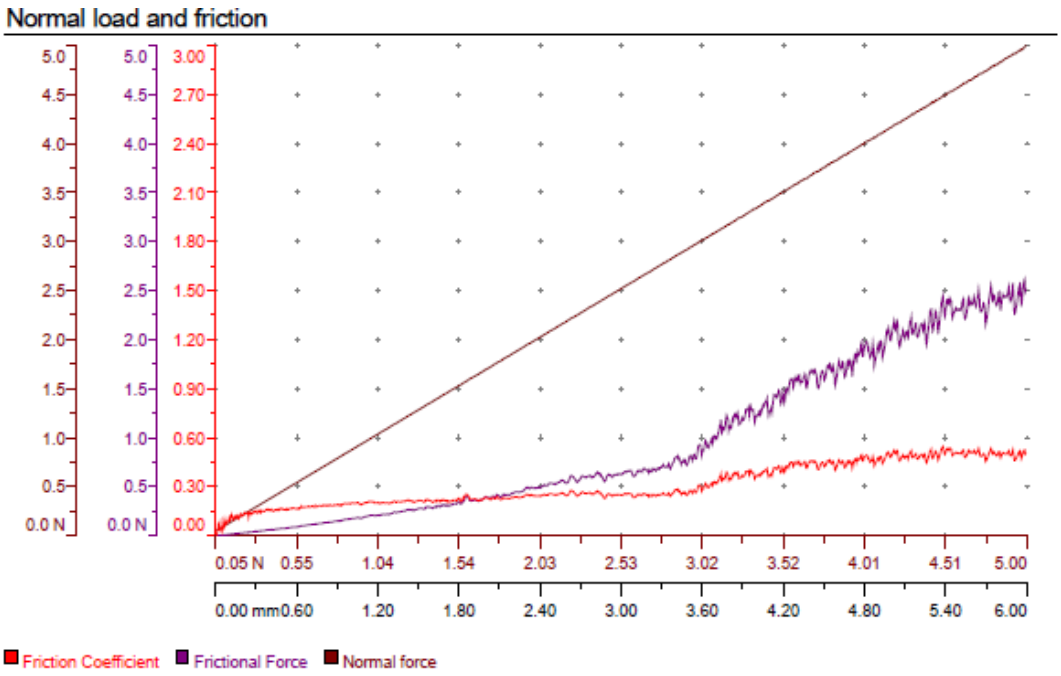

Figure 4.51 Normal load and scratch length vs friction coefficient/frictional force/normal force (Sample 35)

As a result increasing RF power also increases the "Restoration Power" (Table 4.9). However as mentioned before too high RF power is destructive for the film. Actually about 2142 W film becomes unstable and unpredictable peeling points can be observed on the film (Figure 4.50). Furthermore at 850 W (this is the upper machine limit in our case) the film cannot stand even for a single day and generally it is peeled off after the run immediately (two runs were done at this upper limit). Although there is not enough data, we observed and may state that friction coefficients also increases with increasing RF power.

Table 4.9 Scratch test results for samples 18, 34, 35, 37

Al Sample No	Thickness (nm)	Bias Voltage (V)	Max. RF Power (W)	Penetration Depth (nm)	Residual Depth (nm)	Restoration Power	Friction Coefficient	Total Destruction Length (mm)
18	2489	700	1812	5800	2489	1.33	0.18	4.2
34	963	300	963	3650	1957	0.87	0.17	4.1
35	2142	800	2142	6500	2471	1.63	0.20	Unpredictable
37	2410	850	2410	-	-	-	-	(Already Destructed)

4.4.6 Structure Analysis (XPS)

In this phase XPS measurements and analysis are done to characterize RF power effect on the films. Sample 18, sample 34, sample 35, sample 37 are selected to analyze. However films on the sample 35 and sample 37 were peeled off and there was no chance to measure and characterize by XPS. This also proofs that over 700V of bias and respectively over about 1900-2000 W, it is not possible to get films of high durability. Then sample 31 and sample 32 (bias voltages during their runs are below 700V) are selected as subsidies to be measured to get a set of measurement. All of the samples are measured on a spot size of 200 μm and each spot is placed arbitrarily on the surface, in other words measurements are taken from different locations for each sample. It is worth to remember that mean energy levels for sp^3, sp^2 and C-O bonds are respectively 285.20 eV, 284.55 eV and 287 eV and although there is no input to add any oxygen, results show that there are C-O bonds and we deduced that C-O bonds are due to oxidation after the runs exposing the samples to atmosphere. Although 3-6 min argon sputtering process is applied before each measurement, it is not possible to remove oxygen totally.

Almost all results verify that the films are in the class of hydrogenated amorphous DLC films defined by literature (table 2.1). Like in the other two phases there cannot be observed any correlation between RF power and sp^3/ sp^2 ratios. Besides, it seems that distribution of sp^3/sp^2 is random in other words sp^3, sp^2 distribution is not uniform throughout the film. Moreover sp^3/sp^2 ratios also change between 1.43 and 2.37 and show no correlation and very similar to results obtained in the other phases.

Table 4.10 XPS results for samples 18, 34, 35, 37, 31, 32

Al Sample No	H_2 - C_2H_2 Flow Rates (cm^3/s)	RF Coating Step Control Bias Voltage (V)	Coating Time (s)	Profilometer Measured Thickness (nm)	sp^3 ~@285.20 eV (%)	sp^2 ~@284.55 eV (%)	C-O ~@287 eV (%)	sp^3/sp^2
18	150-100	700	3620	2489	63.15	26.66	10.18	2.37
34	150-100	300	3620	1957	60.01	29.61	10.37	2.03
35	150-100	800	3620	2471	no film	no film	no film	no film
37	150-100	850	3620	2496	no film	no film	no film	no film
31	150-100	400	3620	2304	57.95	39.16	2.89	1.48
32	150-100	500	3620	2296	50.01	35.01	3.54	1.43

To sum up considering all the results, sp^3/sp^2 rates are all in a range of 1.32 – 2.37. Although sp^3-sp^2 distribution is always random and different throughout any film regardless of thickness and RF power or hydrogen flow rates, highest sp^3 rate is obtained with highest energy (or RF Power) as in the Table 4.10 which is consistent with literature (Figure 2.7 Incident energy vs relative density, hydrogen content, sp^3 fraction).

4.4.7 Environmental Tests: Humidity + Salt Fog

As mentioned before the environmental tests composed of 10 days humidity test and 5 days salt fog tests. Humidity test is a 5 cycles test and each cycle is composed of 2 days. Temperature is not constant and altered between minimum and maximum temperatures of 20 °C and 60 °C, respectively as seen on Figure 3.9. Besides, 95% relative humidity is conserved throughout the 10 days test in the test chamber.

Please remember that after the humidity test the salt fog test comes. In salt fog test there is temperature constraint that temperature should be kept constant at 35 °C in a

closed test chamber throughout the test run. Duration is 5 days without any interruption. There is a nozzle spraying a solution of 5% NaCl in weight (in other words 5% NaCl and 95% deoinized water). The pH value of the salty solution should be kept between 6.5 and 7.2. The spray should never face directly the film surfaces, the only effect must be the salty fog on the film. Furthermore the speed of solution drop should be kept between 0.0125-0.0375 ml/(cm^3*hour) on the base of the chamber. Moreover, in order not to accumulate solution or salt on the films, the samples placed perpendicularly on an inert (not reacting with the samples during and under the test conditions) holder (this is the same method also applied in humidity test).

As mentioned before all samples (including complete set of samples of three phase) are exposed to the tests together and simultaneously on a sample holder.

Environmental test results show that increase in FR power decreases durability, especially sample 13 coated with 1916 W gets start to fail starting from the edges after the tests. Furthermore sample 35 which is coated with RF power of 2142 W and sample 37 coated with 2410 RF power failed or destructed totally in only hours after the run in normal room conditions, and these films even are not exposed to any environmental test (Figure 4.53).

Increasing RF power by means of increasing bias voltage, decreases elasticity of the film drastically (Table 4.8). Decrease in elasticity is a weakness considering oscillating temperatures during the humidity test. In other words oscillating temperatures cause thermal expansion/contraction cycles and due to these cycles there occurs a thermal fatigue and resultantly the film failed.

The results (Figure 4.45) show that increasing bias and consequently RF power decreases both hardness and elasticity at the same time. Furthermore, although there are only three samples measured, change or decrease can be accepted as linear. This decrease is a powerful sign of again a decrease in sp^3/sp^2 rate. Furthermore the "recovery power" or in other words hardness to elasticity ratio is 0.15 and it will slightly increase to 0.16 as the RF power increases and the hardness values decreases.

Figure 4.53 Effect of RF Power phase samples after environmental tests

4.5 Verification of Amorphous Structure by XRD

At the very beginning of study all assumptions are done by accepting that all the films coated on the samples are amorphous. Indeed results and analyses confirm to what literature says for hydrogenated amorphous diamond like carbon. On the other hand, one of the best way to see and show that all the DLC films coated on the surfaces are amorphous is to look at and characterize them by XRD. Accordingly, a series of XRD measurement and analysis are done for four samples from three distinct sub-studies or phases from this thesis and from a bare/uncoated aluminum sample. Namely sample 5, sample 18, sample 34 and an uncoated aluminum sample is chosen to represent related classes. Results are in the graphs below (Figure 4.54, Figure 4.55, Figure 4.56 and Figure 4.57).

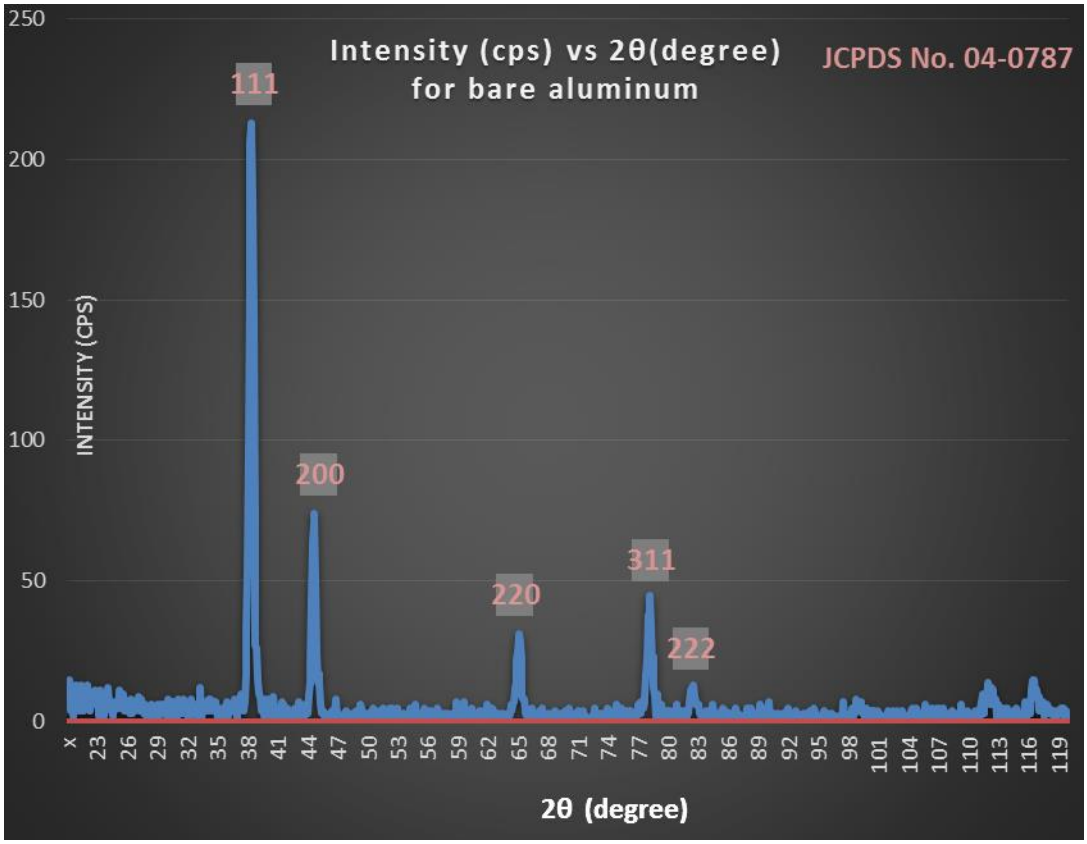

Figure 4.54 XRD spectrum for bare aluminum

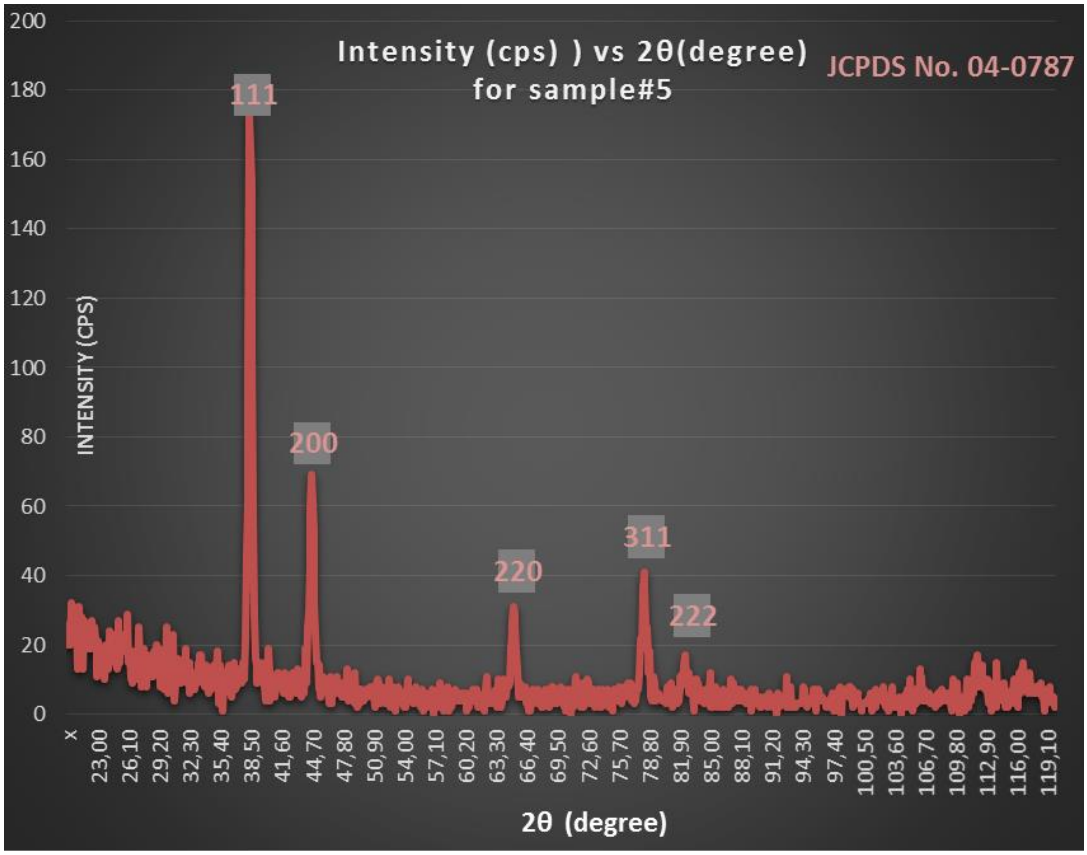

Figure 4.55 XRD spectrum for sample 5
(coating time = 1000 s; thickness = 875 nm; max. coating temp. = 142°C; H_2 flow rate = 150 cm^3/s; bias voltage = 700 V; max. RF power = 1767 W)

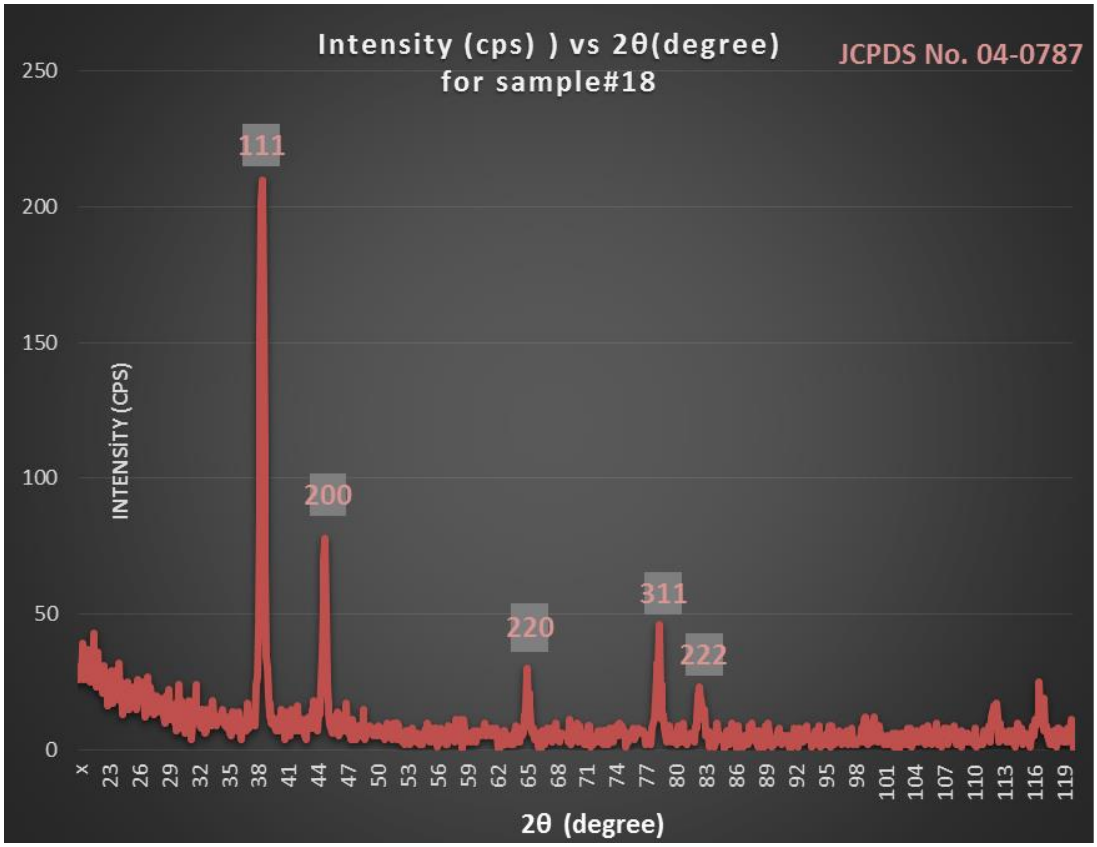

Figure 4.56 XRD spectrum for sample 18
(coating time = 3620 s; thickness = 2489 nm; max. coating temp. = 148°C; H_2 flow rate = 150 cm^3/s; bias voltage = 700 V; max. RF power = 1812 W)

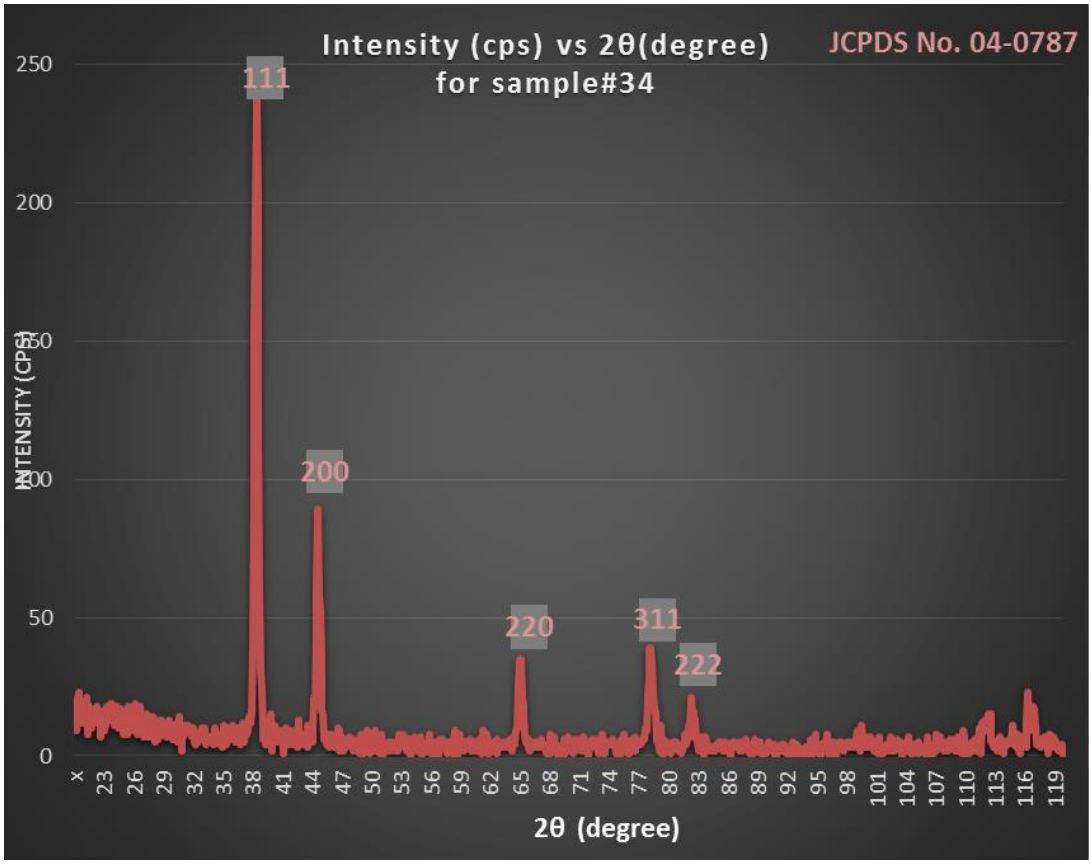

Figure 4.57 XRD spectrum for sample 34
(coating time = 3620 s; thickness = 1957 nm; max. coating temp. = 94°C; H_2 flow rate = 150 cm^3/s; bias voltage = 300 V; max. RF power = 963 W)

All samples including bare aluminum and the three films coated have almost the same peaks on the same locations of intensity peaks of x- axis. Hence the DLC films cannot be distinguished as a different crystal structure than bare aluminum itself. That means all the films are amorphous without a dominant crystallographic structure.

CHAPTER 5

CONCLUSION and FURTHER SUGGESTIONS

We learnt from the interferometer measurements that increasing thickness also increases tension (T) and if this tension overwhelm the adhesion force of the film, the film can be destructed easily. Furthermore, increasing hydrogen content have the reverse effects on intrinsic compressive stress and decreases it, and but this decrease can also be detrimental to the film. Experiments also show that too much energy (an output of high RF Power in our case) reduce hydrogen content, intrinsic compressive stress and resultantly can also harm on and reduces the life of the film. Hence one should care of all these parameters and decide, by making a meaningful trade off, which properties are aimed for the film to have at the end of the day.

Reflectance is directly dependent on the film thickness (t) and refractive index (n). Experiments and characterization works show that 2500 nm film thickness and 150 cm^3/s H_2 flowrates are ideal for maximum reflectance in our case. Besides changing RF power does not change the reflectance noticeably.

We know that refractive index of the DLC films is about 1.931. For the future studies, since high-index layers give enormous reductions in reflectance as mentioned in 2.5.2, it is a good idea to lower the refractive index “n” of the DLC films.

Besides, an elipsometer can give valuable results especially in terms of optical constant “n” and “k” which are the core constants to define reflectivity. If an elipsometer which can make measurements in the infrared band of 8 – 12 micron could be reached, it would be very beneficial for this study.

Experiments show also that thickness of 2500 nm is ideal for hardness, elasticity and the recovery power (H/E) in our case. Furthermore increasing hydrogen content decreases both hardness and elasticity together, on the other hand the recovery power is not decreased, on the contrary it increases from 0.14 - 0.15 to 0.16. Similarly increase in RF power has nearly the same effect on the film.

Frictional analysis prove that increasing only thickness adds nothing to friction coefficient and restoration power but avoids having contact with the aluminum surface. Moreover we observed that as the hydrogen content decreases, the total destruction length elongates, so this makes the film more robust. Furthermore too high RF powers are detrimental for hydrogenated amorphous diamond like carbon films, hence it is not preferred at this case.

XPS results show that sp^3/sp^2 distribution is not uniform throughout the films. On the other hand, it seems that there is a positive correlation between hydrogen content and sp^3 fractions. Though non-uniformity, results show that increase in RF power may result a slight increase in sp^3 content. Furthermore, although sp^3 percentage of sample 18 is over a little than expected literal value, the rest is in the accepted range as shown in the Table 5.1.

Table 5.1 sp^3 percentages for all XPS results

Al Sample No	5	7	15	18	20	26	27	34	31	32
Expected rates (%) of intervals for sp^3 content: 20%-60%	55.09 - 61.88	49.11	54.78	63.15	48.76	58.43	50.72	60.01	57.95	50.01

Furthermore it will be very beneficial to measure hydrogen content by a direct experimental method. The writer advice people who will study further on this subject to find or build an experimental set up for this purpose.

Lastly environmental tests show that since any increase in film thickness also increases total amount of tension, it also decreases the durability of the film considering rated temperature changes. Furthermore, we observed that elasticity is decreased with increasing hydrogen content, hence this decrease in elasticity is another reason to fail in a relatively harsh and unstable environment. Moreover too low or high RF powers cause the similar results with high hydrogen content and make the film more vulnerable to severe environmental conditions.

REFERENCES

[1] C. Donnet, A. Erdemir, «Tribology of diamond-like carbon films: recent progress and future prospects,» Journal of Physıcs D: Applıed Physıcs 39, pp. pp 312-312, 2006.

[2] D. Hofmann, K. Bewilogua ,«History of diamond-like carbon films — From first experiments to worldwide applications,» Surface & Coatings Technology 242, pp. pp 214-215, 2014.

[3] J. A. Byrne, J. McLaughlin, A. Waqar, H. A. Mukhtar, «Study of Human Serum Albumin Adsorption and Conformational Change on DLC and Silicon Doped DLC Using XPS and FTIR Spectroscopy,» Journal of Biomaterials and Nanobiotechnology 4, pp. 194-203, 2013.

[4] H. O. Pierson, Handbook of chemical vapor deposition, New Mexico: Noyes Publications, 1992.

[5] A. Soininen, Studies Of Diamond-Like Carbon And Diamond-Like Carbon Polymer Hybrid Coatings Deposited With Filtered Pulsed Arc Discharge Method For Biomedical Applications., Helsinki: ORTON Research Institute, 2015.

[6] J. Robertson, «Mechanism of sp3 bond formation in the growth of diamond-like carbon,» Diamond & Related Materials 14 , pp. pp 943-947, 2004.

[7] A. Erdemir, J. Fonatine, C. Donnet, «An Overview of Superlubricity in Diamond-like Carbon Films,» %1 içinde Tribology of Diamond -Like Carbon Films, New York, Springer, 2008, pp. 237-262.

[8] A. Mansour, Structural Analysis of Planar sp3 and sp2 Films: Diamond-Like Carbon and Graphene Overlayers, Thuwal: King Abdullah University of Science and Technology, 2011.

[9] Y. Lifshitz, «Diamond-like carbon — present status,» Diamond and Related Materials 8 , p. 1659–1676, 1998.

[10] J. Vlcek, P. Fitl, M. Vrnata, L. Fekete, A. Taylor, F. Fendrych, «UV-laser treatment of nanodiamond seeds—a valuable tool for modification of nanocrystalline diamond films properties,» J. Phys. D: Appl. Phys. 46 , pp. 2-6, 2012.

[11] K. Bewilogua, D. Hofmann, «History of diamond-like carbon films — From first experiments to worldwide applicaitons,» Surface & Coatings Technology 242, pp. pp 215-220, 2014.

[12] S. Pellicori, «Durable Coatings For IR Window Materials,» %1 içinde Durable Coatings For IR Window Materials, 2008.

[13] A. Macleod, Optical Coatings From Design Through Manufacture, Tucson: Thin Film Center Inc, 1999.

[14] A. Erdemir, J. Fonatine, C. Donnet, «Fundamentals of the Tribology of DLC Coatings,» %1 içinde Tribology of Diamond -Like Carbon Films, New York, Springer, 2008, pp. 139-154.

[15] A. Grill, «Electrical and optical properties of diamond-like carbon,» Thin Solid Films 355-356 , pp. 189-193, 1999.

[16] C. Yi-Nan, M. Tian-Bao,Z. Peng-Zhe, Y. Da-Chuan, H. Yuan-Zhong, C. Zhe, W. Hui, «Growth mechanismof hydrogenated amorphous carbon films:Molecular dynamic simulations,» Surface& Coatings Technology 258, pp. 901-907, 2014.

[17] C. Angus, C. Cliff, J. Hayman, «Low-Pressure, Metastable Growth of Diamond and "Diamondlike" Phases,» SCIENCE, VOL. 241, pp. 913-921, 1988.

[18] B. Tian, P.K. Chu, X.M. Cui, H.Q. Zhang, L.H. Li, «Growth and nucleation of diamond-like carbon (DLC) film on aluminum,» Nuclear Instruments and Methods in Physics Research B 206 , p. 691–695, 2003.

[19] G.M. Pharr, Y.J.Park, T.R. Watkins, A.Z. Misra, X. Zhang, C.M. Lepienski, «Factors limiting the measurement of residual stresses in thin films by nanoindentation,» Thin Solid Films 447–448 , p. 251–257, 2004.

[20] Y.Paluleau, «Residual Stresses in DLC Films and Adhesion to Various Substrates,» %1 içinde Tribology of Diamond -Like Carbon Films, Springer, 2008, p. 102.

[21] H. Ronkainen, Tribological properties of hydrogenated and hydrogen-free diamond-like carbon coatings, Espo: VTT Publicaitons, 2001, pp. 1-53.

[22] G.J. KolK, «Wear Resistance of Amorphous DLC and Metal Containing DLC in Industrial Applications,» %1 içinde Tribology of Diamond -Like Carbon Films, New York, Springer, 2008, pp. 484-493.

[23] G. Pagnouxa, S. Fouvryb, M. Peigneyc, B. Delattrea, G. Mermaz-Rolleta, «Influence of scratches on the wear behavior of DLC coatings,» Wear 330-331 , pp. 380-389, 2015.

[24] A. Erdemir, J. Fonatine, C. Donnet, «An Overview of Superlubricity in Diamond-like Carbon Films,» %1 içinde Tribology of Diamond -Like Carbon Films, New York, Springer, 2008, pp. 237-262.

[25] A. Grill, C. Donneta, «Friction control of diamond-like carbon coatings,» Surface and Coatings Technology 94-95, pp. 456-462, 1997.

[26] K.L. Choy, «Chemical vapour deposition of coatings,» Progress in Materials Science 48, p. 57–170, 2003.

[27] C.Jones, M.L. Hitchman, Chemical Vapour Deposition. Precursors, Processes and Applications, Cambridge: Royal Society of Chemistry, 2009.

[28] G. Fedosenkoa, D. Korzeca, A. Schwabedissena, J. Engemanna, E. Bracab, J.M. Kenny, «Comparison of diamond-like carbon films synthesized by 2.45 GHz microwave and 13.56 MHz multi-jet radiofrequency plasma sources,» Diamond and Related Materials 10, pp. 920-926, 2001.

[29] L.Y. Huang, K.W. Xu,J. Lu, B. Guelorget, «Analysis of nano-scratch behavior of diamond-like carbon films,» Surface and Coatings Technology 154, p. 232–236, (2002).

[30] L. Huanga, J. Lub, K. Xua, «Elasto-plastic deformation and fracture mechanism of a diamond-like carbon film deposited on a Ti–6Al–4V substrate in nano-scratch test,» Thin Solid Films 466, pp. 175-182, 2004.

[31] T. Y. Leung, W. F. Man, P.K. Lim, W.C. Chan, F. Gaspari, S. Zukotynski, «Determination of the sp3/sp2 ratio of a-C:H by XPS and XAES,» Journal of Non-Crystalline Solids 254 , pp. 156-160, 1999.

[32] X. Lei, J. X. Ma, "Synthesis and Electrochemical Performance of Aluminum Based Composites," Journal of the Brazilian Chemical Society 21, pp. 209-213, 2009.

[33] M. Cloutier, C. Harnagea, P. Hale, O. Seddiki, F. Rosei, D. Mantovani, «Long-term stability of hydrogenated DLC coatings: Effects of aging on the structural, chemical and mechanical properties,» Diamond & Related Materials 48 , p. 65–72, (2014).

[34] A. K. Gangopadhyay, P. A. Willermet, W. C. Vassell, M. A. Tamor, «Amorphous hydrogenated carbon films for tribological applications II. Films deposited on aluminium alloys and steel,» Tribology International, pp. pp 19-31, 1997.

[35] tydexoptics, «http://www.tydexoptics.com/coatings/DLCcoatings/,» 1994. Available: http://www.tydexoptics.com/. [Retrieved: 10. 06. 2017].

[36] M. Shojiro, I. Junichi, M. Masatoshi, «Dependence ofthefrictiondurabilityofextremelythindiamond-like carbon films on film thickness,» Wear 356-357, p. 66–76, (2016).

APPENDICES

APPENDIX A

Table 6.1 Process parameters for all runs

Al Sample No	Max. Temperature (°C)	Max. RF power (W)	H_2 - C_2H_2 Flow Rates (cm^3/s)	RF Coating Step Control Bias Voltage (V)	Coating Time (s)
1	145	1776	150-100	700	1800
2	140	1799	150-100	700	1600
3	143	1781	150-100	700	1400
4	140	1850	150-100	700	3000
5	142	1767	150-100	700	1000
6	149	1857	150-100	700	2000
7	144	1836	150-100	700	2200
8	142	1872	150-100	700	2500
10	143	1940	150-100	700	3400
11	145	1931	150-100	700	3536
12	142	1944	150-100	700	3620
13	141	1916	150-100	700	3620
14	-	-	150-100	700	3620
15	139	1910	150-100	700	3750
16	-	-	150-100	700	3620
17	139	1920	150-100	700	4000
18	148	1812	150-100	700	3620
19	147	1901	150-100	700	4500
20	107	1319	100-100	700	3620
21	176	2370	200-100	700	3620
22	152	2119	175-100	700	3620
23	86	112	75-100	700	3620

Table 6.1 Process parameters for all runs (cont'd)

Al Sample No	Max. Temperature (°C)	Max. RF power (W)	H_2 - C_2H_2 Flow Rates (cm^3/s)	RF Coating Step Control Bias Voltage (V)	Coating Time (s)
24	164	2394	200-100	700	3620
25	108	1597	125-100	700	3620
26	77	1051	50-100	700	3620
27	96	944	0-100	700	3620
28	91	969	25-100	700	3620
29	164	1897	150-100	700	4250
30	134	1405	150-100	600	3620
32	110	1025	150-100	500	3620
31	92	656	150-100	400	3620
34	94	963	150-100	300	3620
35	166	2142	150-100	800	3620
33	94	961	25-100	700	3620
36	178	2410	150-100	850	3620
37	178	2410	150-100	850	3620

APPENDIX B

Table 6.2 Interferometer, profilometer and FTIR reflectance measurements of all samples

Al Sample No	Interferometer Power (nm) (Uncoated) (-) Convex (+) Concave	Interferometer Power (nm) (Coated) (-) Convex (+) Concave	Δ Interferometer Power (nm) (Coated-Uncoated)	Profilometer Measured Thickness (nm)	FTIR Reflection (coated) (%)
1	-437	-740	-303	1304	81.2
2	-335	-525	-190	1250	82.7
3	-511	-639	-128	1084	83.6
4	101	-227	-328	2041	88.0
5	-40	-215	-175	875	95.2
6	156	-41	-197	1435	75.6
7	9	-155	-164	1640	75.4
8	286	-44	-330	1824	82.9
10	-398	-869	-471	2353	-
11	152	-258	-410	2391	91.2
12	164	-405	-569	2583	-
13	229	-142	-371	2449	92.0
14	354	-22	-376	2560	-
15	139	-505	-644	2515	87.6
16	139	-	-	-	-
17	202	-505	-707	2657	87.0
18	242	-498	-740	2489	90.6
19	536	-295	-831	3026	-
20	560	-226	-786	2371	90.3
21	294	-76	-370	2557	-

Table 6.2 Interferometer, profilometer and FTIR reflectance measurements of all samples (cont'd)

Al Sample No	Interferometer Power (nm) (Uncoated) (-) Convex (+) Concave	Interferometer Power (nm) (Coated) (-) Convex (+) Concave	Δ Interferometer Power (nm) (Coated-Uncoated)	Profilometer Measured Thickness (nm)	FTIR Reflection (coated) (%)
22	166	-284	-450	2548	89.1
23	283	-541	-824	2023	86.0
24	520	549	29	-	-
25	60	-547	-607	2263	87.0
26	190	-699	-889	2066	90.0
27	973	-167	-1140	2024	92.4
28	101	-893	-994	3000	80.6
29	91	-508	-600	2655	89.7
30	134	-565	-699	2249	87.8
32	-	-896	-	2296	93.4
31	302	-460	-763	2304	96.0
34	-52	-599	-548	1957	89.8
35	298	-130	-428	2471	92.2
33	104	230	126	2009	-
36	-	-	-	-	-
37	134	-332	-466	2496	90.5

APPENDIX C

Table 6.3 Measurements for hardness, elasticity and bond structures of all samples

Al Sample No	Hardness - HIT (GPa)	Elasticity - EIT (GPa)	H / E rates (Recovery power)	sp^3 (%)	sp^2 (%)	C-O (%)
1	-	-	-	-	-	-
2	12.7	90	0.14	-	-	-
3	-	-	-	-	-	-
4	-	-	-	-	-	-
5	10.5	84	0.13	61.88	28.06	10.06
6	-	-	-	-	-	-
7	13.3	92	-	49.11	36.39	14.50
8	14.1	92	0.15	-	-	-
10	-	-	-	-	-	-
11	13.4	89	0.15	-	-	-
12	-	-	-	-	-	-
13	-	-	-	-	-	-
14	-	-	-	-	-	-
15	13.4	88	0.15	54.78	37.55	7.67
16	-	-	-	-	-	-
17	13.0	90	0.14	-	-	-
18	14.9	95	0.16	63.15	26.66	10.18
19	-	-	-	-	-	-
20	19.5	132	0.15	48.76	36.99	14.25
21	-	-	-	-	-	-
22	-	-	-	-	-	-
23	-	-	-	-	-	-
24	-	-	-	-	-	-
25	-	-	-	-	-	-

Table 6.3 Measurements for hardness, elasticity and bond structures of all samples (cont'd)

Al Sample No	Hardness - HIT (GPa)	Elasticity - EIT (GPa)	H / E rates (Recovery power)	sp^3 (%)	sp^2 (%)	C-O (%)
26	24.4	180	0	58.43	30.04	11.53
27	23.6	161	0,15	50.72	33.24	16.04
28	-	-	-	-	-	-
29	-	-	-	-	-	-
30	-	-	-	-	-	-
32	-	-	-	-	-	-
31	-	-	-	-	-	-
34	17.7	121	0,15	60.01	29.61	10.37
35	13.8	88	0	-	-	-
33	-	-	-	-	-	-
36	-	-	-	-	-	-
37	-	-	-	-	-	-